UNIVERSITY OF CALIFORNIA

Los Angeles

Evaluation of Soil-Structure Interaction Effects from Field Performance Data

A dissertation submitted in partial satisfaction of the requirements for the degree of Doctor of Philosophy in
Civil Engineering

by

Salih Tileylioglu

2008

The dissertation of Salih Tileylioglu is approved:

Scott J. Brandenberg

Mark Hansen

Robert L. Nigbor

Jian Zhang

Jonathan P. Stewart, Committee Chair

University of California, Los Angeles

2008

To my parents and my brother

TABLE OF CONTENTS

LIST OF FIGURES

LIST OF TABLES

ACKNOWLEDGMENTS

I feel very lucky to be surrounded by great friends and colleagues. The dissertation would not have been complete if it weren't for their persistent support. I would like to extend my gratitude to all those wonderful people.

It was a great privileged to have worked with my research advisor, Dr. Jonathan P. Stewart. His support and guidance throughout my graduate studies here at UCLA not only helped me accomplish an important goal, but also broadened my horizons as a researcher. Furthermore, Chapter 2 is a version of the "Input ground motions for a tall buildings with subterranean levels" published in the Structural Design of Tall and Special Buildings in 2007 coauthored by Dr. Jonathan P. Stewart and me. It was also a great honor to have Dr. Robert L. Nigbor as a co-advisor. His help in my research is greatly appreciated, not to mention our in depth discussions about non-research topics. I consider him a true friend. Chapter 3 was a collaborative effort between me, Dr. Jonathan P. Stewart, Dr. Farzad Naeim and Dr. Arzhang Alimoradi. Their help is greatly appreciated. I would also like to thank Dr. Mark Hansen whom I had a chance to work with during the early years of my research. The dissertation committee members are also acknowledged for accepting to be in my committee. Dr. Mladen Vucetic's support during my early days as a graduate student is appreciated. Partial funding from CENS and UCLA was very helpful and is greatly appreciated.

One of the first people I met here at UCLA was Christine Goulet. We became very good friends since then. Her support and encouragement was very helpful. Special

thanks to Kutay Orakcal for helping me out in various ways, especially in my first year at UCLA. I would also like to acknowledge Ethan and Christian Aubert for their great friendship. My friend S. Tansel Karakaya; who persistently called me and gave moral support all the way from Turkey, is yet another special person whom I feel privileged to have known. I met Pirooz Kashighandi in my second year at UCLA and since then we became great friends. His support and friendship is also acknowledged. My office mates Tim Ancheta, Lisa Star and Joe Coe made the office environment fun. I wish all of them the best of luck in their dissertations.

I would also like to extend my appreciation to Dr. M. Ufuk Ergun, Dr. Orhan Erol and Dr. K. Onder Cetin at METU for their kind support.

I will always remember what a great professor and person the late Dr. Erdil R. Tuncer was. His influence will never be forgotten.

Finally, I would like to thank my parents Sansin and Alaeddin as well as my brother Yigit for being extremely supportive of me. I have been blessed with such a loving family.

VITA

November 6, 1978	Born, Adana, Turkey
1999 B.S.,	Civil Engineering Eastern Mediterranean University Famagusta, TRNC
2002 M.S.,	Civil Engineering (Geotechnical Engineering) Middle East Technical University Ankara, Turkey
2002 -03	Site Engineer Turner-Proge JV
2003-04	Site Engineer ICTAS Construction Co.
2004-08	Teaching Assistant and Research Assistant Department of Civil Engineering University of California, Los Angeles

PUBLICATIONS

Baek J., Hansen M., Nigbor R. L, Tileylioglu S., (2006) "Elevators as an excitation source for structural health monitoring," *4th World Conference on Structural Control Monitoring*

Stewart, J.P. and Tileylioglu, S. (2007). "Input ground motions for tall buildings with subterranean levels," *Structural Design of Tall and Special Buildings*, 16(5), 543-557.

Tileylioglu, S., Nigbor, R.L., and Stewart, J.P. (2008). "Determination of soil-structure interaction effects for a model test structure using parametric system identification procedures," in *Geotechnical Engineering and Soil Dynamics IV,*, May 18-22, 2008, Sacramento, CA, ASCE Geotechnical Special Publication No. 181, D. Zeng, M.T. Manzari, and D.R. Hiltunen (eds.), 10 pages (electronic file).

ABSTRACT OF THE DISSERTATION

Evaluation of Soil-Structure Interaction Effects from Field Performance Data

by

Salih Tileylioglu

Doctor of Philosophy in Civil Engineering

University of California, Los Angeles 2008

Professor Jonathan P. Stewart, Chair

Analytical solutions for soil-structure interaction (SSI) problems are well established, but apply for idealized condition, causing their applicability to realistic conditions to be poorly defined. I use field performance data from buildings to gain insight into poorly understood aspects of SSI problems and to test simplified models.

The first problem addressed concerns the earthquake motions in buildings with subterranean levels. I describe simple models that describe the motions at the base of embedded cylinders relative to free-field motions and contrast those procedures with assumptions made in engineering practice. Strong motion data from buildings are analyzed to show that rigid body displacements of foundations explain only 60-80% of the power of ground-level motions. More accurate procedures accounting for

foundation flexibility are implemented for a tall building with subterranean levels. A relatively complex SSI model is created that matches the observed response to the 1994 Northridge earthquake. Selected components of this model are removed one by one, which shows that including the subterranean portion of the building in the model significantly affects structural drifts and their distribution.

The second problem concerns forced vibration testing of buildings, for which I seek to (1) evaluate modal properties for the fixed- and flexible-base conditions and (2) evaluate foundation-soil stiffness and damping characteristics. Modal properties are developed using parametric system identification techniques that take shaker motion as input and total roof motion as output for flexible-base and a combination of shaker acceleration, foundation acceleration and rotation of foundation as input and translation of the roof motion relative to the base as output for fixed-base. The procedure is applied to a test structure and is shown to provide results comparable to those derived from earthquake data.

Nonparametric system identification procedures for analysis of foundation stiffness and damping under translational and rotational vibration are developed. The impedances are calculated in the frequency domain as ratios of base shear to displacement and base moment to base rotation. The procedure is applied for the same test structure; the observed impedance coefficients match theoretical predictions at low frequencies but decay more rapidly with frequency.

1 INTRODUCTION

1.1 INTRODUCTION

Foundation motions deviate from free-field motions for two principal reasons: (1) the imposition of stiff foundation systems on (or in) a geologic medium experiencing non-uniform shaking will result in foundation motions being reduced relative to those in the free-field and (2) inertial forces developed in the structure will cause base shear and moment, which in turn will induce relative foundation/free-field motions due to the foundation compliance. These phenomena are commonly termed Soil-Structure Interaction (SSI). The general SSI problem is subdivided into kinematic SSI, which is concerned with first factor identified above, and inertial SSI, which is concerned with the second factor. Depending mainly on the relative stiffness of the soil and structure, SSI can have an impact on the response of the structure.

There are two ways of including soil-structure interaction effects into a response analysis of a structure. The *direct method* models the complete soil-foundation-structure system and analyzes its response in a single step. The number of degrees of freedom especially in the soil region is high and the solution would involve sophisticated 3D continuum analysis using finite element or finite different methods. A

recent study with this method is the Humboldt Bay bridge by Yang et al. (2004). The substructure method, involves separate and independent analyses of kinematic and inertial interaction. The substructure approach involves superposition and hence is strictly applicable only to linear systems. However, it is often applied to nonlinear systems using strain-compatible equivalent-linear soil properties.

1.2 OBJECTIVES AND ORGANIZATION OF THE THESIS

The principal objective of this thesis is to use field performance data from instrumented structures to "measure" certain soil-structure interaction effects. Work of this type is extremely important because there is very little data that is available to validate SSI analytical models. The use of field performance data from earthquake excitation has been previously investigated (Stewart et al., 1999a,b), and was not a principal thrust of this research. Instead, the emphasis is on forced vibration tests to: (1) examine the effects of soil-structure interaction (2) to develop system identification procedures that enable the evaluation of fixed and flexible-base parameters (frequency and damping) through inputs and outputs from a soil structure system, (3) estimate impedance functions from forced vibration tests carried out on a model test structure and to compare results to available theoretical models.

Following this introduction, this thesis begins in Chapter 2 with review of and critique of SSI analysis methods used for buildings with subterranean levels. Current practice varies widely, but generally fails to take into account the reduction of translational components of ground motion with depth, the rocking components of base

excitation that can be introduced to embedded foundations, and the effects of foundation-soil interaction along basement walls and base slabs. Chapter 2 describes modeling procedures that would be expected to realistically simulate this soil-foundation-structure interaction problem and contrasts those procedures with modeling approaches commonly used in practice. Data from buildings with subterranean levels is analyzed to investigate the degree to which the foundation acts as a rigid body during earthquake excitation, and the results provide insight into the reliability of some commonly used models.

Chapter 3 expands upon the work from Chapter 2 by performing detailed analysis of a single building with subterranean levels. The selected building is instrumented and has recorded the 1994 Northridge earthquake. A model of the building is created that includes a series of relatively complex soil-structure interaction effects. That model is slightly calibrated (in terms of superstructure modal damping ratios) so as to produce a close fit with recordings. When elements of the SSI model are stripped away, the resulting errors are examined one-by-one. This provides insight into the impact of different modeling procedures on various metrics of building response.

In Chapter 4, I develop parametric system identification procedures to identify modal frequencies and damping ratios from forced vibration test data for flexible-base conditions (inclusive of translational and rotational foundation movements associated with inertial forces) and fixed-base conditions (no effect of inertial soil-structure interaction). This work builds upon similar previous work that was specific to the case of earthquake excitation (Stewart and Fenves, 1998). The developed procedure is

applied using data collected from forced vibration tests of the NEES model test structure in Garner Valley, California (www.nees.ucsb.com). Results are also obtained for earthquake excitation, and those results are compared to each other and to theoretical predictions.

In Chapter 5, field performance data from the same model test structure is used to evaluate the frequency-dependent stiffness and damping associated with foundation-soil interaction. During forced vibration testing, relative foundation/ground displacements occur due to inertial interaction. By measuring those displacements and the causative inertial forces/moments, I seek to infer the aforementioned stiffness and damping characteristics. It is of interest to compare those results to theoretical predictions of impedance functions from the literature. Those impedance functions were developed for simplified conditions such as a rigid foundation and depth-invariant soil conditions. Because of the simplifying assumptions used in the development of theoretical impedance functions, there is a need to verify their accuracy through data. I first review the limited previous experimental studies on the topic, then describe the mathematical procedures used to infer stiffness and damping, and then present results for the Garner Valley model test structure using data from forced vibration testing.

Chapter 6 summarizes the scope and findings of the work. Recommendations for additional research are also provided.

2 INPUT GROUND MOTIONS FOR TALL BUILDINGS WITH SUBTERRANEAN LEVELS

2.1 INTRODUCTION

When earthquake ground motions are characterized for use in structural design and response simulations, the developed motions generally correspond to a "free-field" and "ground surface" condition. The term *free-field* implies no significant effect of structures on the characteristics of ground shaking. The term *ground surface* indicates that the estimated motions are at the surface of the earth.

Neither the free-field nor the ground surface conditions are generally satisfied for tall buildings in California's urban centers. Most tall buildings are embedded, having their foundation level at some depth below the ground surface to accommodate subterranean levels. In some cases, the embedded portion of the structure has a different shape in plan view than the above-ground portion. The embedded portion is often much larger in plan, which is referred to as a podium.

A significant problem in earthquake engineering practice concerns the manner by which free-field, ground surface motions should be utilized for the analysis of

buildings with subterranean levels. Current practice varies widely, but generally fails to take into account the reduction of translational components of ground motion with depth, the rocking components of base excitation that can be introduced to embedded foundations, and the effects of foundation-soil interaction along basement walls and base slabs.

One purpose of this chapter is to describe modeling procedures that would be expected to realistically simulate this soil-foundation-structure interaction problem and to contrast those procedures with modeling approaches commonly used in practice. The chapter also presents the results of past research investigating ground motions in embedded structures, and evaluates the effectiveness of those approaches using available data from instrumented buildings, and identifies knowledge gaps that should be addressed by future research.

This chapter was previously published as a journal paper (Stewart and Tileylioglu, (2008)). The work was performed as Task 8 of the Tall Buildings Initiative organized by the Pacific Earthquake Engineering Research Center.

2.2 MODELING PROCEDURES FOR EMBEDDED STRUCTURES

A schematic illustration of a building with subterranean levels is shown in Figure 2.1. The actual soil-foundation-structure system is excited by a wave field that is incoherent both vertically and horizontally and which may include waves arriving at various angles of incidence. These complexities of the ground motions cause foundation motions to deviate from free-field motions. This complex ground excitation acts on

stiff, but non-rigid, foundation walls and the base slab, which in turn interact with a flexible and nonlinear soil medium having a significant potential for energy dissipation. Finally, the structural system is connected to the base slab, and possibly to basement walls as well.

There are two classical methods for modeling the problem defined in Figure 2.1. The first is a *direct approach*, in which a computational model of the full structure, foundation, and soil system is set up and excited by a complex and incoherent wave field. An example of a direct model using linear soil and structural elements in the program OpenSees (McKenna and Fenves, 2001) is given in Figure 2.2. This problem is difficult to solve from a computational standpoint, especially when the system contains significant nonlinearities, and hence the direct approach is rarely used in practice.

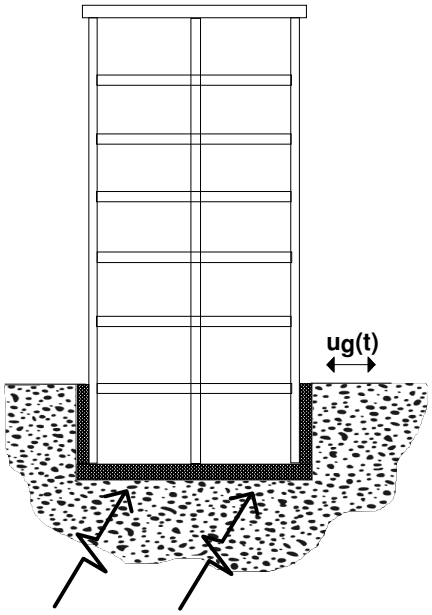

Figure 2.1. Schematic illustration of soil-foundation-structure system

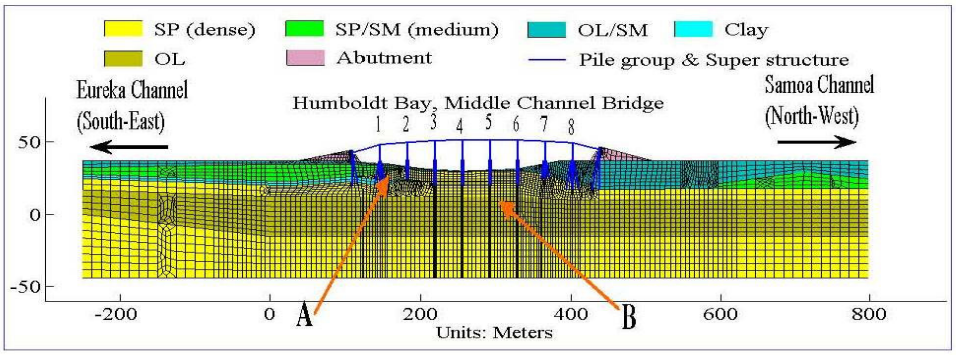

Figure 2.2. Example of direct model of soil-foundation-structure system using OpenSees (Zhang et al., 2003)

In the second approach (referred to as the *substructure approach*), the complex soil-foundation-structure interaction problem is divided into three steps as illustrated in Figure 2.3.

As shown in Figure 2.3(b), the first step in the substructure approach involves evaluating the motion that would be expected to occur on the foundation slab if the superstructure was absent and the foundation had no mass. This motion is termed the *foundation input motion* (FIM), and it accounts for the complexities of the incident wave field and its interaction with the stiff foundation system. For deeply embedded foundations, the dominant mechanism affecting base slab motions are embedment effects associated with ground motion reductions that occur below the original ground surface. The analysis of the foundation input motion is commonly referred to as a *kinematic interaction* analysis.

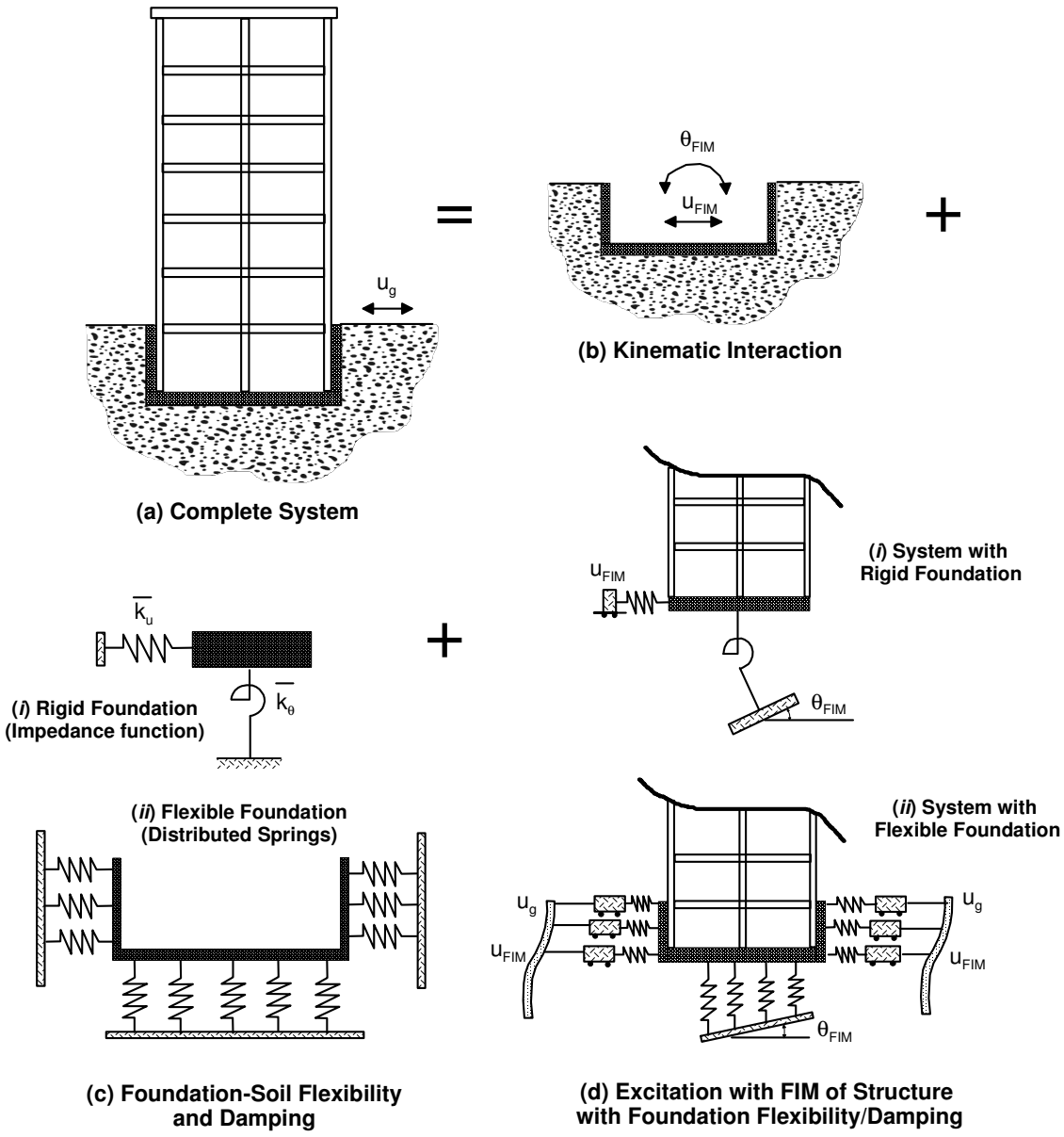

Figure 2.3 Schematic illustration of substructure approach to solution of soil-foundation-structure interaction problem using either (i) rigid foundation or (ii) flexible foundation assumption

In the second step the stiffness and damping characteristics of the foundation-soil interaction are characterized using either relatively simple impedance function models

(e.g., Gazetas, 1991) for rigid foundations (illustrated in Figure 2.3(c-i)) or a series of distributed springs and dashpots acting around the foundation (illustrated in Figure 2.3(c-ii)). The later case of distributed springs is needed for non-rigid foundations and if internal moments and shears and relative displacements of the foundation are a required outcome of the analysis. Only springs are depicted in Figure 2.3(c) for simplicity, but dashpots can easily be added in parallel to the springs (or the springs can be visualized as being complex-valued, which accounts for damping).

As shown in Figure 2.3(d), the final step involves placing the superstructure atop the foundation and exciting the system through the foundation by displacing the ends of the springs using the rocking and translational components of the foundation input motion. Note that in the case of the distributed spring/flexible foundation model, differential ground displacements over the height of the basement walls (= depth of embedment) should strictly be applied given the vertical incoherence of ground motion.

Members of the Task 8 advisory panel have experience in structural design (both from a designer and reviewer perspective) in the Seattle, San Francisco, and Los Angeles areas. The panel members were asked about their experience with respect to the modeling of structures with subterranean levels. It was found that models of the type depicted in Figure 2.3 are not being used. Figure 2.4 shows the most common modeling approaches. In all cases, the foundation input motion is assumed equal to the free-field motion (i.e., $u_{FIM} = u_g$; $\theta_{FIM} = 0$), meaning that kinematic interaction effects

are ignored. The stiffness and flexibility of the soil-foundation interaction are also often ignored by assuming a fixed base, as illustrated in Models 1 and 2 in Figure 2.4. The only distinguishing factor between Models 1 and 2 is the height of the structure, which is taken as the height above ground level for Model 1 and as the height above the foundation level for Model 2. Model 3 includes the flexibility of the soil-foundation interaction through the use of springs (damping effects are ignored) and excites the structure using the free-field motion applied at the ends of the horizontal springs. While better than Models 1 and 2, Model 3 fails to account for kinematic interaction effects on the base excitation and fails to account for ground excitation entering the system through stresses applied on the basement walls.

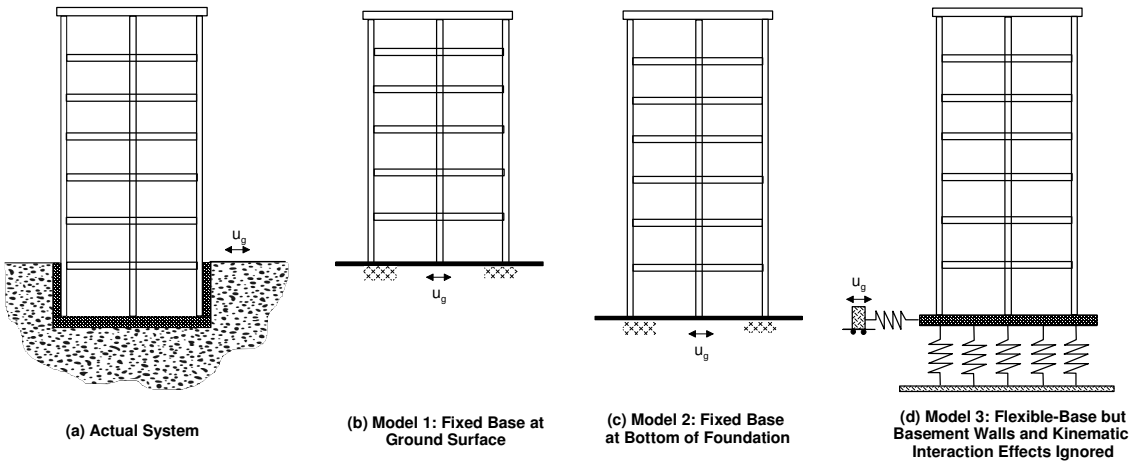

Figure 2.4. Schematic illustration of three models used in engineering practice to represent the actual soil-foundation-structure interaction problem

2.3 THEORETICAL MODELS FOR GROUND MOTIONS AT THE BASE OF RIGID EMBEDDED FOUNDATIONS

Solutions exist in the literature for most of the critical components of the substructure analysis depicted in Figure 2.2 (e.g., Kramer and Stewart, 2004). Most critical for the subject of this article, solutions are available that describe the foundation input motion for embedded foundations as a function of the free-field motion. The available solutions apply for rigid cylinders embedded in a uniform soil of finite or infinite thickness (halfspace). When subjected to vertically propagating coherent SH waves, the embedded cylinders experience a reduction in base-slab translational motion relative to the free-field due to ground motion reductions with depth and wave scattering effects. In addition, rotations in the vertical plane are introduced, which are caused by incompatible shear strains along the sides of the excavation and the free-field.

Kausel et al. (1978) and Day (1978) developed analytical transfer functions relating base-slab translational and rotational motions to free-field translations for an incident wave field consisting of vertically propagating, coherent SH waves. Day (1978) used finite element analyses to evaluate the base motions of a rigid cylindrical foundation embedded in a uniform elastic half space (hysteretic soil damping $\beta = 0$, Poisson's ratio $\nu = 0.25$). Kausel et al. (1978) performed similar studies but for the case of a visco-elastic soil layer of finite depth over a rigid base ($\beta = 0.05$ and $\nu = 0.33$). The amplitude of the halfspace and finite soil layer transfer functions are shown together in Figure 2.5(a) for foundation embedment / radius ratio e/r = 1.0. The primary difference between the two solutions is oscillations in the finite soil layer case

at high frequencies. Also shown in Figure 2.5(a) is the following approximate transfer function amplitude model developed by Kausel et al. (1978):

$$\left|H_u(\omega)\right| = \cos\left(\frac{e}{r}a_0\right) = \cos\left(\frac{e\omega}{v_s}\right) > 0.453 \qquad (2.1)$$

where $\left|H_u\right|$ indicates the FIM/free-field transfer function (i.e., ratio of the Fourier amplitudes of the two motions), e = foundation embedment, r = effective foundation radius (selected to match the actual foundation area), ω = circular frequency in rad/sec, V_s = soil shear wave velocity, and $a_0=\omega r/V_s$.

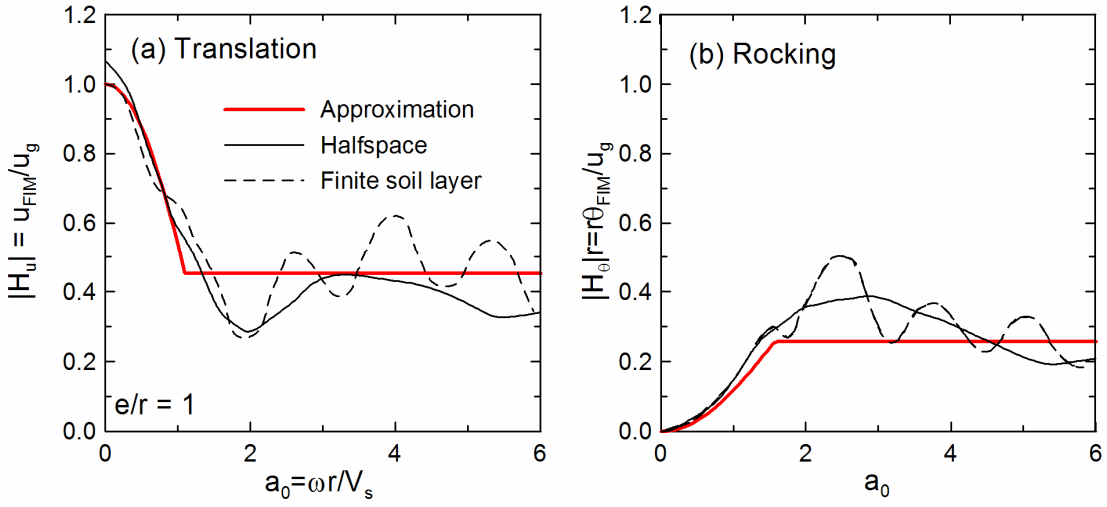

Figure 2.5. Solutions for the transfer functions between input motions and free-field motions for translation and rocking of embedded rigid cylinders. Halfspace solution is from Day (1978) and finite soil layer case is from Kausel et. al. (1978)

Figure 2.5(b) shows similar results for the rocking component of the foundation input motion. In this case, the approximate transfer function is given by:

$$\left|H_\theta(\omega)\right| = \frac{0.257}{r}\left[1-\cos\left(\frac{e}{r}a_0\right)\right] < \frac{0.257}{r} \qquad (2.2)$$

The amount of rocking increases with frequency as shown in Figure 2.5(b).

These results for an embedded rigid cylinder subjected to vertically incident coherent SH waves have been extended for cases of (1) soil properties varying with depth (Kausel et. al. 1978), (2) horizontally propagating coherent SH waves (Day, 1977), and (3) non-circular foundations (Mita and Luco, 1989) as follows:

- For soil properties which vary with depth, Kausel et al. found that the approximate transfer functions represented by Eq. 2.1-2.2 remain valid provided averaged V_S across the embedment depth is used.
- For the case of horizontally propagating coherent SH waves, Day found that the base rocking was practically negligible, the filtering of horizontal motions was significant but was relatively insensitive to *e/r*, and a significant torsional response was induced at high frequencies (a_0 > 1.5). It should be noted, however, that horizontally propagating shear waves are generally of negligible engineering significance in soil-structure interaction problems because components of ground motion with frequencies above about 1 Hz tend to attenuate rapidly with distance (e.g., Chen et al., 1981).
- Mita and Luco found that an embedded square foundation could be replaced by an equivalent cylinder without introducing significant error. The radius of the equivalent cylinder was defined as the average of the radii necessary to match the area and moment of inertia of the square base.

2.4 VERIFICATION OF THE THEORETICAL MODELS

The analytical model presented in Eqs. 2.1-2.2 has been verified with respect to two sites that have deeply embedded circular foundations. One is referred to as Site A3, and consists of a deeply embedded nuclear containment structure in California. This site has a ratio of embedment to foundation radius of e/r = 26.2/9.0 m = 2.9. The second site is referred to as Site A46, and consists of a model of an embedded nuclear containment structure in Lotung, Taiwan. The site has a ratio of embedment to radius of e/r = 4.6/5.0 m = 0.9. Kim (2001) computed transmissibility function amplitudes $|H|$ for these sites, which are shown in Figure 6 along with the simplified analytical transfer functions in Eqs. 2.1-2.2. The simplified transfer functions for translation are generally consistent with the observations. Only Site A46 has sufficient instrumentation to enable an evaluation of rocking. The rocking transfer functions for Site A46 are generally consistent with the data, but show some errors at low frequencies. These errors are likely due to significant rocking induced by inertial interaction, which is pronounced for this structure. Overall, the approximate procedure for estimating FIMs of embedded foundations appears to be well verified by the data from these deeply embedded circular structures.

The validation presented in Figure 2.6 provides confidence that the characteristics of foundation input motions can be estimated with reasonable accuracy for embedded, stiff circular foundations using Eq. 2.1-2.2. However, a number of issues remain unresolved with respect to the specification of input motions for buildings with

subterranean levels. One of the key issues involves the degree to which transient soil displacements over the depth of embedment affects the foundation response through interaction with the basement walls.

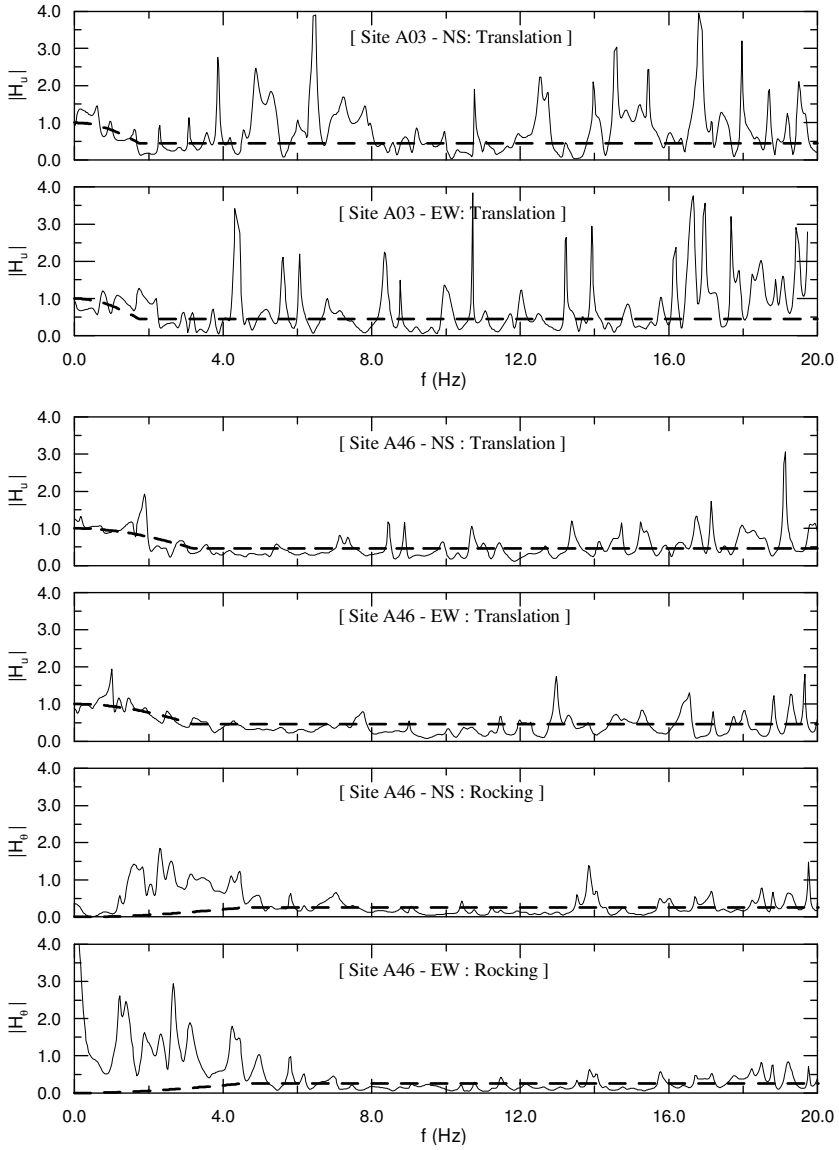

Figure 2.6. Comparison of simplified model for FIM with transmissibility function amplitudes for two sites with deeply embedded foundations (figure from Kim, 2001)

These foundation wall-soil interaction issues are accounted for by the simplified model (Eqs. 2.1-2.2) because the finite element analyses used to develop the transfer functions shown in Figure 2.5 include this interaction. However, the results only apply for a *rigid* embedded structure. As the basement walls become relatively flexible, the transfer functions would be expected to change, especially for rocking. To help visualize how flexible basement walls would affect foundation response, consider a pile embedded in a soil profile as shown in Figure 2.7. Bending of the pile occurs because of the transient displacements of the adjacent soil; similarly, bending of basement walls is also possible if they are relatively flexible. It is obvious that for any given pile (or wall) depth, the displacements of the flexible pile at that depth would differ from those for a rigid pile. In the extreme case of a perfectly flexible pile, there is no rotational component to the FIM and the translation matches exactly the soil column response at the foundation elevation.

The effects of foundation flexibility on the kinematic response of embedded foundations have not been evaluated in the archived literature to our knowledge. Foundation flexibility effects on impedance functions have been investigated (Iguchi and Luco, 1982; Riggs and Waas, 1985; Liou and Huang, 1994; Todorovska et al. 2001), but for the kinematic problem all of the available theoretical solutions are for rigid foundations (Kausel et al., 1978; Day, 1978; Mita and Luco, 1989). In the following section, we examine data from instrumented buildings to provide some preliminary insights into possible foundation flexibility effects on foundation motions.

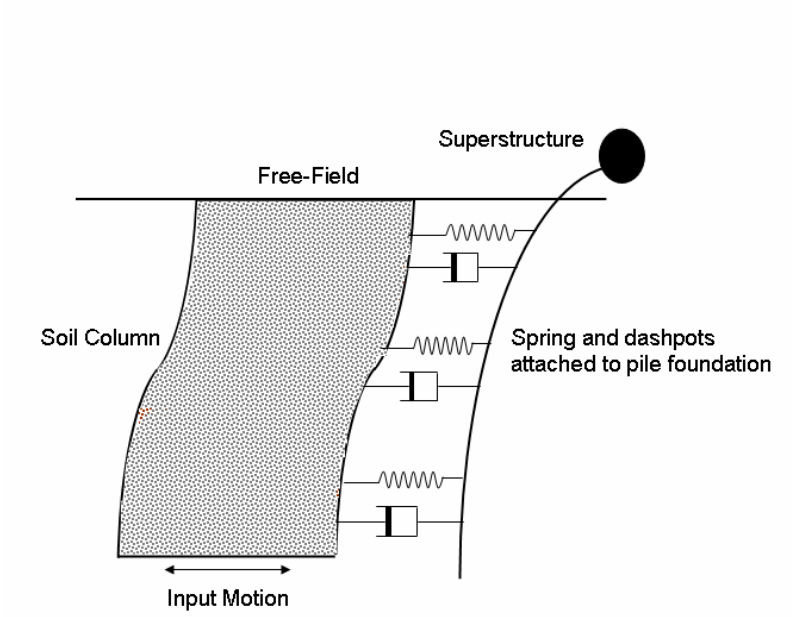

Figure 2.7. Schematic of flexible pile foundation subject to bending as a result of vertical incoherence of ground motion. Although an extreme case with respect to subterranean levels of buildings, the schematic is intended to show how free-field ground response can affect the bending of flexible basement walls, which in turn affects the characteristics of shaking in the subterranean levels of the structure

2.5 EMPRICAL EVALUATION OF FOUNDATION FLEXIBILITY EFFECTS ON FOUNDATION MOTIONS

In this section, we examine data from structures with embedded foundations having the instrumentation shown in Figure 2.8. If the foundation is rigid, the motion at ground level (denoted u_{fg}) should be perfectly explained by the foundation base motion (u_{FIM}) and the foundation rocking ($\theta = (v_1 - v_2)/2r$). As depicted in Figure 2.8, that relationship would be as follows for a rigid foundation:

$$(u_{fg})_{rigid} = u_{FIM} + e\theta \tag{2.3}$$

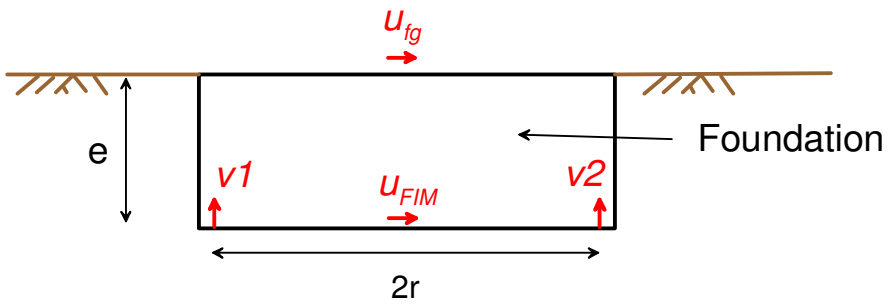

Figure 2.8. Schematic of minimal level of instrumentation needed to evaluate the effects of foundation flexibility on the motions at the ground level of the structure.

The data are used to evaluate the extent to which the real foundation motion at ground level (u_{fg}) is consistent with $(u_{fg})_{rigid}$. Sites from the database of Stewart et al. (1998) were reviewed and sites in Table 1 were identified as having the required instrumentation. As can be seen in Table 2.1, of the five sites with the required instrumentation, only three sites can be used because of missing data from specific instruments.

Table 2.1. Sites having required instrumentation for evaluating foundation flexibility effects

		SITE ATTRIBUTES					
No	Name	T(s)	e(m)	r_θ (m)	v_s (m/s)	Earthquakes Recorded	Data Utilization
A 23	LA 6 Story Office Building	0.9	4.3	14.10	93	1994 Northridge	Recording u_{fg} not available
B3	San Francisco 47 story Office	5.3	8.2	24.10	146	1989 Loma Prieta	Recording u_{fg} not available
B4	San Francisco Transamerica	3.6	12.8	30.30	244	1989 Loma Prieta	Data used
B12	LA 32 Story Office	1.9	13.0	27.80	408	1994 Northridge	Data used
B13	LA 54 Story Office	5.9	14.0	26.40	402	1994 Northridge	Data used

The right side of Figures 2.9-2.11 show acceleration histories for u_{fg}, $(u_{fg})_{rigid}$ (calculated per Eq. 2.3), u_{FIM}, and $e\theta$ for sites The left sides of Figures 2.9-2.11 show power spectral density functions with 4X smoothing using Welch's method (Welch, 1967) for each of the acceleration histories. As can be seen from all the figures, ground level motion u_{fg} is not perfectly described by $(u_{fg})_{rigid}$, although the differences appear to be relatively small. The ground level motion derived from foundation rotation ($e\theta$) is small compared to the motion derived from foundation translation (u_{FIM}), particularly at low frequencies.

The power of each signal from the Figures 2.9-2.11 is calculated as follows:

$$P_x = \int_{\omega_1}^{\omega_2} S_{xx}(\omega) d\omega \tag{2.4}$$

where $S_{xx}(\omega)$ is the power spectral density function for signal x, ω denotes circular frequency (in rad/sec), and ω_1 and ω_2 denote the lowest and highest useable frequency per the signal filtering criteria. Table 2.2 lists for all the sites with available data the power ratios for the following motions: $(u_{fg})_{rigid} / u_{fg}$, u_{FIM} / u_{fg}, $e\theta / u_{fg}$. Also shown in Table 2.2 are the limiting frequencies ω_1 and ω_2 used in the calculations (expressed in Hz).

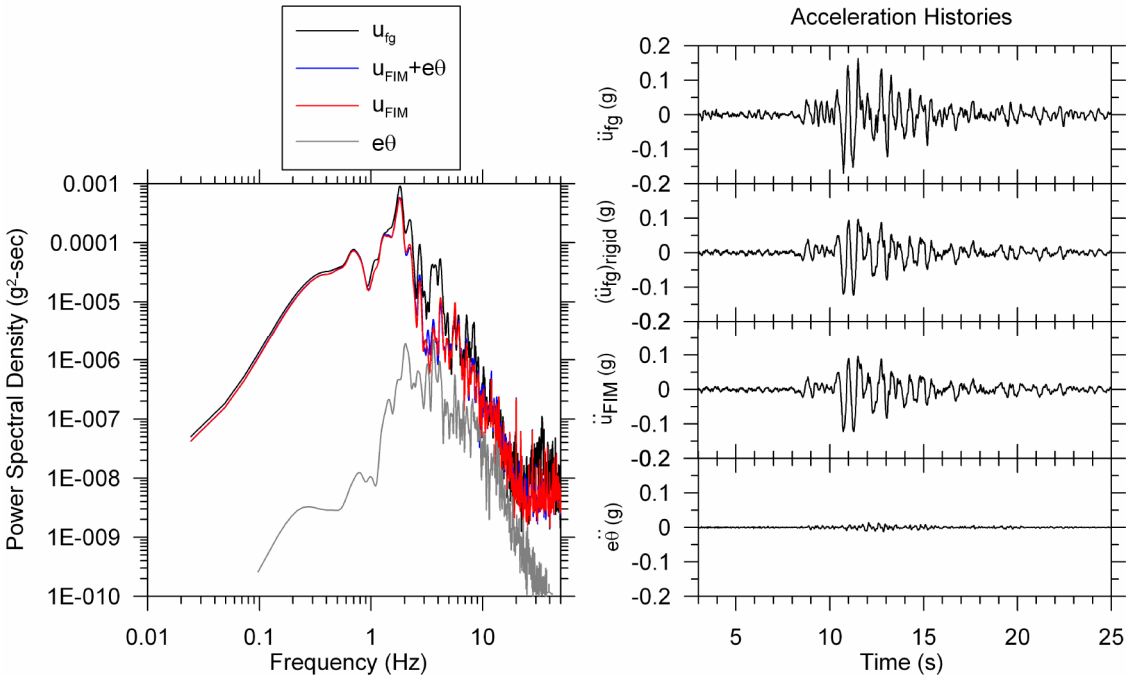

Figure 2.9. Power spectral density functions and acceleration histories for Site B4 (SF Transamerica Building), showing contribution of base translation (u_{FIM}) and rotation ($e\theta$) to motion at top of foundation and also showing contribution of rigid body motions ($u_{FIM} + e\theta$) to top of foundation motion (u_{fg}). Nyquist frequency for the selected records after decimation is 100 Hz.

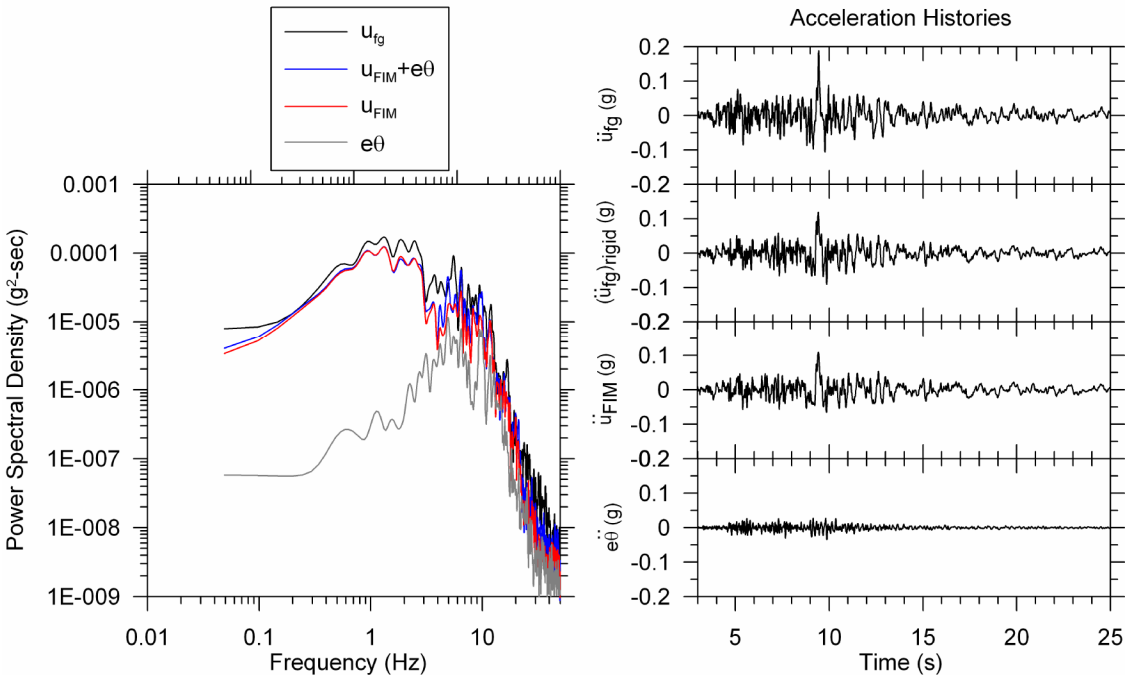

Figure 2.10. Power spectral density functions and acceleration histories for Site B12 (LA 32 Story), showing contribution of base translation (u_{FIM}) and rotation ($e\theta$) to motion at top of foundation and also showing contribution of rigid body motions (u_{FIM} + $e\theta$) to top of foundation motion (u_{fg}). Nyquist frequency for the selected records after decimation is 100 Hz

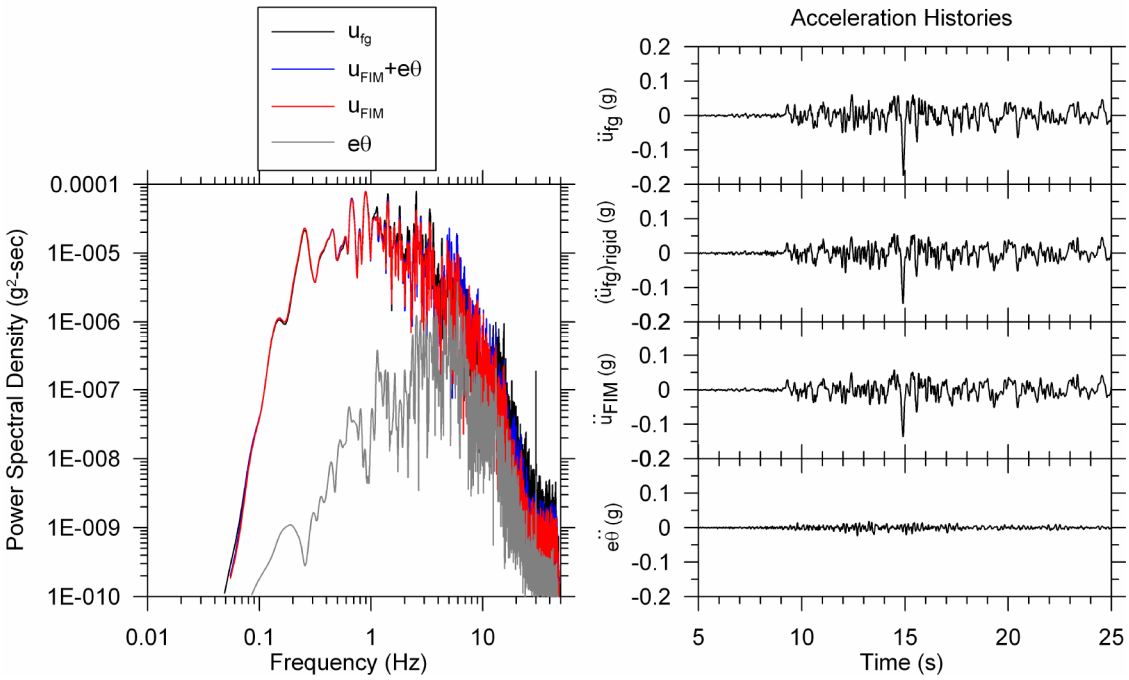

Figure 2.11. Power spectral density functions and acceleration histories for Site B13 (LA 54 Story), showing contribution of base translation (uFIM) and rotation (eθ) to motion at top of foundation and also showing contribution of rigid body motions (u_{FIM} + eθ) to top of foundation motion (u_{fg}). Nyquist frequency for the selected records after decimation is 50 Hz

Table 2.2 Power ratios and amplitude ratios for buildings with instrumented foundations

			Power Ratios from Data			Weighted Amplitude Ratios			
Site	**f_1(Hz)**	**f_2(Hz)**	**$(u_{fg})_{rigid}/u_{fg}$**	**u_{FIM}/u_{fg}**	**eθ/u_{fg}**	**Data: u_{FIM}/u_{fg}**	**Theory: $u_{FIM}/(u_{fg})_{rigid}$**	**Data: eθ/u_{fg}**	**Theory: eθ/$(u_{fg})_{rigid}$**
B4	0.17	100	0.59	0.58	0.01	0.74	0.97	0.06	0.03
B12	0.13	100	0.63	0.54	0.06	0.72	0.90	0.19	0.10
B13	0.66	50	0.87	0.81	0.04	0.88	0.96	0.13	0.04

As can be seen from the column of Table 2.2 labeled $(u_{fg})_{rigid}/u_{fg}$, 60-80% of the power of the ground level motion can be explained by rigid-body motion. Moreover, most of

the rigid body motion (85 – 95%) can be explained by base translation. This suggests that base rocking is not a significant contributor to the motion at the ground level of the selected buildings. The rocking contributions may become more significant further up in the superstructure.

To facilitate comparisons of the data to the theoretical model for rigid foundations (represented by Eq. 2.1-2.2), we compute transfer function amplitudes for the ground motion ratios listed under the "Weighted Amplitude Ratios" portion of Table 2.2. Those ground motion ratios represent the relative contributions of foundation base translation and base rocking on the top-of-foundation translations. Results are shown in Figures 2.12-2.14 for sites B4, B12, B13 respectively. The transfer functions marked as "data" are calculated as the square root of the corresponding power spectral ratios, the square root being necessary because the power spectrum corresponds roughly to the square of the Fourier amplitude spectrum (Pandit, 1991). The corresponding model predictions are obtained from the functions given in Eq. 2.1-2.2 as:

$$\frac{u_{FIM}}{(u_{fg})_{rigid}} = \frac{1}{1+\frac{e}{r}\left(\frac{|H_\theta|}{|H_u|}\right)}$$
$$\frac{e\theta}{(u_{fg})_{rigid}} = \frac{1}{1+\frac{r}{e}\left(\frac{|H_u|}{|H_\theta|}\right)} \qquad (2.5)$$

The results in Figures 2.12-2.14 show that the data generally follow the trends predicted by the rigid foundation model. However, for translation the data generally lie

below the model, which we attribute to the relatively large ground level motion used for the data versus the model (i.e., $u_{fg} > (u_{fg})_{rigid}$). For rotation, the data lie slightly above the model for Sites B4, B12, and B13. Recall from Figure 2.6 that the base rotations at Lotung were significantly larger than the kinematic model at low frequencies. Sites B4, B12 and B13 are very tall, long period structures with first-mode periods corresponding to a_0=0.22, 0.23, and 0.07 respectively.

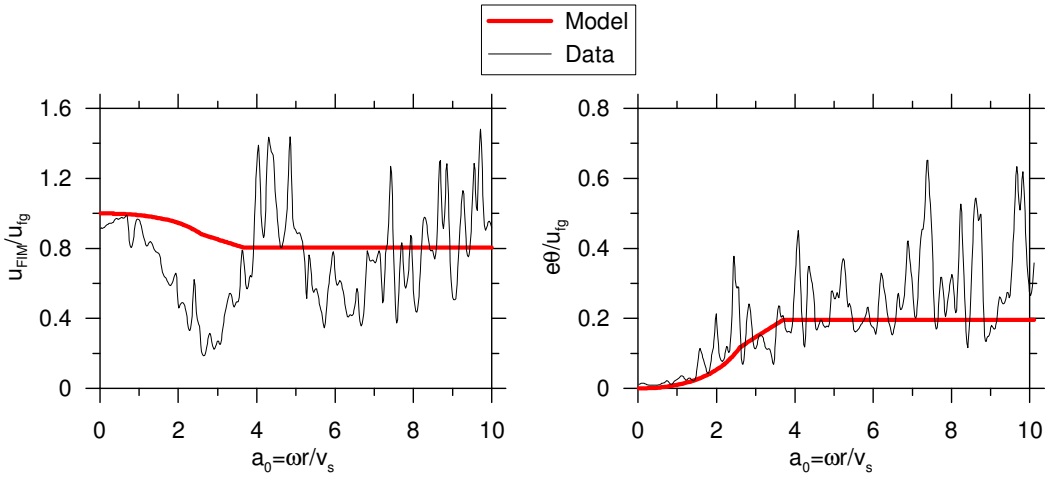

Figure 2.12. Comparison of transfer functions from rigid foundation model to data for transfer functions representing the relative contributions of base-of-foundation translation (u_{FIM}) and rocking (θ) on top-of-foundation displacement (u_{fg}). Data is from Site B4 (SF Transamerica).

Because the effects of inertial interaction on base-of-structure motions tend to be concentrated at the first-mode building frequency (e.g., Kim and Stewart, 2003), most of the frequency range shown in Figures 2.12-2.14 is relatively unaffected by inertial interaction. We speculate that this causes the kinematic interaction model to provide a relatively good estimate of the data. On the other hand, the first mode period at Lotung

occurs at a_0=3.1, which causes inertial interaction to introduce rotations beyond those expected from kinematic interaction alone over the low end of the plotted frequency range in Figure 2.6.

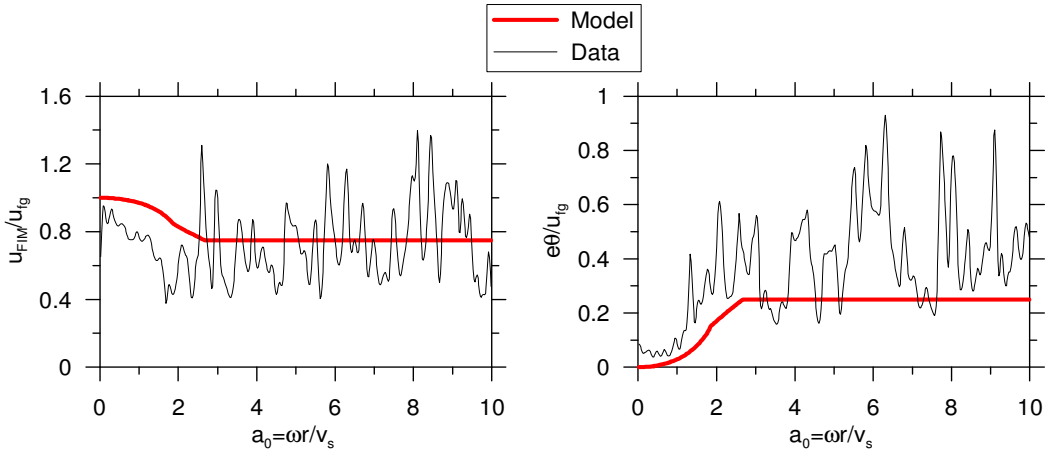

Figure 2.13. Comparison of transfer functions from rigid foundation model to data for transfer functions representing the relative contributions of base-of-foundation translation (u_{FIM}) and rocking (θ) on top-of-foundation displacement (ufg). Data is from Site B12 (LA 32 Story).

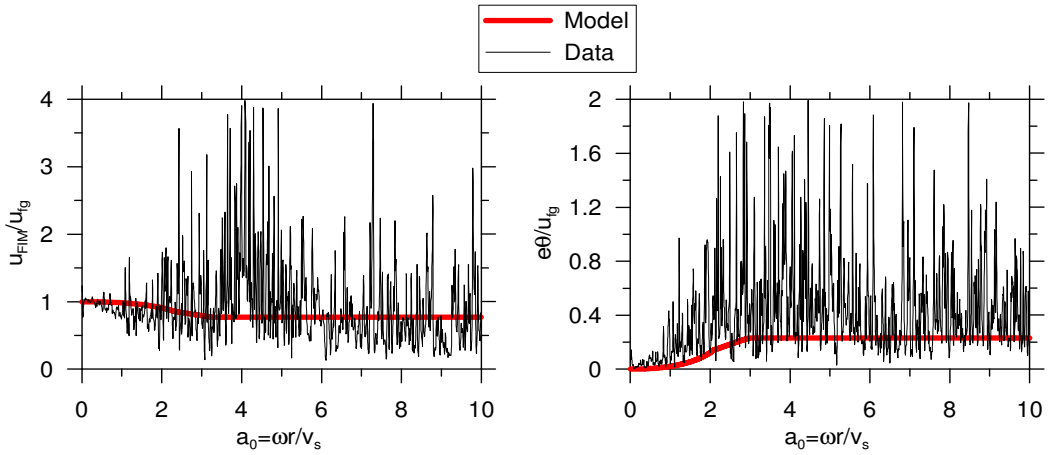

Figure 2.14. Comparison of transfer functions from rigid foundation model to data for transfer functions representing the relative contributions of base-of-foundation translation (u_{FIM}) and rocking (θ) on top-of-foundation displacement (ufg). Data is from Site B13 (LA 54 Story).

Lastly, a weighted average of the transfer function amplitudes across the frequency range of the motions, in which the weight for a given frequency is the corresponding power spectral density ordinate normalized so that the sum of the weights across all frequencies is one is calculated. This effectively establishes the average value of the transfer function amplitudes, but weighted according to the dominant frequency band of the ground motion. The results are shown on the right side of Table 2.2 in the columns under the heading "Weighted Amplitude Ratios." The results in the "data" columns are very similar to the square root of the corresponding power ratios, as expected. The ratios from theory exceed those from data for translation and are smaller for rotation, which is consistent with the aforementioned trends from Figures 2.12-2.14.

The principal findings from this data analysis are as follows:

(1) The rigid foundation models for kinematic interaction of embedded foundations produce estimates of top-of-foundation ground motions that are biased on the low side. There are a number of possible explanations for this difference, including amplification through the subterranean portion of the structure (which is affected by the mass and flexibility of those portions of the structure), effect on demand introduced to the system of foundation non-rigidity between the base and top of the foundation, possible torsional effects on the ground-level motions, and potential effects of surface waves (stronger at the ground surface than at depth).

(2) For the structures investigated here, the top-of-foundation motion estimated by the rigid foundation models are dominated by base translation; base rocking could be neglected without any significant loss of accuracy.

(3) The base rocking for very tall, long period buildings is reasonably well predicted by rigid cylinder models for kinematic interaction. Short-period buildings, such as at the Lotung site (Figure 2.6) can have much larger base rotations than what is predicted by rigid cylinder models.

2.6 SUMMARY AND CONCLUSIONS

In this chapter we have described on a schematic level how the soil-foundation-structure interaction problem for tall buildings with subterranean levels can be solved using a substructure approach (Figure 2.3). The modeling approaches used in current practice, as represented by the diagrams in Figure 2.4, fail to capture many of the key attributes of soil-structure interaction. One of the key missing attributes is the effects of kinematic interaction on the motions of embedded foundations. We review the attributes of an existing model for the reduction of translation and the introduction of kinematic rocking, and show the model to provide good results when compared to recordings from actual structures with very stiff cylindrical foundations.

Recordings from tall buildings with subterranean levels are then examined to evaluate the degree to which the foundations are truly rigid and to further test the aforementioned model. The main results of this work are summarized in the bullets above, and are not repeated here.

3 IMPACT OF FOUNDATION MODELING ON THE ACCURACY OF RESPONSE ANALYSIS OF A TALL BUILDING

3.1 INTRODUCTION

In analyzing the seismic response of a building with a basement, various approaches for modeling the base of the building can be employed. While some of these modeling approaches are very simple, others are complex and require significant effort in modeling the linear or nonlinear soil-structure interaction. What is not clear, however, is whether these more complex and time-consuming approaches actually produce substantially more accurate results.

Currently, over 180 buildings have been instrumented by California Motion Instrumentation Program (CSMIP). Out of these, about 35 have subterranean floors and records from at least one earthquake (Naeim, et al. 2005). The focus of this chapter is on the response of LA 54 story building during the 1994 Northridge earthquake (Figure 3.1). The building has four levels embedded. The site consists mainly of alluvium.

The analysis begins with the development of a three-dimensional model, which is called the "most accurate" (MA) model. The MA model includes soil-foundation-structure interaction in the vertical and horizontal directions, including rocking, with a series of no tension springs and dampers reflecting site soil properties. The MA model of the building includes the embedded portion of the building and its foundations. Seismic demands imposed on the MA model include base translation and rocking (generally from recordings) as well as kinematic loading of basement walls (simulated by displacement histories applied to the ends of horizontal springs attached to basement walls).

Using the aforementioned specification of "seismic demand," the MA model is calibrated to match the response interpreted from the recorded motions. Once the MA model successfully matches the recorded data, components of the specified seismic demand and soil-foundation-structure interaction model (i.e., portions of the MA model that are below ground), are replaced one or more at a time, with various simplifications common in practice and assess the errors induced by each simplification on estimates of various metrics of seismic response.

Many previous studies have been similar to the "MA" component of this work, in that they have developed mathematical models that replicate the recorded response of buildings (e.g., Chajes et al., 1996; Ventura et al., 2003; Kunnath et al., 2004; Liu et al., 2005). The novel aspect of the present work follows the MA model development. Those subsequent models simplify the MA model (without further calibration) so that the degree of error associated with each simplification can be evaluated. The objective

is to find the simplest models which produce results of sufficient accuracy for engineering applications.

Following this introduction, the attributes of the LA 54 story building is described. Section 3.3 describes how the robust SFSI modeling procedures described in Chapter 2 were applied to the LA54 building while Section 3.4 outlines various simplifications to that procedure that are considered here. Section 3.5 describes some challenges faced while implementing the components of the SFSI model in a conventional structural analysis software package (ETABS). Finally, Sections 3.6 and 3.7 present the results of the study and conclusions, respectively.

This chapter was previously published as a conference paper by Naeim et al. (2008). This work represents the efforts of a team of researchers at UCLA (including the author) and John A. Martin and Associates (JAMA). The contribution of the author to this work was principally in the specification of the SSI and ground motion elements of the model (Sections 3.3-3.4) and the presentation and interpretation of the results (Sections 3.6-3.7).

Figure 3.1. Los Angeles 54 story office building

3.2 DETAILS OF THE LOS ANGELES 54 STORY BUILDING

3.2.1. Structural and Foundation Systems

The building is 52 stories tall above ground level with a penthouse and a four-level basement. As shown in Figure 3.2, the building is roughly rectangular in plan with base dimensions of approximately 64.6 m. by 41.45 m, tapering inward at the 36^{th} and 46^{th} floors to 196 by 36.9 m and 176 by 36.9 m, respectively. The vertical load carrying system consists of composite concrete slabs (6.4 cm thick) over a 7.6 cm. steel metal deck with welded metal studs, supported by steel frames. The spans between gravity columns vary from about 3 m to 14.3 m. The lateral load resisting system consists of moment resisting perimeter steel frame (framed tube) with 3 m column spacing. There

are Virendeel trusses and 121.9 cm deep transfer girders at the setbacks at the 36th and 46th floors.

The foundation system consists of a reinforced concrete mat that is 2.9 m thick in load bearing areas and 2.1 m thick in intermediate areas. Concrete basement walls surround the subterranean levels.

3.2.2 Geotechnical Conditions

Geotechnical conditions at the site were characterized by LCA (1981) and are summarized by Stewart and Stewart (1997). The site exploration by LCA generally encountered 20 m of sands with variable layers of silts and clays overlying siltstone and shale bedrock, which extended to the maximum depth explored of 40 m. The shear wave velocities shown in Figure 3.3 are based on in situ downhole measurements by LCA (1981).

3.2.3 Recorded Motions

The building is instrumented with 20 accelerometers (sensors) as shown in Figure 3.2. Sensors 1 and 2 installed on the top of the mat foundation measure vertical acceleration. The earthquakes recorded at the site are from 1992 Big Bear and Landers, 1994 Northridge, 2001 Hector Mine, and 2008 Chino Hills. The Northridge earthquake produced horizontal ground motions of about 0.14 g at the site whereas horizontal accelerations produced by Big Bear, Landers, Hector Mine and Chino Hills

earthquakes were about 0.03 g, 0.04 g, 0.06 g and 0.02g, respectively. In this chapter, the Northridge recordings are focused upon.

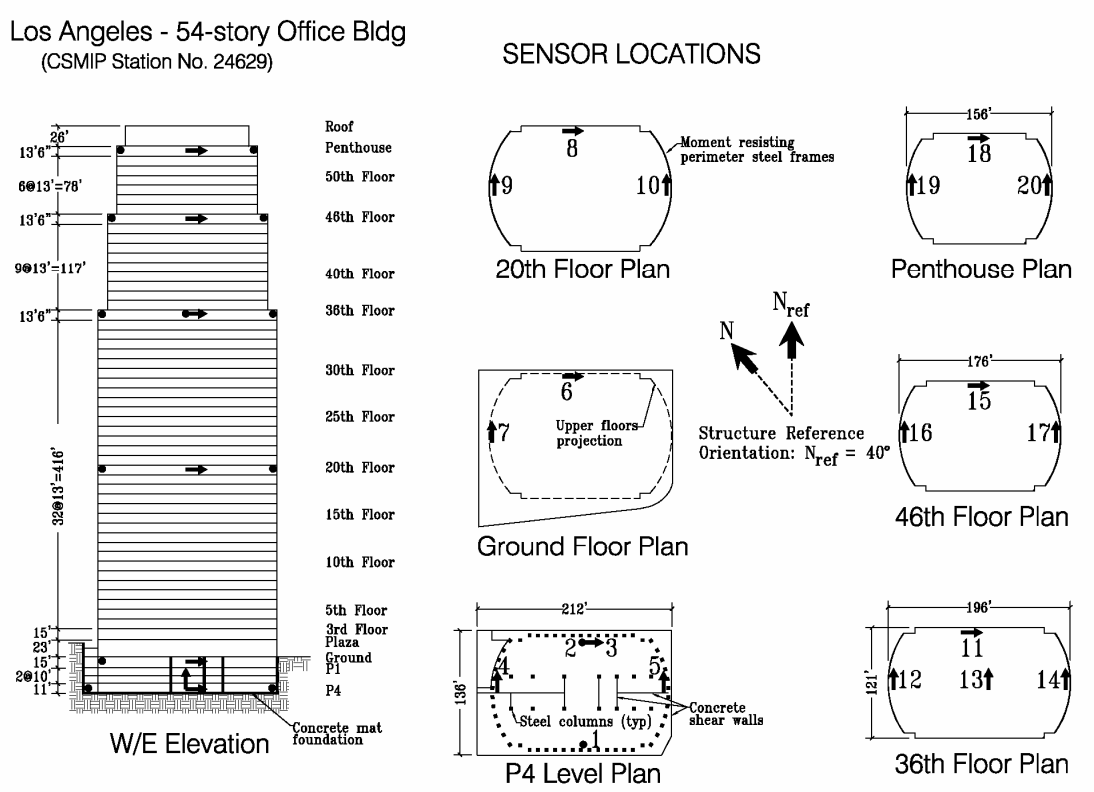

Figure 3.2. Instrumentation plan of the Los Angeles 54 Story Building

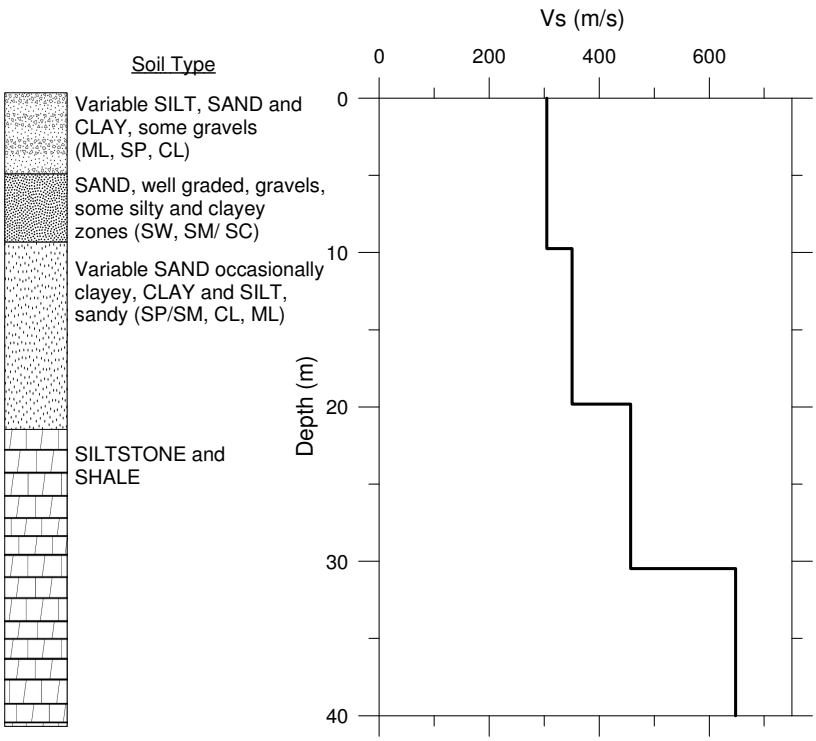

Figure 3.3. Geotechnical and shear wave velocity profile at LA 54 story building site

3.3 SOIL-FOUNDATION-STRUCTURE INTERACTION (SFSI) MODELING PROCEDURES

3.3.1 General Procedures

SFSI modeling procedures have been presented in Chapter 2. Figure 2.4 summarizes the substructure approach and is referred to throughout this chapter.

3.3.2 Application to the LA 54 Story Building

There is not a free-field instrument at the LA 54 story building, hence u_g is unknown. What is known is the horizontal translation at the base of the building and

the rotation in the short (transverse) direction of the structure (because of the two vertical instruments on the base slab).

The recorded horizontal translation provides a good estimate of u_{FIM}. In reality, the recording is also affected by inertial soil structure interaction effects, which cause the foundation base translation to differ from u_{FIM}. However, those effects are small for buildings such as the LA 54 story building with weak inertial soil-structure interaction effects. Even when they are strong, such effects are narrow-banded at the first mode system frequency (Kim and Stewart, 2003). Hence, u_{FIM} is taken as the base mat horizontal recording. Conversely, the base rotation is likely to be dominated by inertial interaction effects, so recordings are not relied upon to estimate this quantity. Instead, it is estimated based on predictions of validated theoretical models (Stewart and Tileylioglu, 2007). Those models allow the estimation of transfer functions that relate free-field motion u_g to the translational and rotational FIMs:

$$\left|H_u\right| = \frac{u_{FIM}}{u_g},\ \left|H_\theta\right| = \frac{\theta_{FIM}}{u_g} \tag{3.1}$$

where $\left|H_u\right|$ and $\left|H_\theta\right|$ are translational and rotational transfer functions (respectively) that can be evaluated as a function of frequency knowing the soil shear wave velocity and foundation dimension (see Chapter 2). Figure 3.4(a) presents these functions for the LA 54 building site using the aforementioned expressions. Given $\left|H_u\right|$ and $\left|H_\theta\right|$, base rotation can be estimated from u_{FIM} through manipulation of Eq. 3.1 to yield:

$$\theta_{FIM} = u_{FIM} \frac{|H_\theta|}{|H_u|} \tag{3.2}$$

To summarize, the translational motion applied at the end of the foundation spring attached to the base slab is u_{FIM} (taken from recordings). The vertical motions applied at the end of vertical springs are defined from the product of θ_{FIM} and horizontal distance to the foundation centroid.

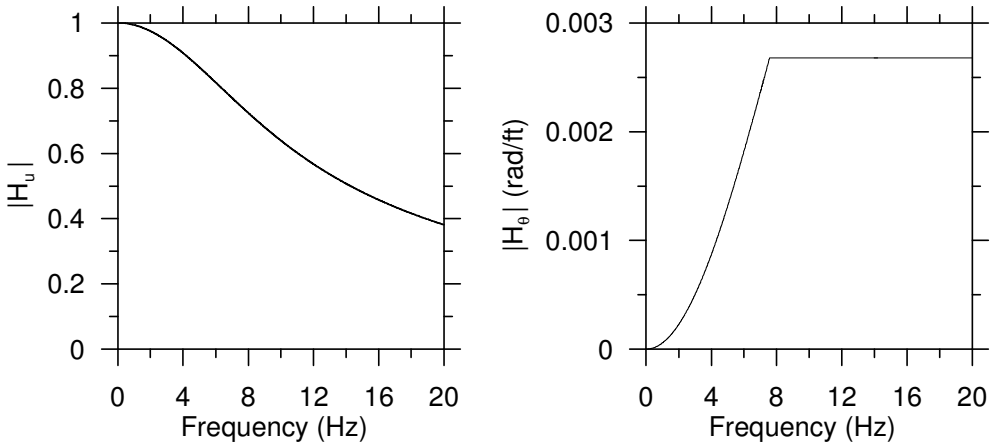

Figure 3.4(a). Theoretical transfer functions between foundation input motions and free-field motion

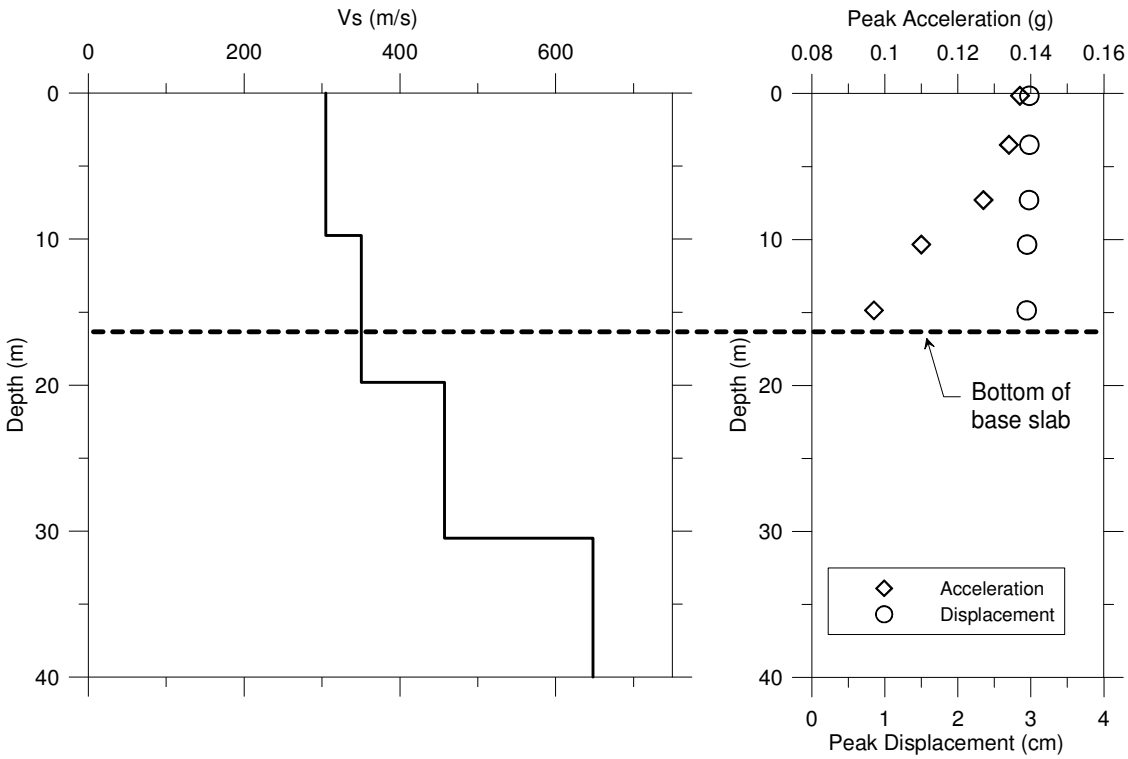

Figure 3.4(b). Variation of peak acceleration with depth at ends of foundation springs, as calculated from ground response analysis.

The remaining issue for ground motion specification is the distribution of translations over the embedment depth, as illustrated in Figure 2.3 (d). This is evaluated by performing equivalent-linear ground response analysis with the input consisting of u_{FIM} at the average foundation depth of 52 ft as an outcropping motion. Those analyses were performed with SHAKE04 (Youngs, 2004), which is a modified version of SHAKE91 (Idriss and Sun, 1992). The velocity profile is shown in Figure 3.5(b). Nonlinear modulus reduction and damping curves were used from EPRI (1993), Vucetic and Dobry (1991) and Seed and Idriss (1970) for various layers in the profile.

Figure 3.4(b) shows that the variation of ground motion over the embedment depth is minor in displacements but is significant in accelerations.

The foundation springs and dashpots are evaluated by first calculating translational (K_x, K_y) and rotational (K_{xx}, K_{yy}) stiffnesses for rectangular rigid foundations (Mylonakis et al., 2002). Dashpot coefficients (C_x, C_y, C_{xx}, C_{yy}) can be similarly evaluated using equations from Mylonakis et al. (2002). Foundation stiffnesses are shown in Figure 3.5(a) for the LA 54 story building site. For translation, the portion of the stiffness that can be attributed to the base slab is calculated using surface foundation equations in conjunction with the seismic velocities of materials below the mat. That stiffness is applied as a spring at the elevation of the foundation mat (Figure 2.3(c)). The total translational stiffness of the foundation is higher due to embedment, and the difference is applied as horizontal springs distributed along the basement walls. For rotation, vertical springs are distributed along the base of the foundation as shown in Figure 3.5(b). Higher stiffnesses are assigned at the boundaries, but the overall rotational stiffness associated with the vertical springs matches that from the impedance function. This is accomplished by ensuring that the following equalities hold:

$$K_{xx} = \sum_i k_{z,i} \cdot y_i^2$$
$$K_{yy} = \sum_i k_{z,i} \cdot x_i^2 \qquad (3.3)$$

where K_{xx} and K_{yy} = overall rotational stiffness of foundation (Figure 3.5(a)), $k_{z,i}$ = stiffness of vertical spring at location indexed by i, x_i=closest horizontal distance from spring i to the y-centroidal axis of foundation, and y_i=closest horizontal distance from spring i to the x-centroidal axis of foundation. Distances x and y are measured from the centroid as illustrated in Figure 3.5(a). The vertical stiffness values given in Figure 3.5(b) satisfy Eq. 3.3.

Both the horizontal and vertical springs are specified as "compression-only," meaning that no tension is allowed to develop. This allows a gap to form, although the implementation does not track gap width.

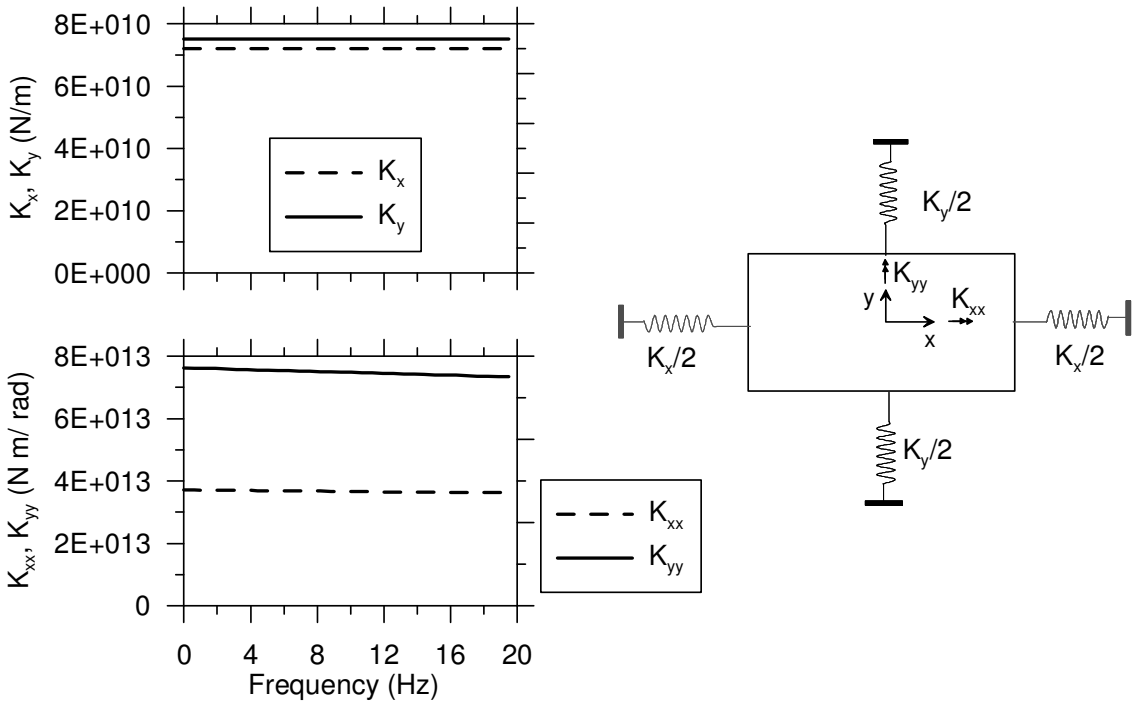

Figure 3.5(a) Foundation impedance functions (stiffness portion) for overall foundation system

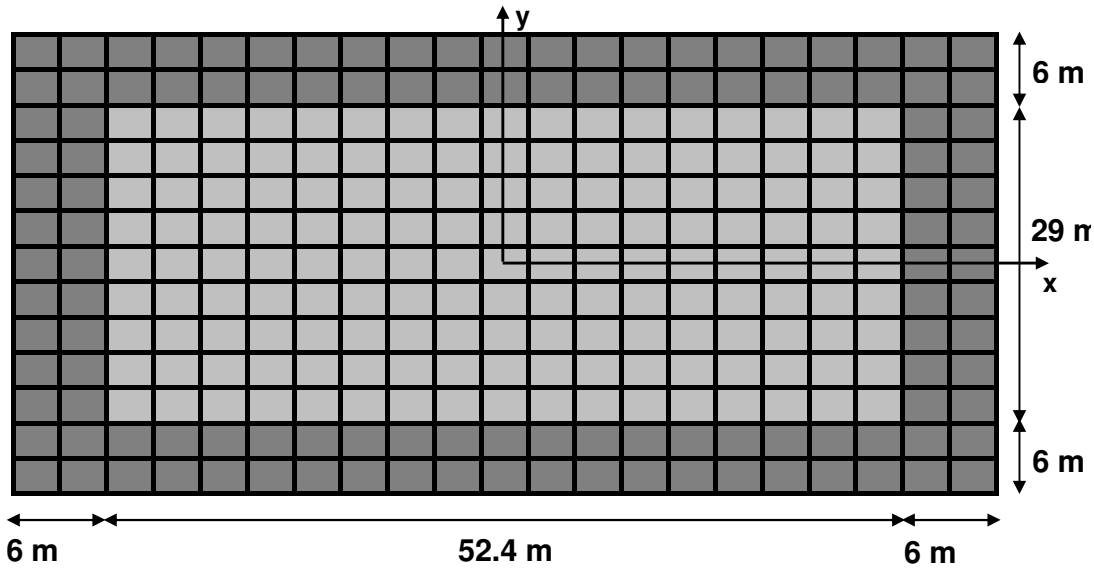

	k_z (N/m)	c_z (N.s/m)
	3.50E+09	9.50E+07
	8.70E+08	2.40E+07

Figure 3.5(b). Distribution of vertical foundation springs and dashpots across base slab

3.4. SIMPLIFICATIONS TO SFSI MODELING CONSIDERED IN PRESENT STUDY

The simplifications to the MA model fall into three categories, as illustrated in detail in Table 3.1:

Model 1: Replacement of compliant foundation structural elements (i.e., base slab and basement walls) representing actual cracked section properties with rigid elements.

Models 2a-c: Modification of the seismic demand to remove various aspects of the kinematic response and depth-variable ground motions.

Models 3a-d: Modification (or removal) of foundation springs.

Table 3.1 Summary of the properties of the MA model and the simplified models considered

Model	Compliant Found. Elements	Seismic Demand			Soil Flexibility				
		Kinematic base rocking ($\theta_{FIM} \neq 0$)	Depth variant ground motion	Kinematic base translation ($u_{FIM} \neq u_g$)	No-tension springs	H & V springs at base slab	H springs on basement walls	Ignore soil; fix structure at base slab level	Ignore soil; fix structure at ground surface
MA	●	●	●	●	●	●	●		
1		●	●	●	●	●	●		
2a	●		●	●	●	●	●		
2b	●	●		●	●	●	●		
2c	●		●		●	●	●		
3a	●	●	●	●		●	●		
3b	●						●		
3c								●	
3d									●

Details of the specific modifications to the MA model are explained in the following:

1. The embedded portion of the building is assumed to be rigid. The specification of seismic demand is not modified. The objective here is to specifically investigate the effects of compliance in structural elements below ground line.

2. Change the manner in which seismic demand is specified. Three deviations from the MA model are investigated:

a. Ignore the effect of base rocking in the specification of seismic demand (note that rocking from inertial interaction is still allowed; essentially the ends of the vertical springs on the base slab are not provided with excitations compatible with the rocking that would normally be expected from kinematic interaction).

b. Ignore the effect of kinematic loading of basement walls associated with depth-variable displacement histories applied to the ends of horizontal foundation springs. Essentially, this analysis deviates from the MA model only by fixing the ends of the horizontal springs attached to the basement walls.

c. Neglect kinematic interaction altogether by replacing the recorded motions at the base of the building by equivalent free-field motions (u_g calculated from u_{FIM} using Eq. 3.1 and Fig 2.3(a); rotation taken as zero).

3. Change the manner in which soil flexibility is modeled. Specifically, the following are investigated:

   a. Allowing springs to develop tension (removal of no-tension interface elements).

   b. Neglect entirely soil flexibility at the level of the base slab (i.e., the base

slab is fixed vertically and horizontally), and simulate soil flexibility along the basement walls with horizontal springs with ends fixed to match the free-field ground motion. Seismic demand consists only of horizontal motions (equivalent free-field condition) at the base slab level and at the ends of foundation springs. This simulates a condition commonly used in structural design offices.

c. Same as 3(b), except soil flexibility along basement walls is neglected (no soil springs). In this model, the height of the structure is effectively lengthened by the embedment depth and the model is fixed at the level of the base slab. This simulates another condition commonly used in some structural design offices.

d. The below ground portion of the building is ignored and the superstructure is assumed to be fixed at the ground level. Seismic demand consists only of horizontal motions (equivalent free-field condition) applied at ground level. This is the third (and final) condition commonly used in some structural design offices.

3.5 IMPLEMENTATION

Several computing platforms for conducting SFSI analyses were considered. Since the objective was to produce modeling recommendations suitable for adaptation by design offices, a software system that is most commonly used for dynamic structural

analysis of buildings by reputable firms was utilized. Therefore, the ETABS computer program (Computers and Structures, 2008) was used for this study. Use of more powerful software such as OpenSees (PEER, 2008) may have reduced the troubles encountered, but would not have produced recommendations that were directly applicable to a design office environment. The main implementation problem was the lack of integration in the computer program. The implementation issues encountered are given in more detail in Naeim et al. (2008).

3.6 RESULTS

3.6.1 Results for the MA Model

The best match of MA model to recordings was obtained with all modal damping values set to 1.0% of critical except for modes 1 and 4 where the damping values were set to 1.8%. The same damping values were used for all approximations. A summary of 50 Ritz vectors provided a level of accuracy that did not improve by inclusion of more vectors (up to 300 Ritz vectors were utilized to see if there is any significant difference in the results). As indicated by Table 3.2 all five computed periods are very close to those identified from recorded data using the CSMIP-3DV software (Naeim et al. 2005; 2006). A summary of the first five periods associated with Ritz vectors for various models is presented in Table 3.3

Table 3.2 Comparison of MA model periods and those obtained from system identification

Direction	Identified Periods (sec.)		MA Model Periods (sec.)	
	Mode 1	Mode 2	Mode 1	Mode 2
E-W	6.07	1.95	6.06	1.92
N-S	5.12	1.86	5.18	1.81
Torsional	2.78		2.76	

Table 3.3. Summary of periods associated with the first five Ritz vectors for various models.

Model	Reported vibration periods for first five Ritz vectors (sec.)				
	1	2	3	4	5
MA*	6.06	5.18	2.76	1.92	1.81
1	6.03	5.15	2.75	1.91	1.81
2A	6.06	5.18	2.76	1.92	1.81
2B	6.06	5.18	2.76	1.92	1.81
2C	6.06	5.18	2.76	1.92	1.81
3A	6.04	5.18	2.78	1.92	1.82
3B	5.79	4.99	2.76	1.92	1.82
3C	5.79	4.99	2.76	1.92	1.82
3D	5.63	4.90	2.74	1.89	1.80

Displacement histories obtained from the calibrated MA model are compared to recordings in Figure 3.6. The match in both horizontal directions at the ground level is also virtually perfect (Figures 3.6(f) and 3.6(g)). Elsewhere over the height of the building the quality of the match is generally better in the E-W direction than in the N-S direction. However, the matching of both maximum amplitudes and phasing are very good in both directions. At the foundation level, Figure 3.6(h) shows that the base rocking produced by the model matches very well with observation, suggesting that the

rotational foundation impedance is well represented by the MA model. However, this base rocking is a small contributor to the roof translation, as shown in Figure 3.6(i).

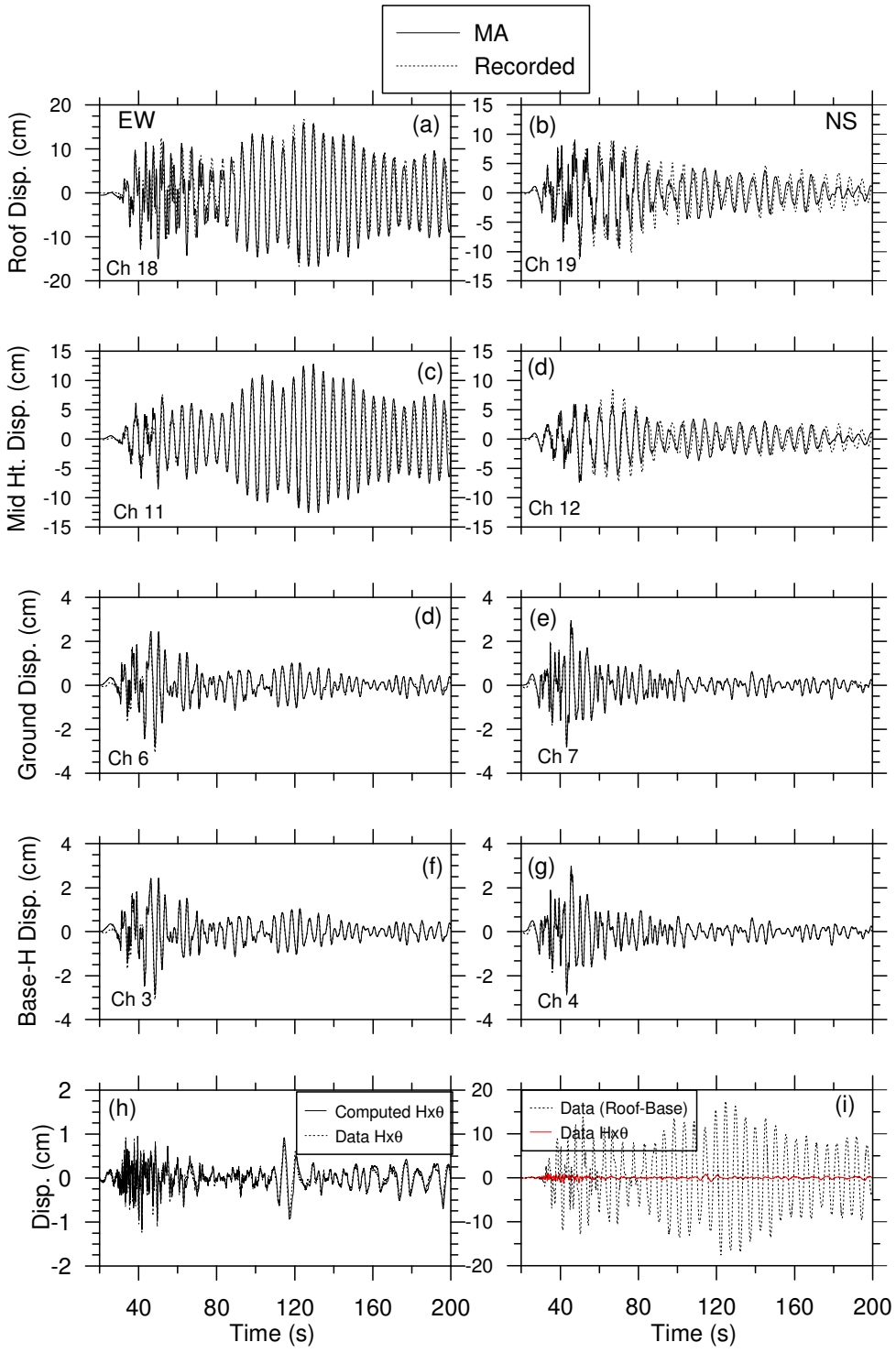

Figure 3.6 Comparison of recorded displacements with those computed for the MA model

3.6.2 Results for selected approximations

The analyses of the models that are simplified relative to MA are presented relative to the MA results instead of the recordings. This allows for a direct evaluation of the impact of changes in model attributes.

Allowing tension in the soil with no other changes (Model 3A) does not affect the results by much. Table 3.3 shows that the building vibration periods are very slightly affected and Figure 3.7 shows the errors induced in displacement history response throughout the height are negligible (e.g., less than 4% at roof level). As illustrated in Figure 3.7(g) and 3.7(h), error in maximum story drift ratios for floors above ground level are less than 10% and 5% in the E-W and N-S directions, respectively. The error in the maximum interstory drift ratios for subterranean floors are significantly larger at about 32% in the E-W direction and 46% in the N-S direction.

Ignoring the subterranean levels by assuming a rigid base at ground level (Model 3D) significantly alters the vibration periods of the building (see Table 3.3). As a result, many of the displacement history responses are out of phase with those of obtained for the MA model. The roof peak displacement in the E-W direction for the MA and 3D models while having similar amplitude occurs at very different times during the response. The error in peak roof displacement is less than 20%. Interestingly, the distribution of interstory drifts over the height of the structure is also significantly affected, with drifts increasing at lower levels and decreasing at higher levels of the building for Model 3D relative to MA.

Fixing the far ends of horizontal soil springs, and subjecting these fixed ends to free-field ground accelerations (Model 3B) is one of the two common methods used by engineering offices to bound the SFSI problem. As shown in Table 3.3, this approximation also significantly affects the dynamic characteristics of the model by shortening its period because the fixed-end springs provide more resistance to the below-ground structure. Note that in this model the ground accelerations are used as input and ETABS does not calculate the displacements at the fixed ends of the horizontal springs. Therefore, the displacements reported at the ground line consist only of the in-plane displacements of the ground floor diaphragm which are very small. The peak roof displacement in the E-W direction happens to be close to twice of the MA model.

Ignoring the embedment effect by running the structure down to the foundation level and ignoring the horizontal stiffness of the surrounding soil is another common assumption that is used in design offices to bound the SFSI problem (Model 3C). Many engineers will be surprised to see that the 3C model is stiffer and has a shorter fundamental period than the MA model (Table 3.3). As shown in Figure 3.8 (c)-(d), the displacement time histories at the ground floor for the 3C and MA model are virtually identical. The error in maximum roof displacement is small at less than 5% and 10% in E-W and N-S directions. Figure 3.8 (g)-(h) shows that as with Model 3D, Model 3C story drift ratios increase relative to MA at lower levels of the building, although this effect is principally in the E-W direction.

If all MA model characteristics are retained but foundation structural elements (i.e., mat and basement walls) are assumed to be rigid (Model 1), building periods are practically unaffected, as shown in Table 3.3. The displacement histories at the ground floor for the 1 and MA model are virtually identical. The frequency match with the MA model results for the displacement histories are good throughout the height of the building. However, Model 1 overestimates the displacements of the upper portions of the building in the E-W direction in the first one-third of the response duration where the peak displacement in this direction occurs resulting in an overestimation of the maximum roof displacement in this direction by about 25%. In the N-S direction, the reverse occurs. That is, the displacement amplitudes in the early part of the response where peak displacement occurs is very close to those obtained from the MA model but in the later part of the response Model 1 underestimates the amplitude of displacements. As a result, the maximum story displacements in the N-S direction are much closer to the values reported by the MA model. The maximum error for displacements in this direction is less than 8%. The maximum error in interstory drifts in the E-W direction occurs at the 22^{nd} floor and is about 28%. The maximum interstory drift errors at above ground floors in the N-S direction are significantly smaller at less than 5%. However, the same error in the subterranean levels in the N-S direction is significantly larger in the N-S direction compared to the E-W direction (65% compared to 20%).

Elimination of kinematic base rocking with no other changes (Model 2A) has negligible effect on the vibration periods of the building (Table 3.3). Moreover, as

shown in Figure 3.9, the maximum displacements and interstory drifts throughout the height of the building, with the exception of subterranean drifts, are almost identical.

Eliminating kinematic loading from relative soil displacements adjacent to basement walls (Model 2B) virtually affects nothing as the displacement and inter-story drift histories and maximum values are nearly identical to those obtained from the MA model (Figure 3.10).

Finally, ignoring kinematic interaction effects on the base horizontal motion (Model 2C) produces results which are virtually identical to the MA model at all floor above the ground level (Figure 3.11). However, use of Model 2C results in significant underestimating of maximum interstory drifts in the subterranean levels (Figures 3.11(g) and 3.11(h)).

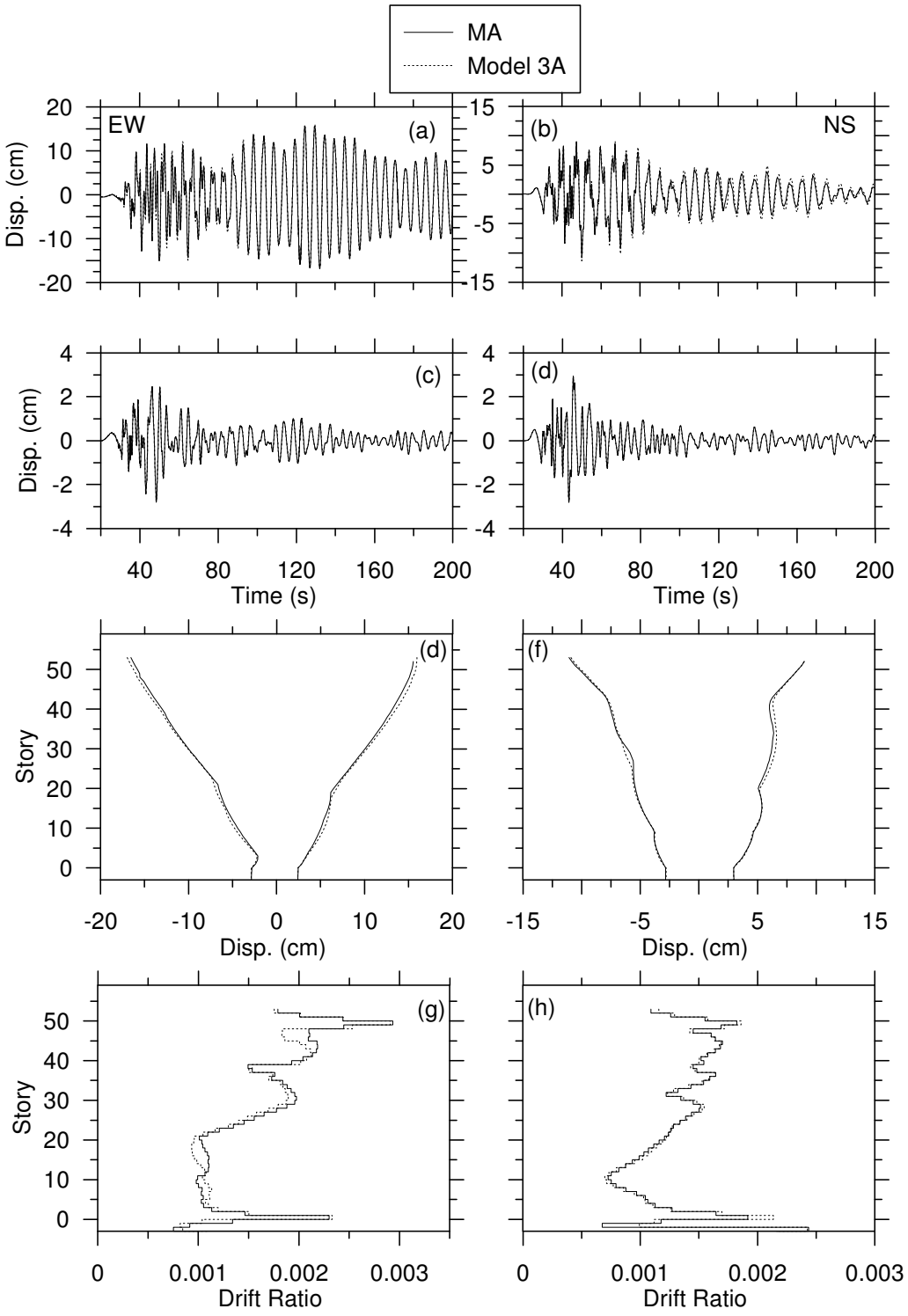

Figure 3.7 Comparison of displacement histories obtained from the MA and 3A models

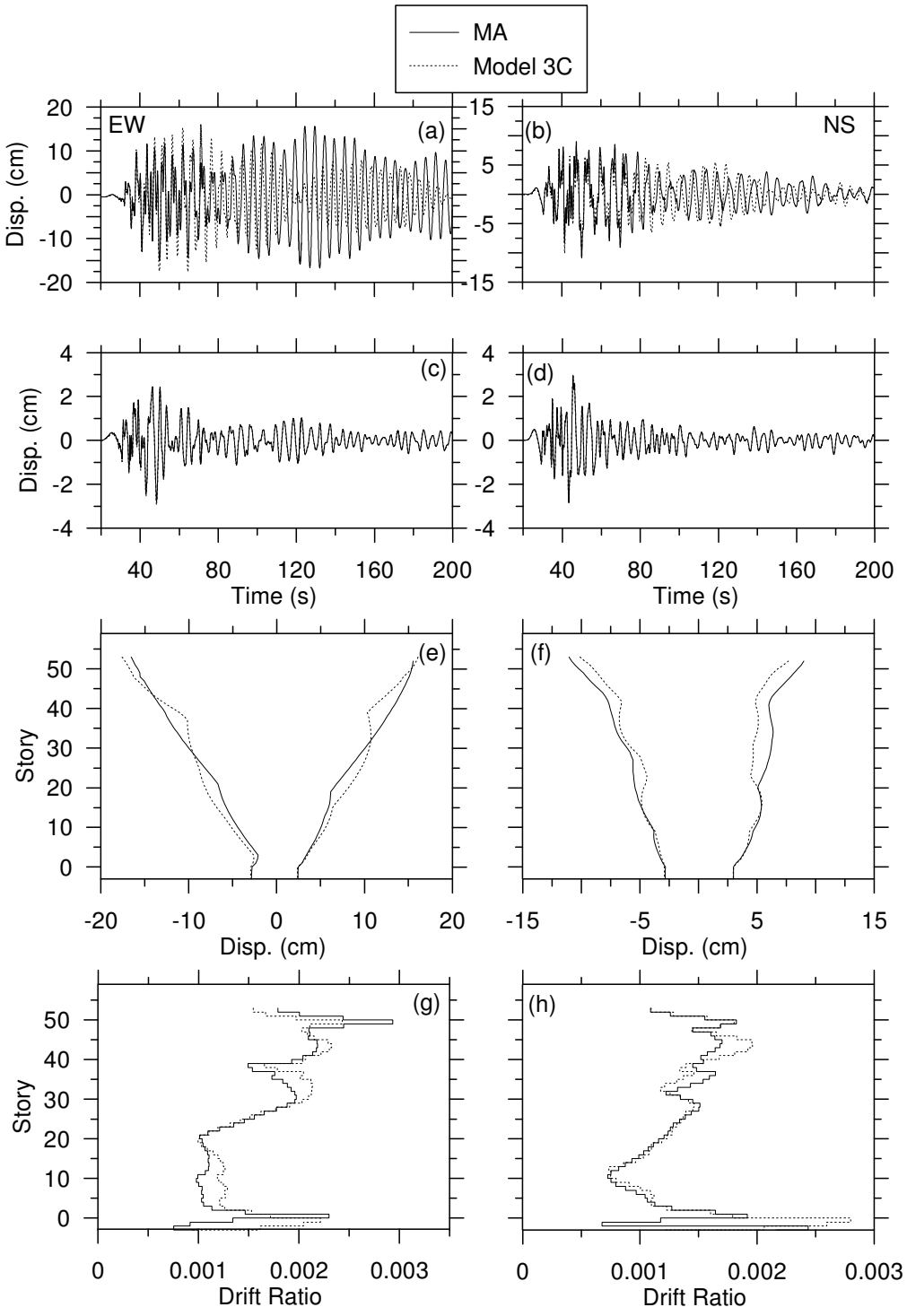

Figure 3.8. Comparison of displacement histories obtained from the MA and 3 models

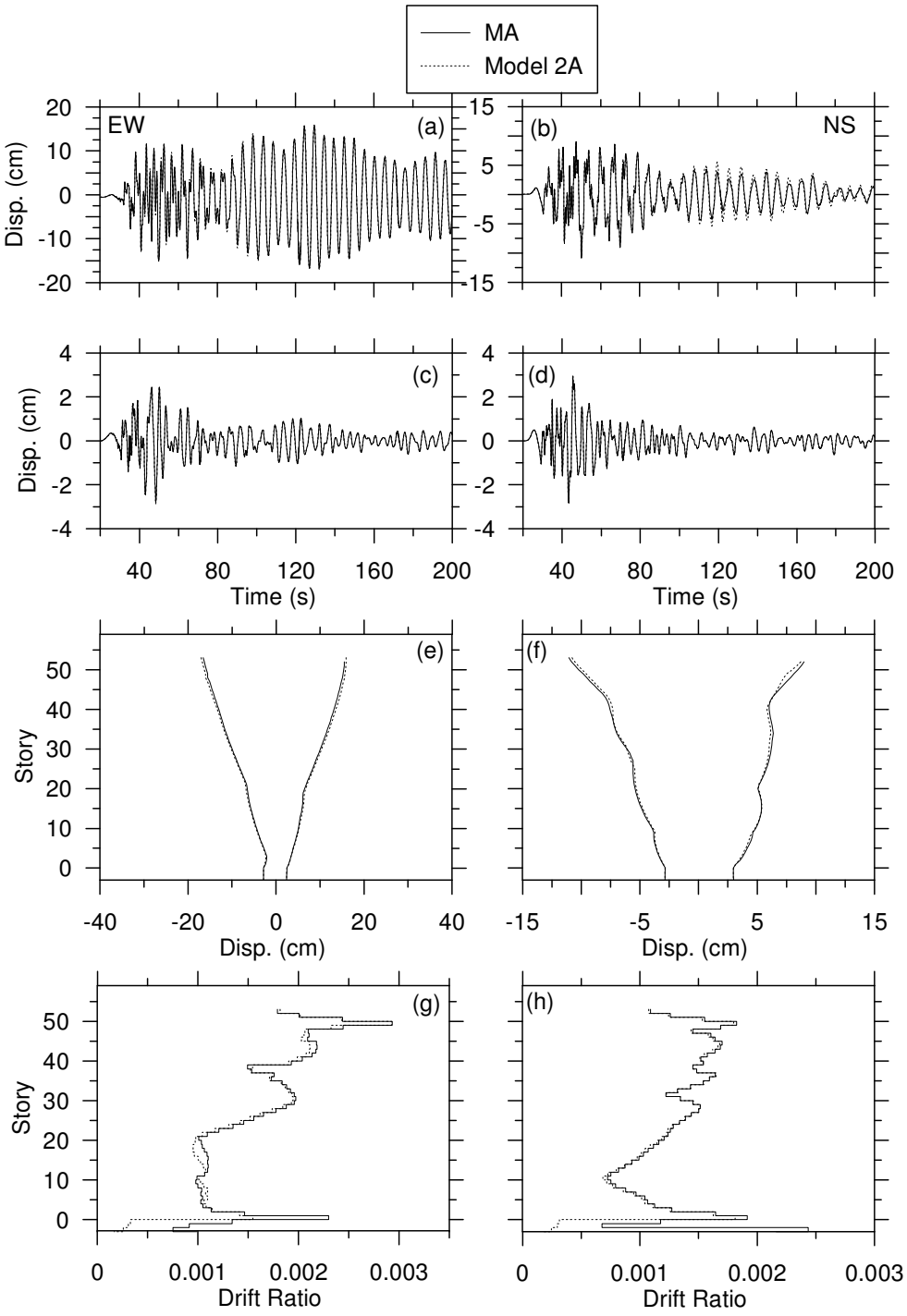

Figure 3.9 Comparison of displacement histories obtained from the MA and 2A models

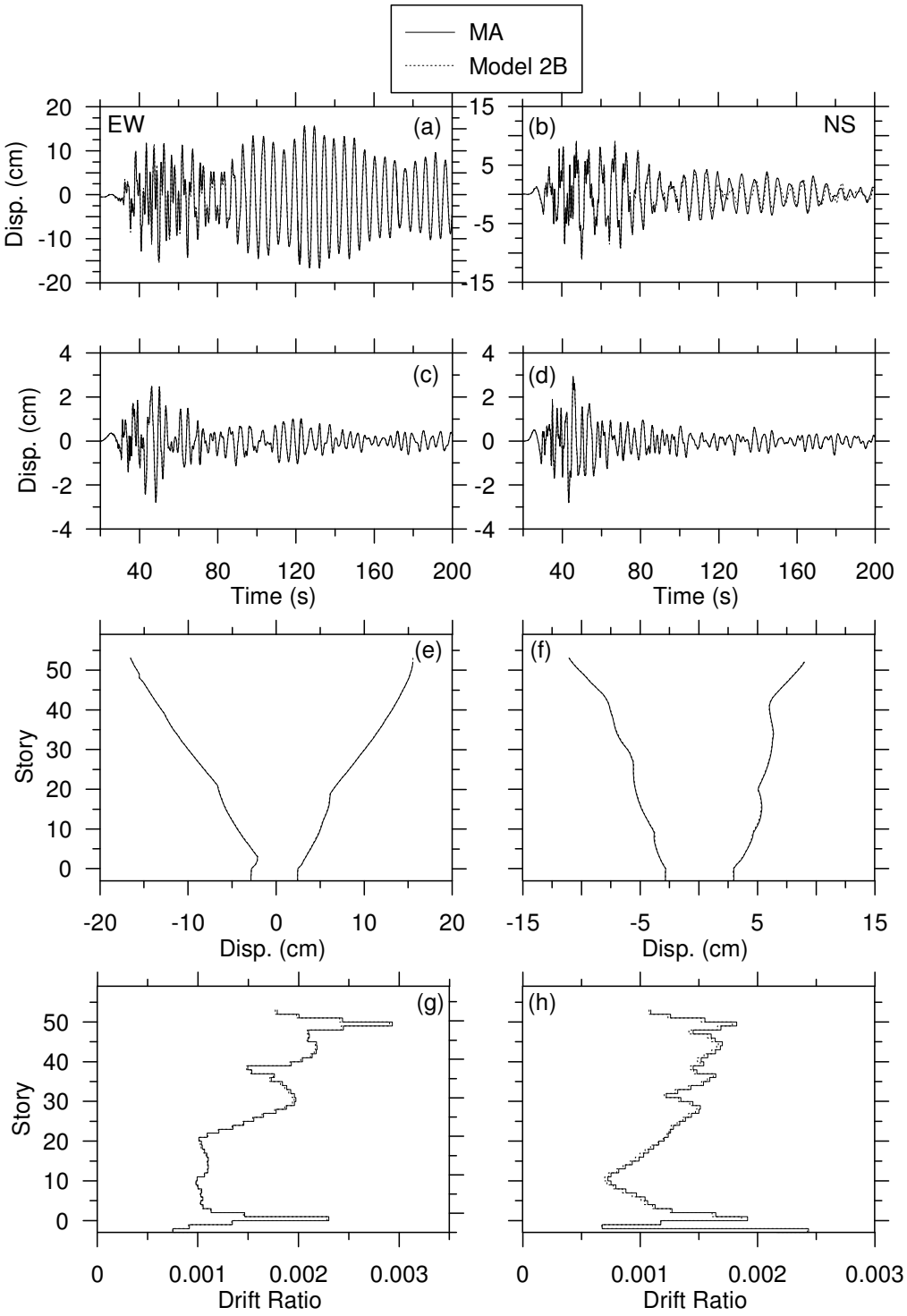

Figure 3.10 Comparison of displacement histories obtained from the MA and 2B models

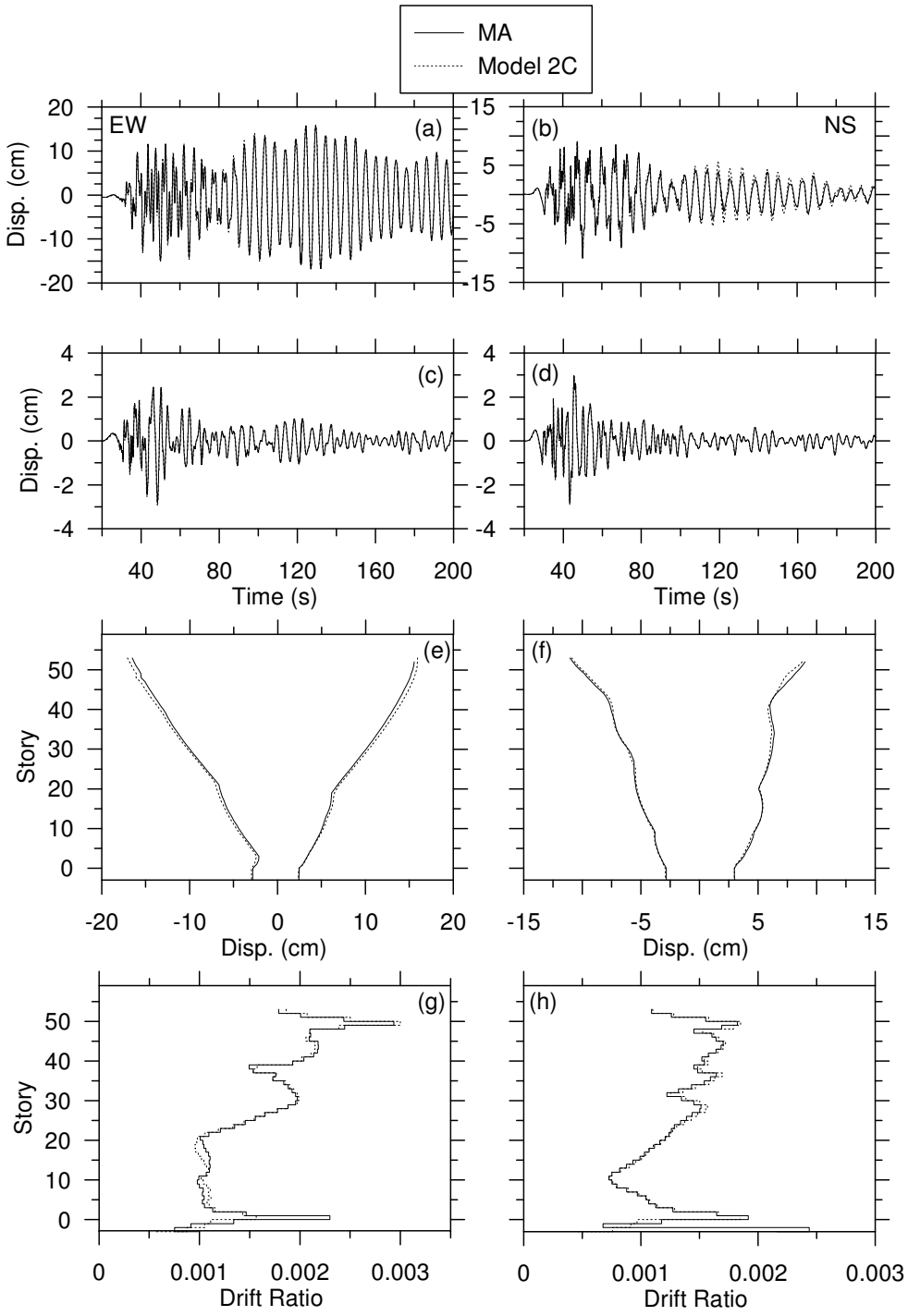

Figure 3.11 Comparison of displacement histories obtained from the MA and 2C models

3.7 SUMMARY AND CONCLUSIONS

Soil-structure interaction can affect the response of buildings with subterranean levels by modifying the characteristics of input motions relative to those in the free-field and through the added system compliance associated with relative foundation/free-field translation and rocking. While procedures are available to account for these effects, they are seldom utilized in engineering practice. The objective is to examine the importance of these effects on the seismic response of a 54 story building with four subterranean levels. First, a "most accurate" (MA) model that accounts for kinematic interaction effects on input motions, depth-variable ground motions along basement walls, compliant structural foundation elements, and soil flexibility and damping associated with translational and rocking foundation deformation modes is generated.

With reasonable tuning of superstructure damping, the MA model accurately reproduces the observed response to the 1994 Northridge earthquake. While the MA modeling exercise was ultimately successful, the process highlighted several major hurdles to the implementation of soil-structure interaction effects in practice for these types of structures. The principal implementation problems are lack of a direct integration scheme in ETABS and existence of nonphysical acceleration spikes in the acceleration results.

Selected components of the MA model were removed one-by-one to test their impact on building response. Factors found to generally have a modest effect on building response above ground level include compliance of structural foundation

elements, kinematic interaction effects (on translation or rocking), and depth-variable ground motions applied to the ends of horizontal soil springs/dashpots. However, those factors did generally affect below-ground response as measured by interstory drift.

Properly accounting for foundation/soil deformations does not significantly affect vibration periods for this tall building (which is expected), but does impact significantly the distribution of inter-story drifts over the height of the structure. To the best of my knowledge, the latter observation is new to this study.

The exclusion of kinematic effects on base rocking and translation do not change the vibration periods of the building or interstory drifts above ground. However, kinematic interaction does significantly affect below-ground drifts. Hence, to accurately characterize the demand in subterranean levels, kinematic interaction effects should be considered. Exclusion of depth variable ground motions did not significantly affect below-ground or above-ground response for this building.

Two approximations commonly used in practice are shown to provide poor results: (1) fixing the structure at ground line with input consisting of free-field translation and (2) fixing the structure at the base level, applying free-field motions as input at the base level, and using horizontal foundation springs along basement walls with their end condition fixed to the free-field ground motion.

4 PARAMETRIC SYSTEM IDENTIFICATION OF MODAL PROPERTIES OF STRUCTURES FROM FORCED VIBRATION TESTS

4.1 INTRODUCTION

The objective of system identification is to evaluate the unknown properties of a system using a known input into, and output from, that system. For applications to buildings, system identification can be used to estimate modal frequencies, damping ratios, mode shapes, and participation factors (Safak, 1991). Depending on the selected input-output motions, modal vibration parameters can be identified that describe the behavior of the structure alone (i.e. fixed-base parameters) and the soil-foundation-structure system (i.e. flexible-base parameters). Fundamental-mode frequencies and damping ratios can be distinct for the two base fixity conditions. The differences, such as the ratio of flexible/fixed base fundamental mode periods, are a useful quantification of Soil-Structure Interaction (SSI) effects.

For a given input-output motion pair, system identification can be performed in two general ways. Non-parametric system identification procedures estimate the ratio

of output/input motions in the frequency domain without fitting an underlying model (Ljung, 1987 and Pandit, 1991). The locations of peaks are used to identify modal periods and the width and height of peaks can be used to estimate damping (Chopra, 2007). Parametric system identification (PSI) procedures fit a model to data in the discrete time domain (Safak, 1991). After transforming to the Laplace domain, a transfer function can be evaluated that represents the ratio of output/input motions. Modal periods and damping ratios are related the position of "poles" (i.e., peaks) in the transfer function ((Safak, 1991, Stewart et. al, 1999). The emphasis of the present work is on parametric system identification procedures.

For the case of earthquake excitation, Stewart and Fenves (1998) derived the input and output data pairs required to evaluate fixed- and flexible-base modal parameters. The system considered is depicted in Figure 4.1(a) and the input-output pairs are listed in Table 4.1. Note that differences between the input-output motions correspond to flexibilities in the identified system. For example, for the fixed-based case the only difference between the input and output motions is the lateral deflection of the structure itself, whereas for the flexible-base case the difference also includes the foundation translation and the contribution of foundation rocking to roof translation.

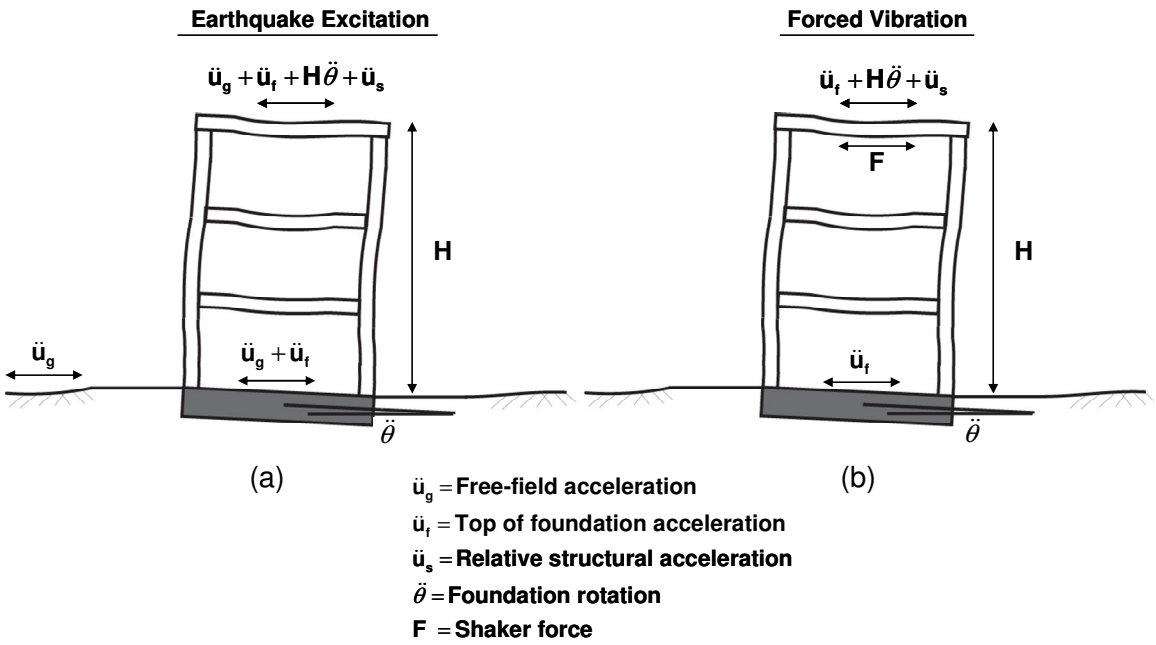

Figure 4.1. Recordings required for parametric system id with (a) Earthquake excitation (Stewart et.al (1998) and (b) Forced vibration (this study)

Table4.1 Input and output pairs from earthquake excitations for various base fixity conditions (Stewart, J.P. (1998))

Base Fixity	Input	Output
Flexible -Base	u_g	$u_g+u_f+H\theta+u_s$
Pseudo Flexible -Base	u_g+u_f	$u_g+u_f+H\theta+u_s$
Fixed- Base	$u_g+u_f+H\theta$	$u_g+u_f+H\theta+u_s$

For many practical situations it is desirable to estimate modal parameters based on controlled experiments rather than wait for earthquake excitation. In this study, I consider the case of excitation imposed by a shaker mounted on the roof of a structure, as depicted in Figure 1b. I evaluate the input and output pairs required to estimate fixed- base and flexible-base modal properties for this configuration. The results are

verified by performing system identification for a system with known properties. The procedure is demonstrated by evaluating modal vibration parameters for a test structure in Garner Valley, California using data from forced vibration tests. Those results are compared to identified modal parameters from earthquake excitation for the same structure.

4.2. SOLUTION OF EQUATION OF MOTION IN THE LAPLACE DOMAIN

I begin by deriving the solution of the equation of motion in the Laplace domain for a multi degree-of-freedom system subject to forced vibration at the roof level. The derivation presented here is similar to that in Stewart and Fenves (1998), but differs in that the excitation consists of forced vibration in lieu of earthquake excitation. For simplicity, a fixed-base system is considered first, which is subsequently extended to incorporate foundation compliance. As shown in Figure 4.2, the linear structure consists of n degrees of freedom having a mass matrix **m**, a stiffness matrix **k** and a damping matrix **c** of classical form (i.e. the damping does not couple modal responses). While modal damping can be coupled in actual structures, the classical damping assumed here is appropriate for simplified system response analyses.

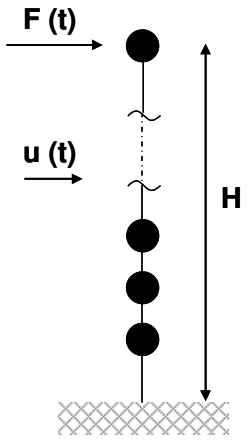

Figure 4.2. Linear lumped mass structure (fixed base) with shaker force F applied on top

The relative displacements of the n degrees-of-freedom in the structure relative to the base are described by an $n\times1$ vector $\mathbf{u}$, with corresponding velocity and acceleration vectors $\dot{\mathbf{u}}$ and $\ddot{\mathbf{u}}$, respectively. The well-known equation of motion of the superstructure is (Chopra, 2007):

$$\mathbf{m}\ddot{\mathbf{u}}(t)+\mathbf{c}\dot{\mathbf{u}}(t)+\mathbf{k}\mathbf{u}(t)=F(t)\mathbf{1} \tag{4.1}$$

where $\mathbf{1}=(0,0,0,.....1)^T$.

Equation (4.1) can be solved by superposition of vibration modes such that:

$$\mathbf{u}(t)\approx\sum_{j=1}^{J}\boldsymbol{\varphi}_j q_j(t) \tag{4.2}$$

where $q_j(t)$ is the generalized coordinate for mode j, $\boldsymbol{\varphi}_j$ is the $n\times1$ mode shape for mode j, and J is the number of modes considered in the analysis ($J < n$). The approximation results from the use of a subset of modes.

Equation (4.2) and its derivatives can be inserted into equation (4.1), followed by pre-multiplication by $\boldsymbol{\varphi}_i^T$, to yield:

$$\sum_{j=1}^{J} \boldsymbol{\varphi}_i^T \mathbf{m} \boldsymbol{\varphi}_j \ddot{q}_j(t) + \sum_{j=1}^{J} \boldsymbol{\varphi}_i^T \mathbf{c} \boldsymbol{\varphi}_j \dot{q}_j(t) + \sum_{j=1}^{J} \boldsymbol{\varphi}_i^T \mathbf{k} \boldsymbol{\varphi}_j q_j(t) = F(t) \boldsymbol{\varphi}_i^T \mathbf{1} \tag{4.3}$$

Assuming orthogonality of modes, the expressions in the sums are only non-zero for *i=j*, and hence, equation (4.3) simplifies to

$$m_j^* \ddot{q}(t) + c_j^* \dot{q}(t) + k_j^* q(t) = F(t) \boldsymbol{\varphi}_j^T \mathbf{1} \tag{4.4}$$

where $m_j^* = \boldsymbol{\varphi}_\mathbf{j}^\mathbf{T} \mathbf{m} \boldsymbol{\varphi}_\mathbf{j}$ is the modal mass for mode *j* and c_j^* and k_j^* are similarly defined as modal damping and stiffness, respectively. Invoking the familiar expressions for modal frequency ($\omega_j = \sqrt{k_j^* / m_j^*}$) and fraction of critical damping ($\zeta_j = c_j^* / \left(2\omega_j m_j^*\right)$), and dividing equation (4.4) by m_j^*, we obtain

$$\ddot{q}(t) + 2\zeta_j \omega_j \dot{q}(t) + \omega_j^2 q(t) = \frac{F(t) \boldsymbol{\varphi}_j^T \mathbf{1}}{m_j^*} \tag{4.5}$$

Equation (4.5) can be converted from the time domain to the Laplace domain using the Laplace transform $g(t) = \hat{g}(s) e^{st}$, in which *s* is the Laplace operator:

$$s^2 \hat{q} + 2\zeta_j \omega_j s \hat{q} + \omega_j{}^2 \hat{q} = \frac{\hat{F} \boldsymbol{\varphi}_j^T \mathbf{1}}{m_j^*} \tag{4.6}$$

Generalized coordinate $\hat{q} = \hat{q}(s)$ can then be written as:

$$\hat{q} = \frac{1}{s^2 + 2\zeta_j \omega_j s + \omega_j^2} \frac{\hat{F}\boldsymbol{\varphi}_j^T \mathbf{1}}{m_j^*} \tag{4.7}$$

Entering equation (4.7) into (4.2) (after transformation of (4.2) to Laplace domain) gives:

$$\hat{\mathbf{u}} \approx \hat{F} \sum_{j=1}^{J} \boldsymbol{\varphi}_j \boldsymbol{\varphi}_j^T \mathbf{1} \frac{1}{s^2 + 2\zeta_j \omega_j s + \omega_j^2} \frac{1}{m_j^*} \tag{4.8}$$

Because parametric system identification estimates a transfer function between a known input and output, I seek to re-write equation (4.8) in the form of a transfer function. Taking the shaker force as input, transfer functions for each structural degree-of-freedom can be defined as:

$$\hat{\mathbf{H}}(s) \equiv \frac{\hat{\ddot{\mathbf{u}}}}{\hat{F}} \tag{4.9}$$

where $\hat{\mathbf{H}}$ is an $n \times 1$ vector of transfer functions. Recognizing that $\hat{\ddot{\mathbf{u}}} = s^2 \hat{\mathbf{u}}$, equation (4.9) can be re-written by substituting $\hat{\mathbf{u}}$ from equation (4.8),

$$\hat{\mathbf{H}}(s) = \sum_{j=1}^{J} \boldsymbol{\varphi}_j \boldsymbol{\varphi}_j^T \mathbf{1} \frac{\hat{H}_j}{m_j^*} \tag{4.10}$$

where

$$\hat{H}_j = \frac{s^2}{s^2 + 2\zeta_j \omega_j s + \omega_j^2} \tag{4.11}$$

Different recording locations within a structure exhibit the same poles, so generally it is adequate to consider only the output at the roof for identifying parameters for the lower, most significant modes. Hence, we use single-output system identification analysis, as done previously for the case of earthquake excitation

(Stewart and Fenves, (1998)). This reduces the vector $\hat{\mathbf{H}}$ to a scalar function for the roof response. It should be noted that contributions from all *J* modes are represented in the single-output solution.

The amplitude of a particular component of $\hat{\mathbf{H}}$ is a continuous surface with peaks (also known as poles) for each mode that occur at a position on the horizontal plane which can be related to modal frequencies and damping ratios. When a component of $\hat{\mathbf{H}}$ is evaluated along the imaginary axis, the transmissibility function H(iω) is obtained, which gives the ratio of output-to-input motion as a function of frequency ω. The roof component of $\hat{\mathbf{H}}$ for the Garner Valley structure is presented subsequently.

The transfer function $\hat{\mathbf{H}}$ can be evaluated from motions recorded during a forced vibration test at suitable input and output points (discussed in the following section) using parametric system identification procedures. Those procedures are described elsewhere (Safak, 1991, Stewart and Fenves, 1998), but the essential feature for the present work is that the fitting of the parametric model to the data is performed so as to minimize the error between the model output and the measured output over the full duration (in the time domain) of the signal. This is referred to as the *Cumulative Prediction Error Method* by Safak, E. (1991).

The roots of the denominator of equation (4.11) are the poles of $H_j(s)$. Accordingly, the poles are located as follows:

$$s_j, s_j^* = -\zeta_j \omega_j \pm i\omega_j \sqrt{1-\zeta_j^2} \tag{4.12}$$

from which the modal frequencies and damping ratios can be computed as:

$$\omega_j = \sqrt{s_j s_j^*}$$

$$\zeta_j = -\frac{\mathrm{Re}(s_j)}{\omega_j} \tag{4.13}$$

4.3. EVALUATION OF SSI EFFECTS THROUGH TRANSFER FUNCTION

The simple model in Figure 4.3 is considered to derive the input-output pairs for fixed- and flexible-base conditions. The intent is to use those motion pairs with the parametric system identification methods described in Section 4.2 to evaluate modal parameters for the two cases of base fixity. The compliance of the soil is modeled through springs that enable foundation translation (u_f) and rotation (θ_f). Deformation of degree of freedom i in the structure relative to the translated and rotated foundation is denoted u_{si}.

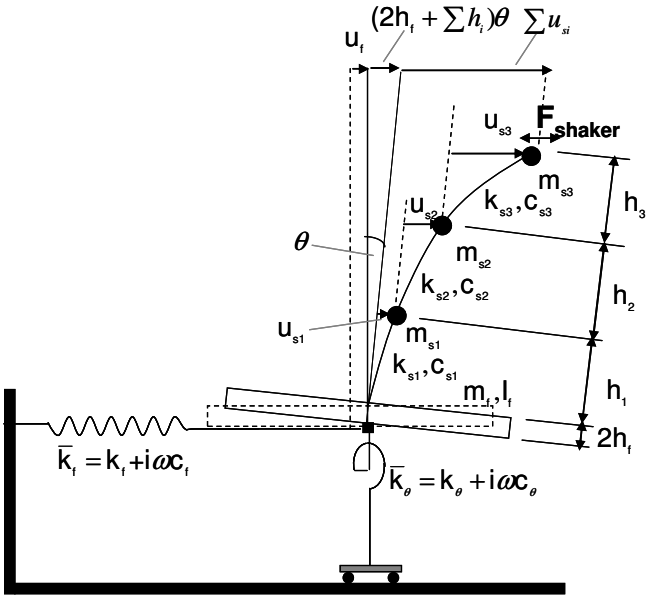

Figure 4.3 Simple SSI model subjected to an external force

The equations of motion for the model in Figure 4.3 subjected to forced vibration have been modified from Crouse et. al (2001) which presents the equations for ground motions.

$$\mathbf{M}\ddot{\mathbf{U}} + \mathbf{C}\dot{\mathbf{U}} + \mathbf{K}\mathbf{U} = \mathbf{F} \tag{4.14}$$

Crouse et al. (2001) present the mass, damping, and stiffness matrices for use with equation (4.14), which are not repeated here for brevity. The force vector is presented in Crouse et. al (1984). The displacement vector is defined as:

$$\mathbf{U} = \begin{bmatrix} u_f & \theta_f & u_{s1} & u_{s2} & u_{s3} \end{bmatrix}^T \tag{4.15}$$

For the case of a single degree-of-freedom superstructure subject to forced vibration, the terms in the equation of motion can be written as (adapted from Crouse et. al (2001):

$$\mathbf{M} = \begin{pmatrix} m_f + m_s & m_f h_f + m_s h & m_s \\ m_f h_f + m_s h & I_f + m_f {h_f}^2 + m_s h^2 & m_s h \\ m_s & m_s h & m_s \end{pmatrix} \tag{4.16a}$$

$$\mathbf{C} = \begin{pmatrix} c_f & c_{\theta f} & 0 \\ c_{f\theta} & c_\theta & 0 \\ 0 & 0 & c_s \end{pmatrix} \mathbf{K} = \begin{pmatrix} k_f & k_{\theta f} & 0 \\ k_{f\theta} & k_\theta & 0 \\ 0 & 0 & k_s \end{pmatrix} \tag{4.16b}$$

$$\mathbf{U} = \begin{bmatrix} u_f & \theta_f & u_s \end{bmatrix}^T \mathbf{F} = \begin{bmatrix} F_s & hF_s & F_s \end{bmatrix}^T \tag{4.16c}$$

where $c_{\theta f} = c_{f\theta}$ and $k_{\theta f} = k_{f\theta}$ are the coupled damping and stiffness terms for foundation translation-rotation, respectively. For the sake of brevity, our subsequent evaluation of input-output motions focuses on this relatively simple single degree-of-

freedom representation of the superstructure. We subsequently verify the applicability of the results obtained to a multi-degree-of-freedom superstructure model (Section 4.5).

Equations of motion at each degree of freedom can be obtained by entering the terms from equation (4.16) into equation (4.14) and completing the matrix multiplication. Excluding the $m_f h_f^2$ term, $m_f h$ term, and the coupled foundation stiffness and damping terms, the equations are:

$$m_s(\ddot{u}_f + h\ddot{\theta}_f + \ddot{u}_s) + m_f\ddot{u}_f + c_f\dot{u}_f + k_f u_f = F_s \text{ foundation translation} \quad (4.17a)$$

$$m_s h(\ddot{u}_f + h\ddot{\theta}_f + \ddot{u}_s) + I_f\ddot{\theta}_f + c_\theta\dot{\theta}_f + k_\theta\theta_f = hF_s \text{ foundation rotation} \quad (4.17b)$$

$$m_s(\ddot{u}_f + h\ddot{\theta}_f + \ddot{u}_s) + c_s\dot{u}_s + k_s u_s = F_s \quad \text{structure translation} \quad (4.17c)$$

Equations (4.17) are transformed into the Laplace domain, and after some re-arranging of terms, we obtain:

$$\left(m_s + m_f\right)\hat{u}_f A_f + s^2 m_s h\hat{\theta}_f + s^2 m_s\hat{u}_s = \hat{F}_s \quad (4.18a)$$

$$s^2 m_s\hat{u}_f + s^2 m_s\hat{u}_s + m_s A_\theta h\hat{\theta}_f = \hat{F}_s \quad (4.18b)$$

$$s^2 m_s\hat{u}_f + s^2 m_s h\hat{\theta}_f + m_s\hat{u}_s A_s = \hat{F}_s \quad (4.18c)$$

The *A* coefficients in equations 4.18 are defined as:

$$A_f = s^2 + \frac{sc_f}{m_s + m_f} + \frac{k_f}{m_s + m_f} \quad (4.19a)$$

$$A_\theta = s^2\left(1 + \frac{I_f}{m_s h^2}\right) + s\frac{c_\theta}{h^2 m_s} + \frac{k_\theta}{h^2 m_s} \quad (4.19b)$$

$$A_s = s^2 + 2\zeta_s\omega_s s + \omega_s^2 \quad (4.19c)$$

In equations (4.19), ω_s, ζ_s are the fixed base frequency and damping.

Equations (4.18) have three equations and three unknown responses $(\hat{u}_s, \hat{u}_f, \hat{\theta}_f)$. The solutions of the equations are presented in the next section.

4.4 SOLUTIONS OF THE EQUATIONS OF MOTION IN THE LAPLACE DOMAIN

Equation (4.18b) can be written as:

$$m_s h\hat{\theta}_f = \frac{\hat{F}_s}{A_\theta} - \frac{s^2 m_s \hat{u}_s}{A_\theta} - \frac{s^2 m_s \hat{u}_f}{A_\theta} \tag{4.20}$$

Equation (4.18c) can be written as:

$$m_s h\hat{\theta}_f = \frac{\hat{F}_s}{s^2} - m_s \hat{u}_f - \frac{m_s \hat{u}_s A_s}{s^2} \tag{4.21}$$

Equating equations 4.20 and 4.21 gives:

$$\frac{\hat{F}_s}{A_\theta} - \frac{s^2 m_s \hat{u}_s}{A_\theta} - \frac{s^2 m_s \hat{u}_f}{A_\theta} = \frac{\hat{F}_s}{s^2} - m_s \hat{u}_f - \frac{m_s \hat{u}_s A_s}{s^2} \tag{4.22}$$

Rearranging equation (4.22) and defining $B_\theta = A_\theta - s^2$ yields:

$$m_s \hat{u}_s = \frac{B_\theta \left(-\hat{F}_s + s^2 m_s \hat{u}_f\right)}{s^4 - A_\theta A_s} \tag{4.23}$$

Inserting equation (4.23) into equation (4.18b) and noting that $s^4 - A_s A_\theta = -A_s B_\theta - s^2 B_s$ gives

$$m_s h\hat{\theta}_f = \frac{B_s}{\left(s^4 - A_\theta A_s\right)}\left(-\hat{F}_s + s^2 m_s \hat{u}_f\right) \tag{4.24}$$

Subsequently inserting equation (4.23) and (4.24) into equation (4.18a), assuming $m_f = 0$ and defining $B_f = A_f - \mathrm{s}^2$, $B_s = A_s - \mathrm{s}^2$ gives:

$$\frac{m_s \hat{u}_f}{\hat{F}_\mathrm{s}} = \frac{\left(s^4 - A_\theta A_s + s^2(B_\theta + B_s)\right)}{\left(A_f(s^4 - A_\theta A_s\right) + s^4\left(B_s + B_\theta\right)} \tag{4.25}$$

Inserting equation (4.25) into equation (4.23) yields:

$$\frac{m_s \hat{u}_s}{\hat{F}_\mathrm{s}} = \frac{B_\theta\left(s^2 - A_f\right)}{\left[A_f\left(s^4 - A_\theta A_s\right) + s^4\left(B_s + B_\theta\right)\right]} \tag{4.26}$$

Finally inserting equation (4.26) back into (4.24) yields:

$$\frac{m_s h\hat{\theta}_f}{\hat{F}_\mathrm{s}} = \frac{B_s(-A_f + s^2)}{\left(A_f(s^4 - A_\theta A_s) + s^4(B_s + B_\theta)\right)} \tag{4.27}$$

Defining $C_s = -\left(A_f(s^4 - A_\theta A_s) + s^4(B_s + B_\theta)\right)$ yields the following equations:

$$\frac{m_s \hat{u}_f}{\hat{F}_\mathrm{s}} = \frac{-\left(s^4 - A_\theta A_s + s^2(B_\theta + B_s)\right)}{C_s} \tag{4.28}$$

$$\frac{m_s \hat{u}_s}{\hat{F}_\mathrm{s}} = \frac{-B_\theta\left(s^2 - A_f\right)}{C_s} \tag{4.29}$$

$$\frac{m_s h\hat{\theta}_f}{\hat{F}_\mathrm{s}} = \frac{-B_s(-A_f + s^2)}{\left(s^4 - A_\theta A_s\right)C_s} \tag{4.30}$$

Further writing $C_s = s^2(B_u B_s + B_u B_\theta + B_s B_\theta) + B_u B_s B_\theta$ yields:

$$\frac{m_s \widehat{u}_s}{\widehat{F}_s} = \frac{B_\theta B_f}{C_s}, \quad \frac{m_s \widehat{u}_f}{\widehat{F}_s} = \frac{B_\theta B_s}{C_s}, \quad \frac{m_s h \widehat{\theta}_f}{\widehat{F}_s} = \frac{B_s B_f}{C_s} \tag{4.31}$$

Equation (4.31) represents the complete solution for single degree-of-freedom superstructure model, so any transfer function of interest can be directly evaluated from these results. Two input-output pairs for flexible- and fixed-base conditions are considered.

(a) *Flexible-base case*. For the flexible-base case, the shaker force is taken as the input and the inertial force associated with roof acceleration is the output. The transfer function is defined as the ratio of these two forces in the Laplace domain:

$$\widehat{H} = \frac{m_s s^2 \left(\hat{u}_s + \hat{u}_f + H \hat{\theta}_f \right)}{F_s} = \frac{s^2 \left(B_\theta B_f + B_\theta B_s + B_s B_f \right)}{C_s} \tag{4.32}$$

The poles for this case are values of s for which C_s=0. We demonstrate in Section 4 that those poles are associated with the flexible-base frequency and damping.

The accuracy of this solution can be demonstrated theoretically for the case of a foundation with zero mass and zero rotational inertia. For this case, the roots of C_s are in the same form as equation (4.12) but with the system frequency $\tilde{\omega}$ and damping $\tilde{\zeta}$ defined as:

$$\tilde{\omega}^2 = \frac{\omega_\theta^2 \omega_f^2 \omega^2}{\omega^2 \omega_f^2 + \omega_\theta^2 \omega_f^2 + \omega^2 \omega_\theta^2} = \frac{1}{1/\omega^2 + 1/\omega_\theta^2 + 1/\omega_f^2} \tag{4.33}$$

$$\tilde{\zeta} = \left(\frac{\tilde{\omega}}{\omega_f} \right)^3 \zeta_f + \left(\frac{\tilde{\omega}}{\omega} \right)^3 \zeta + \left(\frac{\tilde{\omega}}{\omega_\theta} \right)^3 \zeta_\theta \tag{4.34}$$

where $\omega_f = \sqrt{k_f / m_s}$, $\omega_\theta = \sqrt{k_\theta / \left(m_s h^2\right)}$, $\zeta_f = c_f / \left(2\omega_f m_s\right)$, and $\zeta_\theta = c_\theta / \left(2\omega_\theta m_s h^2\right)$. Equations (4.33-4.34) demonstrate the accuracy of the proposed input-output pair because they match known theoretical solutions for flexible-base frequency and damping (Luco, 1980, Stewart and Fenves 1998).

(b) *Fixed base case.* For the fixed-base case, we take the input as the difference between the shaker force and the sum of the inertial forces due to foundation translation and rocking. The output is the inertial force caused by relative structural translation at the roof. The transfer function for this case is:

$$\hat{H} = \frac{m_s \hat{u}_s}{\hat{F}_s - m_s\left(\hat{u}_f + H\hat{\theta}_f\right)} = \frac{s^2 B_\theta B_f}{C_s - s^2\left(B_s B_\theta + B_s B_f\right)} \tag{4.35}$$

The denominator can be reduced to the product of a first and second order polynomial in s,

$$C_s - s^2\left(B_s B_\theta + B_s B_f\right) = \left[2s\left(\zeta_u \omega_u \omega_\theta^2 + \zeta_\theta \omega_\theta \omega_u^2\right) + \omega_\theta^2 \omega_u^2\right]\left(s^2 + 2\zeta\omega_s s + \omega^2\right) \tag{4.36}$$

The second-order polynomial in equation (4.36) has the same form as (4.11). Hence, the roots of equation (4.36) are the fixed-base fundamental mode frequency and damping (equation 13 for j=1).

To summarize, the input-output pairs to evaluate flexible- and fixed-base parameters are listed in Table 4.2. The forces have been re-written in terms of accelerations through normalization by m_s. The relationships between the inputs-

outputs shown in Table 4.2 and recordings on a typical building are illustrated in Figure 4.4.

Table 4.2. Input and output pairs to evaluate flexible- and fixed-base modal parameters

Base Fixity	Input	Output
Flexible-Base	$\frac{F_s}{m_s}$	$\ddot{u}_f + H\ddot{\theta} + \ddot{u}_s$
Fixed-Base	$\frac{F_S}{m_s} - \ddot{u}_f - H\ddot{\theta}$	$\ddot{u}_s$

The flexible base input involves the measurement of shaker mass acceleration $\ddot{u}_{sh}$, shaker mass m_{sh}, and equivalent single degree-of-freedom structural mass m_s. In the case of an MDOF superstructure system the same input and output pairs given in Table 2 can be used. The Mass m_s can be taken as the effective fundamental modal mass defined as

$$m_s = m_1 = L_1^2 / \boldsymbol{\varphi}_1^{\mathrm{T}} \mathbf{m}' \boldsymbol{\varphi}_1 \tag{4.37}$$

where,

$$L_1 = \boldsymbol{\varphi}_1^{\mathrm{T}} \mathbf{m}' \mathbf{1} \tag{4.38}$$

Note that in equation (4.37) and (4.38) the mass matrix $\mathbf{m}'$ for the structure is diagonal, which can be achieved by a coordinate transformation of the degrees of freedom.

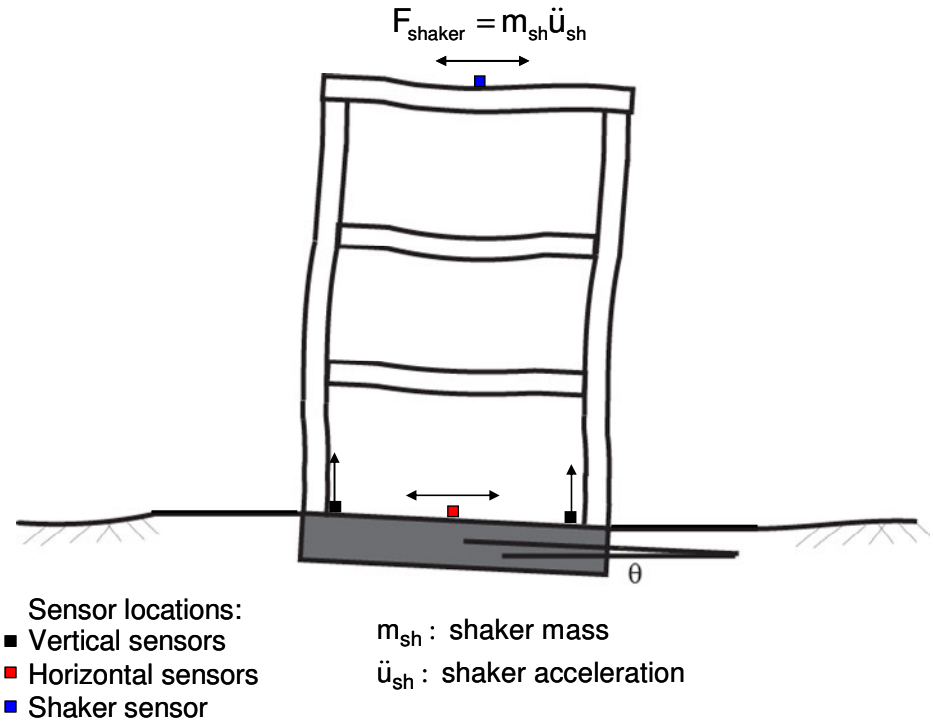

Figure 4.4 Schematic of multi-story building with sensor locations indicated

4.5 VERIFICATION OF PARAMETER ESTIMATION PROCEDURES

To verify the input-output pairs identified in the previous section, we analyze the response of linear soil-foundation-structural systems. As shown in Figure 4.5, three structural systems are considered, each having the same uniform soil condition with depth-invariant shear modulus = *G*. The three structures include two single degree-of-freedom (dof) systems with low and high stiffness and one three dof system. Fixed-based modal parameters are specified as shown in Figure 4.5 for the single dof structures. For the three dof structure, the floor stiffnesses and masses are specified as

shown in Figure 4.5 and eigenvalue analysis (Chopra, 2007) provides the fixed-base frequencies and mode shapes shown in the figure.

Flexible-base fundamental-mode frequencies and damping ratios can be computed for these structures using the theoretical model of Veletsos and Meek (1974). The lengthening of the fundamental mode period is given as:

$$\frac{\tilde{T}}{T} = \sqrt{1 + \frac{k_s}{k_f} + \frac{k_s h^2}{k_\theta}} \tag{4.39}$$

where k_f and k_θ are the foundation stiffnesses for translation and rocking. Those are calculated using the theoretical model of Veltsos and Verbic (1973). The flexible base damping is given as:

$$\tilde{\zeta} = \tilde{\zeta}_0 + \frac{\zeta}{(\bar{T}/T)^3} \tag{4.40}$$

where $\tilde{\zeta}_0$ is the foundation damping computed using closed form expressions given in Velotsos and Nair (1975).

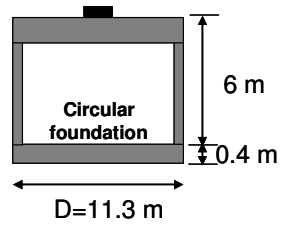

System 1 Properties	
m_f (kg)	25000
m_s (kg)	35000
k_s (N/m)	1.2E+07
ζ_s (%)	1
G (N/m^2)	3.6E+07

System 2 Properties	
m_f (kg)	25000
m_s (kg)	35000
k_s (N/m)	4.5E+08
ζ_s (%)	6
G (N/m^2)	3.6E+07

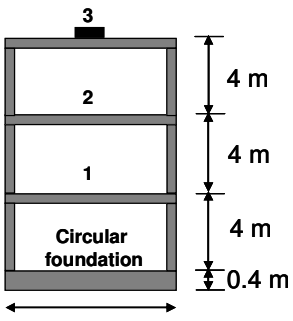

System 3 Properties	
m_f (kg)	25000
m_{s1} (kg)	35000
m_{s2} (kg)	35000
m_{s3} (kg)	35000
k_{s1} (N/m)	3.5E+08
k_{s2} (N/m)	3.5E+08
k_{s3} (N/m)	3.5E+08
$\zeta_{s\,1}$(%)	3
$\zeta_{s\,2}$(%)	6
$\zeta_{s\,3}$(%)	6
G (N/m^2)	3.6E+07

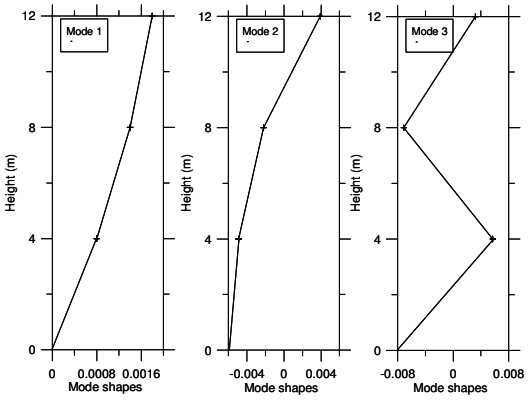

shaker

Figure 4.5 Properties of the systems resting on the same soil with a constant shear modulus G

The responses of the structural systems shown in Figure 4.5 can be computed precisely from theoretical solutions (modified from Crouse et al., 2001) for forced vibration tests. A broadband shaker excitation is specified and the response quantities foundation translation $\ddot{u}_f$, base rotation, $\ddot{\theta}_f$, and total lateral roof acceleration are solved for. Those responses are shown in Figure 4.6.

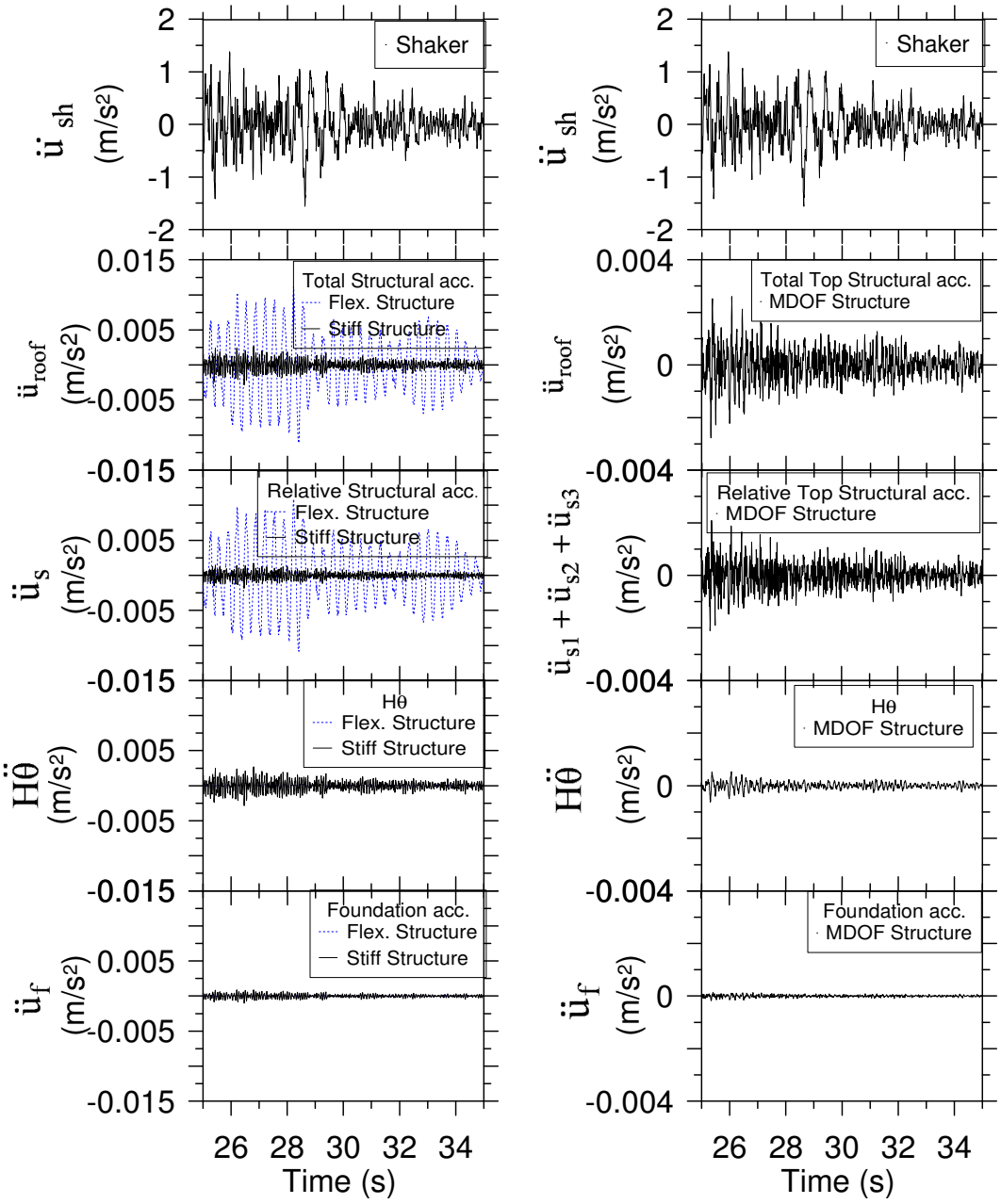

Figure 4.6 Theoretical responses for the sdof structures (left) and mdof structure right with assumed shaker excitation used in the verification models

Parametric system identification is applied to the responses in Figure 4.6 for the SDOF structures. The back calculated frequency and damping are found to exactly

match the assumed frequency and damping values. However, an important check in parametric system identification which describes how well the numerical model's output matches the recorded output does not run due to a numerical instability. The cause of this numerical instability is not presently understood. To overcome this, white noise is added to the computed responses in Figure 4.6 that make up the output motions presented in Table 4.2 before the parametric system identification was carried out.

The responses are then manipulated to form the input and output accelerations indicated in Figure 4.4 and Table 4.2 and parametric system identification is repeated. The identified fixed-base parameters evaluated from parametric system identification are compared in Table 4.3 to the values used to define the numerical model. The match is very good for both frequencies and damping. The comparison of flexible-base frequencies, the theoretical values of which are computed using equations (4.26) and (4.27), is also nearly exact. Note also that the identified parameters for the multi-dof system are reasonably good; indicating that the same input-output pairs derived for the single dof case can apply to multi dof structural systems.

Table 4.3. Summary of assumed and back calculated fixed-base frequency (f) and damping (ζ) results

System	Fixed Base Parameters				Flexible Base Parameters			
	Assumed		System Id		System Id		Theory	
	f (Hz)	ζ(%)	f (Hz)	ζ(%)	f (Hz)	ζ(%)	f (Hz)	ζ(%)
SDOF-Flexible	3.00	1.00	3.00	1.07	2.96	1.21	2.96	1.25
SDOF-Stiff	18.00	6.00	17.59	6.49	12.30	21.00	12.00	22.55
MDOF-Stiff*	7.05	3.00	7.55	3.13	5.65	9.00	5.42	10.00

*For the MDOF system 1st mode parameters are compared

Based on these findings, we conclude that the use of the input-output pairs shown in Table 4.2 in system identification analysis provides accurate estimates of modal parameters. A more detailed presentation of system identification results is deferred to the following section, where these procedures are applied to recorded data from a test structure.

4.5 APPLICATION OF PROCEDURES TO GARNER VALLEY TEST STRUCTURE

In this section, we apply the parametric system identification procedures to a model test structure, which is shown in Figure 4.7. The test structure is located at the Garner Valley Differential Array (GVDA), a permanent test site in Southern California. The test structure is a simple steel frame with reconfigurable bracings and reinforced concrete foundation and roof slabs. The foundation slab dimensions are 4m × 4m in plan and 50cm thickness (no embedment). The roof slab has the same lateral dimensions but is 40 cm thick. The columns are 3.16 m in height from the top of the foundation slab to the base of the roof slab. A 70 kg shaker is installed on the underside of the roof slab, which allows forced vibration experiments to be conducted. Structural response is monitored through an array of 32 sensors on the structure in addition to the nearby ground motion arrays. Further details on the structure and site conditions are provided in www.nees.ucsb.com.

Figure 4.7 The SFSI structure

Recordings at the GVDA test structure are available from numerous earthquakes recorded between 2005 and 2008. In addition, forced vibration testing has been conducted almost daily from 2006 to 2008. Tileylioglu et. al (2008) has previously evaluated some of this earthquake data. In this section, we examine forced vibration test data from 10/24/2006 and 11/4/2006 conducted on the structure with and without bracings respectively. We compare our results to those from recordings at the site from a local M_L=4.2 earthquake (2008) and also the M_w = 5.4 2008 Chino Hills, California earthquake.

The forced vibration tests are conducted by commanding the shaker to produce sinusoidal forces over a frequency range of 5-15 Hz. The excitation begins at 15 Hz and the frequency is gradually decreased over 60 sec until 5 Hz frequencies are achieved.

To illustrate the application of the parametric system identification procedure, we consider the fixed-base input-output data pair for a forced vibration test on the unbraced structure. Parametric system identification requires two user-specified

parameters; the time delay between the input and output signals and the number of modes required to capture the response of the system (Pandit, (1991), Stewart and Fenves (1998). Optimum values of each parameter are evaluated by examining the error between the specified output signal (data) and the model fit (model) as the above parameters are varied. The error is calculated as the sum of the squares of residuals between recorded output and model output in the time domain (Cumulative Prediction Error Method (Safak. (1991)). As illustrated in Figure 4.8, for this input-output pair, the minimum error occurs at a time delay of 0 and decreases gradually for increasing number of modes. A zero time lag and J=6 modes is selected. This produces a very good fit between the data and model output, as shown in Figure 4.9.

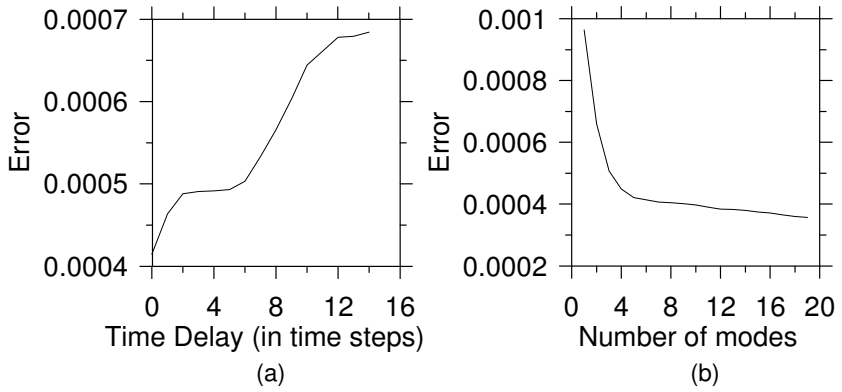

Figure 4.8 Error of system identification model with respect to (a) time delay and (b) number of modes

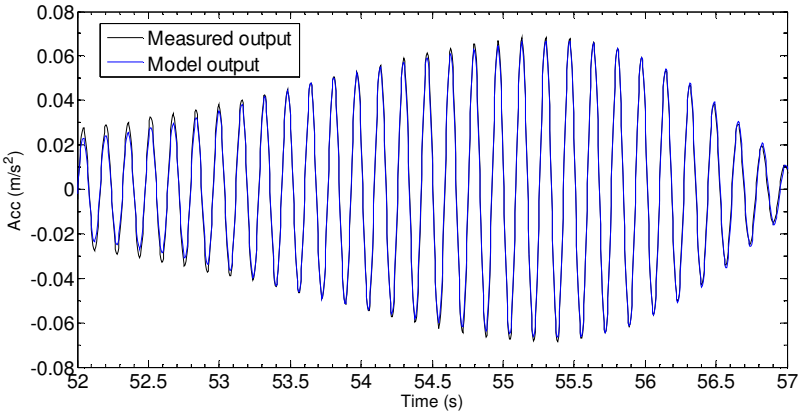

Figure 4.9. Data output and model output

Once the time lag and number of modes are obtained, the transfer function surface in the Laplace domain is identified. The results for the fixed- and flexible-base case for the structure with and without bracing are shown in Figure 4.10. The locations of high points ("poles") define modal frequencies and damping ratios per equations (4.12) and (4.13). As shown in Figure 10, the braced structure has two significant modes within the frequency range of interest. The fixed and flexible base modes of the braced structure occur at 12.76 Hz and 9.88 Hz respectively.

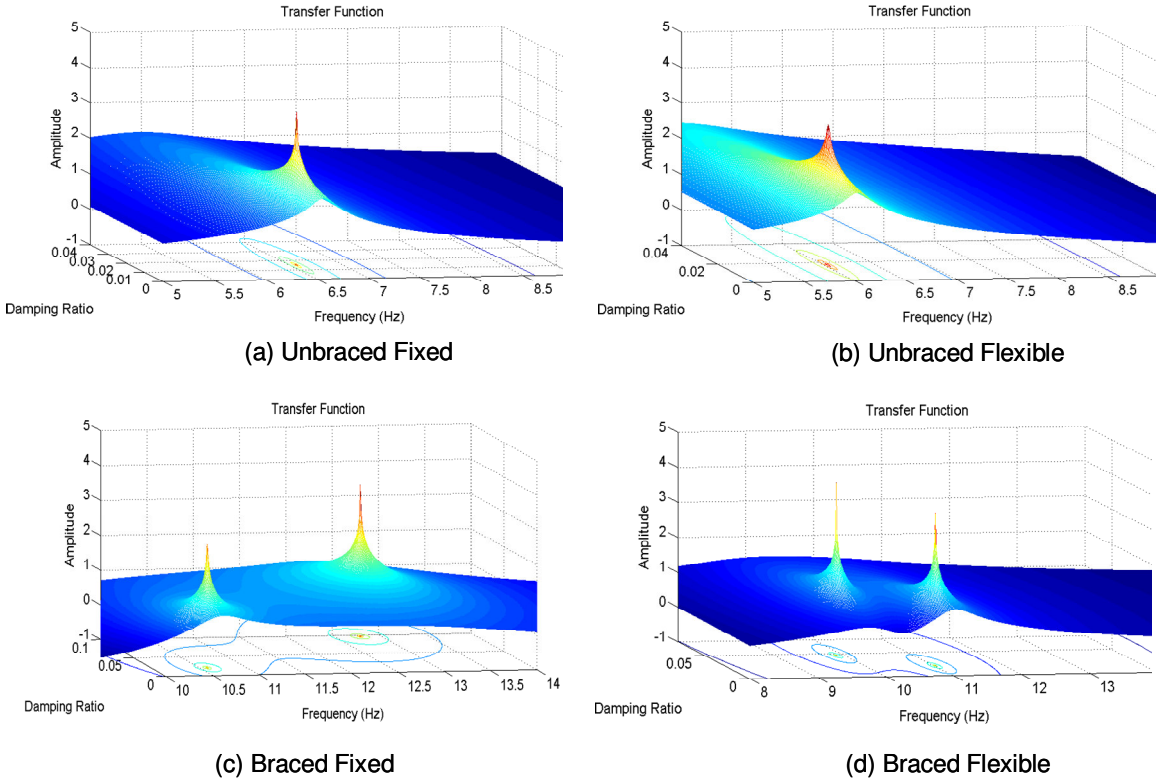

Figure 4.10. Transfer function surfaces

As shown in Figure 4.11, the intersection of the transfer function with a vertical plane on the frequency axis corresponds to the parametric estimate of a transmissibility function, which can be compared to the ratio of ouput/input motions in the frequency domain from nonparametric system identification. The non-parametric transmissibility functions were calculated by taking the square-root of the power spectral density function with 4X smoothing using the Welch's method (Welch, 1967). The peaks correspond to the same frequencies however there is difference between the amplitudes because the non-parametric transmissibility function depends on the smoothing method.

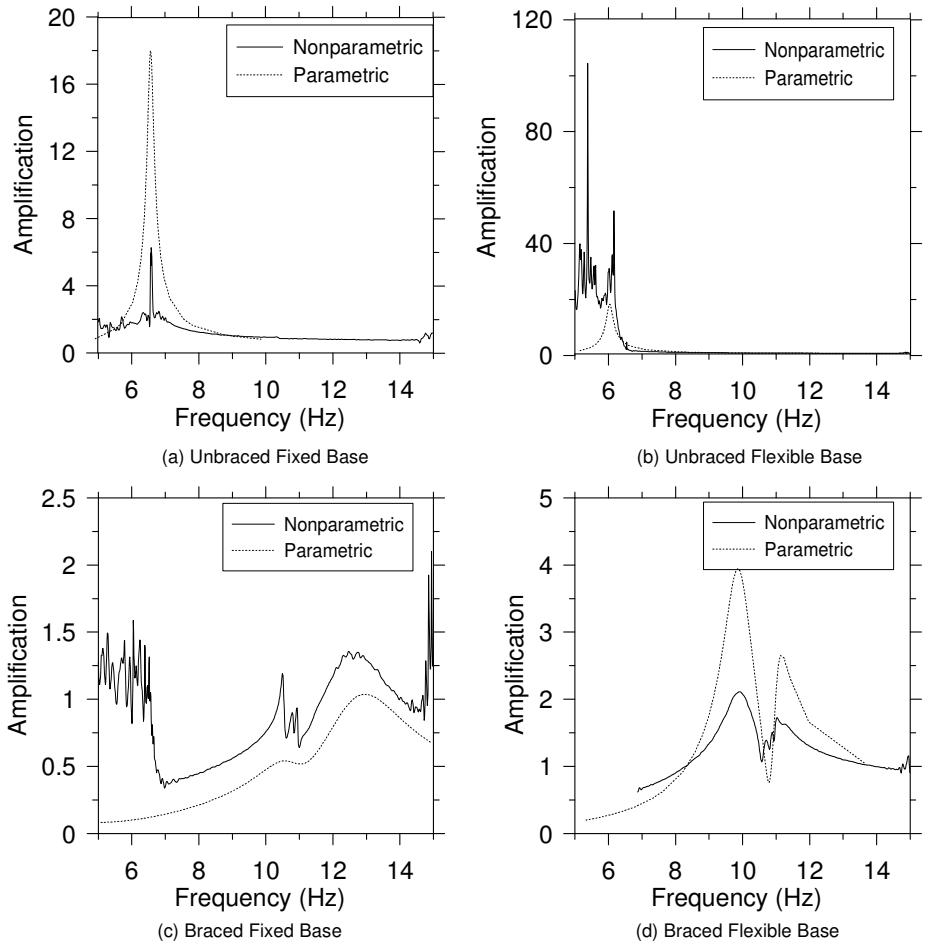

Figure 4.11 Parametric and Non-Parametric transmissibility functions for different base fixity and structure conditions

As indicated in Figures 4.10-4.11, the procedures described above were repeated for forced vibration tests on the structure with and without bracing. The results are shown in Table 4.4 along with calculations of period lengthening and foundation damping per equations (4.26) and (4.27). A stronger soil-structure interaction effect is evident for the braced structure, which is consistent with expected patterns of behavior (higher structure to soil stiffness).

Table 4.4. Summary of system identification and SSI effect

Excitation Source	Structural Configuration	Fixed Base Parameters		Flexible Base Parameters		SSI Effect: Data		SSI Effect: Theory	
		f (Hz)	$\zeta(\%)$	f (Hz)	$\zeta(\%)$	$\bar{T}/T$	ζ_o (%)	$\bar{T}/T$	ζ_o (%)
Forced	Unbraced	6.56	1.48	6.04	1.68	1.09	0.54	1.10	1.40
Forced	Braced	12.76	9.33	9.88	4.60	1.29	0.25	1.55	5.30
Earthquake 1 M_L=4.2	Unbraced	6.71	0.51	5.82	1.25	1.15	0.91	1.10	1.40
Earthquake 2 M_w=5.4	Unbraced	6.70	0.90	5.81	4.11	1.15	3.52	1.10	1.40

Parametric system identification was also performed using the earthquake data. This analysis differs from previous work (Tileylioglu, et. al (2008)) for this site because of availability of free-field recordings for the present data set. Procedures for system identification using earthquake recordings are presented in (Stewart and Fenves (1998)). Using the input-output data pairs listed in Table 4.1, fixed-base and flexible-base parameters for the unbraced structure (the bracing was out at the time of the earthquake) were evaluated. The results are shown in the last two rows of Table 4.4. The earthquakes produced more period lengthening and greater foundation damping than the forced vibration test, which can be attributed to significantly stronger shaking levels from the earthquakes.

As noted previously, the SSI effect for the braced structure is stronger than for the unbraced structure, as evidenced by higher period lengthening. The foundation damping factor for the braced structure, as identified from data, is relatively low. This may be due to the fact that the bracing's vibration mode (around 11 Hz; Figure 4.11d) occurs close to the structure's fundamental mode, which likely contaminates (i.e., introduces unknown errors to) the system identification results for the fixed-base structure.

4.7 CONCLUSIONS

Parametric system identification of data recorded during forced vibration tests provides a useful tool for evaluation of modal frequencies and damping ratios. In this study, I have extended parametric system identification procedures developed for earthquake excitation to the case of forced vibration. To evaluate flexible-base modal parameters, which incorporate flexibility and damping associated with foundation translation and rocking along with structural translation, recordings of shaker acceleration and roof translational acceleration are needed. Shaker mass and fundamental-mode participating mass are also needed. To evaluate fixed-base modal parameters, recordings of foundation translation and base rocking (measured using vertical accelerometers on opposite sides of the foundation) are needed in addition to those for the flexible-base case. The precise input-output pairs for both cases are given in Table 4.2.

The input-output pairs listed in Table 4.2 have been verified using numerical analysis of various structures for which the fixed-base parameters are specified a priori and the flexible-base parameters can be computed using theoretical analysis. The verification involved the use of computed structural motions in parametric system identification procedures, which reproduced the a priori specified (fixed-base) and theoretically derived (flexible-base) parameters. Noise was added to the outputs of the transfer function in order to compute the numerical output and compare it with the actual output. The effect of noise on the results is not fully grasped, however as stated earlier it was essential to add it.

The system identification procedures were applied to recordings obtained during forced vibration testing of a test structure at the Garner Valley Differential Array. The results were generally consistent with those obtained from earthquake recordings, both in terms of the values of fundamental mode vibration properties and the levels of soil-structure interaction effects inferred from comparison of fixed- and flexible-base parameters.

5 IMPEDANCE FUNCTIONS FROM FORCED VIBRATION TESTS

5.1 INTRODUCTION

Impedance functions represent the stiffness and damping characteristics of foundation-soil interaction. Closed form analytical solutions for impedance functions have been available for simplified foundation and soil conditions since the early 1970's. Those analytical models are generally based on a rigid foundation on a homogeneous viscoelastic halfspace, although some adjustments are possible to capture complexities such as a specified depth-variable shear stiffness, embedment, and non-rigid foundations. The ability of these impedance function models to simulate the performance of actual foundations is largely unknown.

In this chapter, forced vibration test data from the Garner Valley SFSI structure are used to infer the impedance functions that develop under realistic field conditions. The chapter begins with a brief overview of analytical impedance functions. Past experimental studies on the topic are described in Section 5.3. Next, the mathematical formulation used to infer impedance functions from field measurements is presented. The derived equations are validated against a known solution in Section 5.5. In Section

5.6 recorded data from the Garner Valley test structure is utilized to calculate impedance functions, which are then compared to theoretical predictions. The effect of groundwater table on impedance functions is presented in Section 5.7. Chapter 5 ends with discussion of the results.

5.2 IMPEDANCE FUNCTIONS AND ANALYTICAL MODELS

Impedance functions are complex valued and frequency dependent. In Figure 4.3 the functions are represented by $\bar{k}_f$ and $\bar{k}_\theta$. Coupling terms $\bar{k}_{f\theta}$ and $\bar{k}_{\theta f}$ can also be included in a more complete model. Veletsos and Wei (1971), Luco and Westman (1971), have expressed the impedance function for a rigid circular disk foundation on the ground surface as follows:

$$\bar{k}_j = k_j(a_o, \nu) + i\omega c_j(a_0, \upsilon) \qquad (5.1)$$

where, j denotes the mode f (translation) or θ (rotation)

ω is the angular frequency (rad/s)

a_0 is a dimensionless frequency which is defined by $a_0=\omega r/Vs$

r is the foundation radius

V_s is the soil shear wave velocity

υ is the Poisson ration of the soil

For non-circular foundations, equivalent foundation radii are computed for both translational and rotational deformation modes to match the area A_f and moment of inertia I_f of the actual foundation through:

$$r_f = \sqrt{A_f/\pi}\ ,\ r_\theta = \sqrt[4]{4I_f/\pi} \tag{5.2}$$

The real part of equation (5.1) represents the stiffness whereas the complex part represents the damping. For both translation and rocking the individual terms in equation (5.1) can be expressed as follows:

$$\begin{aligned} k_f &= \alpha_f K_f;\ c_u = \beta_f \frac{K_f r_f}{V_s} \\ k_\theta &= \alpha_\theta K_\theta;\ c_\theta = \beta_\theta \frac{K_\theta r_\theta}{V_s} \end{aligned} \tag{5.3}$$

where, $\alpha_\theta, \beta_\theta, \alpha_f, \beta_f$ are dimensionless parameters that express the frequency dependence of the impedance terms and K_f, K_θ are the static stiffnesses of the foundation in translation and rocking, respectively. The static stiffnesses are obtained as follows for circular foundations (Veletsos and Verbic, 1973):

$$K_f = \frac{8}{2-\nu} G r_f \tag{5.4}$$

$$K_\theta = \frac{8}{3(1-\nu)} G r_\theta^3 \tag{5.5}$$

where, G is the shear modulus of the soil and is related to the shear wave velocity through the density ρ as $G = \rho V_S^2$.

Luco and Westmann (1971), Veletsos and Wei (1971), and Veletsos and Verbic (1973) have investigated the frequency dependence of the aforementioned α_f , α_θ and β_f, β_θ terms. Figure 5.1 shows representative results for circular foundations for a case with zero hysteretic damping (β=0) and 10% hysteretic damping. There is a tendency for rocking stiffness to reduce with increasing frequency and for rocking damping to increase with frequency. For translation, there is relatively modest frequency dependence of the stiffness and damping terms. The large increase in the β terms near zero frequency is associated with hysteretic damping effects.

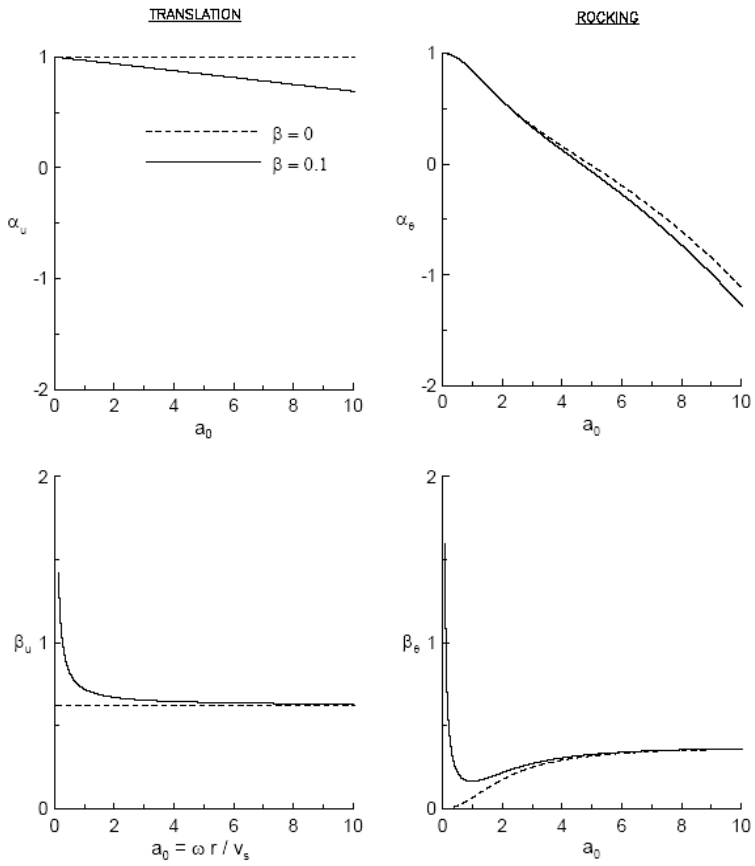

Figure 5.1. Foundation stiffness and damping factors for elastic and viscoelastic halfspace, ν=0.4 (Veletsos and Verbic, 1973)

Most classical solutions for impedance functions apply for a rigid circular foundation on a viscoelastic half-space. In reality, soil profiles are non uniform and the foundation may be non-circular, embedded, and flexible.

Non-uniform profiles can be represented for modeling purposes by an equivalent halfspace with a representative shear wave velocity and damping ratio. The representative shear wave velocity is calculated as the ratio of an effective depth to the shear wave travel time over that depth interval. The effective depth is measured

downward from the base of the foundation. Some effective depth recommendations include $4\times r_u$ for translation and $1.5\times r_\theta$ for rocking (pre 2000 NEHRP), which have been modified to $0.75\times r_u$ for translation and $0.75\times r_\theta$ for rocking (2003 NEHRP; Stewart et al., 2003). Roesset (1980) did not recommend the use of an effective profile depth, but suggested taking the effective velocity as the measured value at a depth of 1/2×r below the foundation (for circular foundations. This generally provides similar representative velocities to those from the effective profile depths noted above.

Frequency dependence of impedance functions for non uniform soil profiles are shown in Figure 5.2 for a surficial layer overlying a stiffer layer (denoted as (1) in figure) and a layer with uniformly varying stiffness overlying a halfspace (denoted as (2) in figure). Note that the frequency-dependence of the translational stiffness is much stronger for the nonuniform profile than the halfspace. For the rotational stiffness term and damping terms, the differences from the halfspace solution are relatively minor.

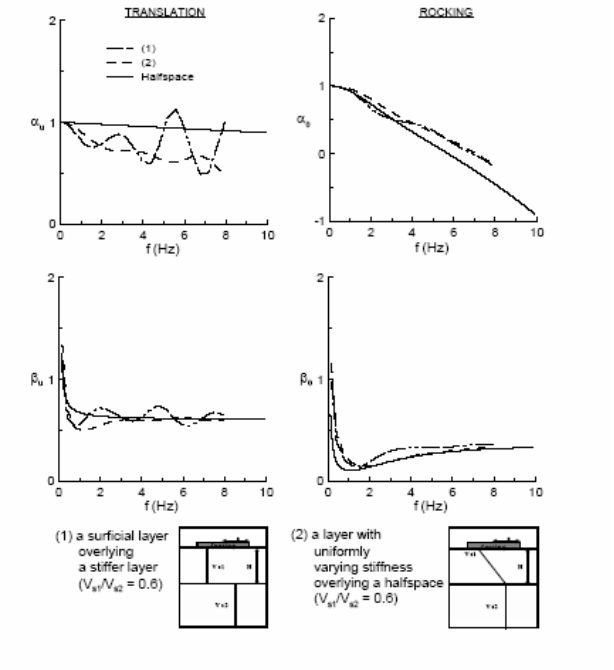

Figure 5.2. Frequency dependence terms for various non-uniform soil profiles (H/r=2, υ=0.45 , β=0.05, Wong and Luco, 1985)

5.3 PAST EXPERIMENTAL STUDIES ON IMPEDANCE FUNCTIONS FROM FORCED VIBRATION TESTS

Forced vibration tests involve actively shaking a structure using a vibration source, usually mounted on the roof, and monitoring motions within the structure. These tests have the advantage of essentially zero free-field motion. This can result in good signal to noise ratios relative to other types of tests (ambient or earthquake vibration), where free-field motions are significant relative to foundation level motions. A variety of forcing techniques are used in forced vibration tests including actuators pushing against a reaction frame, shakers, step relaxation, and various methods of measured impact

(Sohn et al., 2004). The forced vibration test data reported in the literature generally uses eccentric mass shakers that apply harmonic loading. A summary of forced vibration tests with shakers reported in the literature has been presented by Stewart et al. (2005). Table 5.1 shows a summary of these tests.

Table 5.1 Summary of forced vibration tests used to infer impedance functions (from Stewart et al. 2005)

Foundation Dimensions	Embedment (m)	First-mode fixed-base Frequency (Hz)	Soil Vs (m/s)	Excitation		Results			
				Source	Freq. (Hz)	$f / \tilde{f}$	Impedance obtained	Freq. Range (Hz)	Reference
3m×3m	0-1.5	17.5	305	Vibrator on ground	7 - 70	1.3 (e=1.5) - 1.5 (e=0)	$k_u c_u k_\theta c_\theta$	modal freq. only	Lin and Jennings, 1984
23m×25m	4–5.5	NS:2.16 EW:1.26	300	Vibrator on roof	NS:0.8-2.5 EW:0.8-1.75	NS:1.06 EW:1.1	$k_u c_u k_\theta c_\theta$	NS:0.8-2.5 EW:0.8-1.75	Luco et al., 1988 ; Wong et al., 1988
1.3m×1.3m (w/ corner piers)	0	n/a	120	Vibrator on foundation	10 – 60	N/a	$k_u c_u k_\theta c_\theta$	0 – 60	Crouse et al., 1990
1.2m×1.1m	0	n/a	75	Vibrator on foundation	10 - 60	n/a	$k_u c_u k_\theta c_\theta$	0 - 60	
d=10.8m	5.2	9.37	300	Vibrator on roof / foundation	2 - 20	2	$k_u c_u k_\theta c_\theta$ $k_{u\theta} c_{u\theta} k_v c_v$	5 - 14	DeBarros and Luco, 1995

Crouse et al. (1990) performed a series of forced vibration tests on two different foundations each located at different accelerograph sites on soft to moderately stiff alluvial deposits. One of the foundations tested was a 1.27m square slab with corner piers. The second foundation was a 1.22mx1.14m rectangular slab resting directly on the ground. Excitation was provided by a 15.8 kg eccentric-mass shaker bolted to the surface of the foundations (Crouse, et. al. 1990). Experiments were performed over a

frequency range of 10-60 in 5 Hz increments. In order to prevent large non-linear response, the eccentricities were lowered (which in turn lowers the force exerted on the foundation) at 20Hz and 40 Hz. The results of the series of experiments were compared to the theoretical formulation of Apsel and Luco (1987), which provides estimates of impedance functions for surface and embedded circular foundations in a linear, viscoelastic layered soil. The foundation with corner piers was modeled as a rigid cylinder having a radius of 0.73m, which gives the same moment of inertia as the base of the actual foundation. The second foundation was modeled as a rigid rectangular surface with the same plan dimensions as the actual foundation. Three models were created for each foundation: (1) Model 1 has the best estimate of shear wave velocity from the profile and a representative damping, (2) in Model 2, V_s values from the upper 0.6m were increased relative to Model 1 by 30% (to account for the effects of overburden from the overlying structure), (3) Model 3 had the same V_s profile as Model 2 but higher damping (0.08 instead of 0.015). Model predictions are compared to data in Figure 5.3 for the second foundation. The increased soil stiffness (Model 2 vs. Model 1) and the increased damping (Model 3 vs. Model 2) are needed to optimize the fit. It is not clear from this study how these adjustments to velocity and damping would be made for forward (predictive) analysis. As shown in Figure 5.4, model predictions for the slab with corner piers were relatively poor, generally over-predicting translational stiffness and damping and under-predicting rotational stiffness and damping. Possible explanations for the misfit include the complexity of the actual foundation relative to the model and potential soil nonlinearities (Crouse et al., 1990).

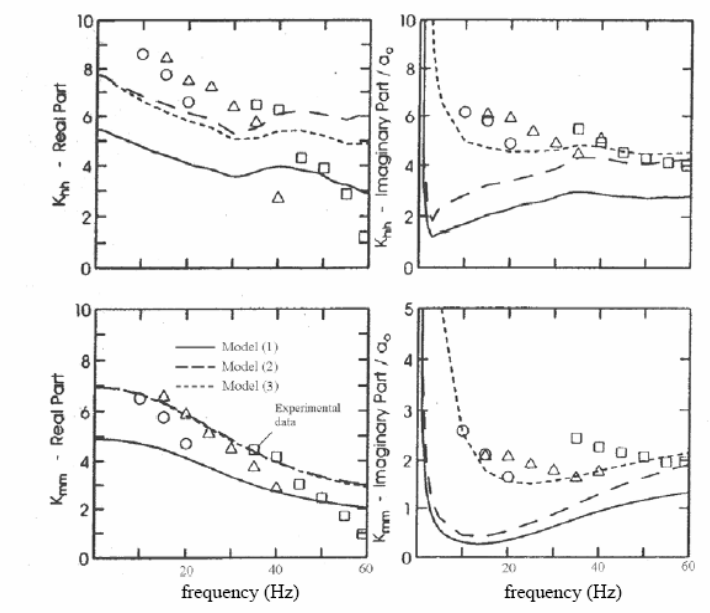

Figure 5.3 Theoretical and experimental foundation impedance functions for a foundation slab without corner piers (a_o is the dimensionless frequency) (from Crouse et al., 1990)

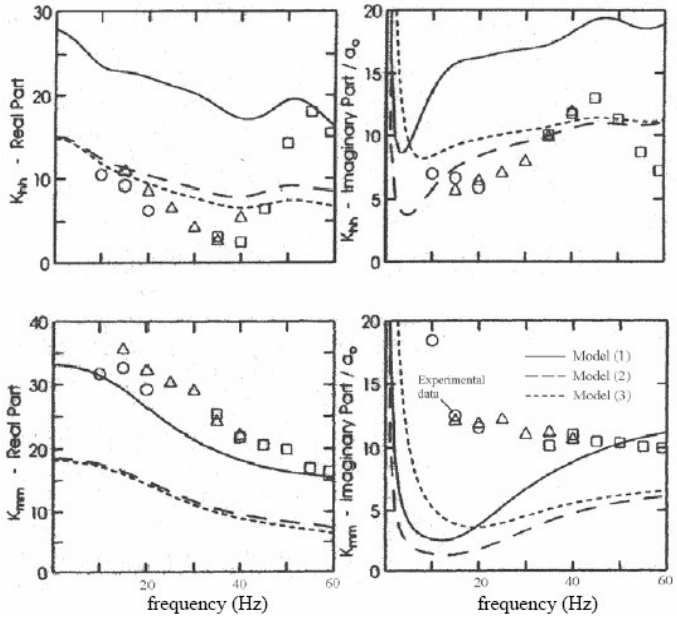

Figure 5.4 Theoretical and experimental foundation impedance functions for a foundation slab with corner piers (from Crouse et al., 1990)

A forced vibration test was carried out by Luco et al. (1988) on the 9 story Millikan Library at the Caltech campus. The lateral load resisting system for this building consists of shear walls along the outside edges of the building for NS shaking and a central core of shear walls for EW shaking. For the analysis of base translation and rocking, the forced vibration test data was reduced with two assumptions. The first, referred to as a flexible foundation assumption, takes the base translations and rotation as averages measured across the foundation. The second, referred to as a rigid foundation assumption, uses the translation and rotation at the base of the shear walls. As shown in Figure 5.5, similar results are obtained using both methods. The impedance functions shown in the figure are normalized to be dimensionless. The normalization takes the following forms:

$$\bar{K}_{ff} = \frac{\bar{k}_f}{GL} \tag{5.6}$$

$$\bar{K}_{\theta\theta} = \frac{\bar{k}_\theta}{GL^3} \tag{5.7}$$

where $\bar{K}_{ff}$ and $\bar{K}_{\theta\theta}$ are the dimensionless impedance coefficients and L is a characteristic foundation length.

The results are compared to predictions from the theoretical model of Apsel and Luco (1987). As shown in Figure 5.5, the model predictions are reasonably good for rocking, but are relatively poor for translation. Moreover, the real part of the impedance functions is generally predicted better than the imaginary parts.

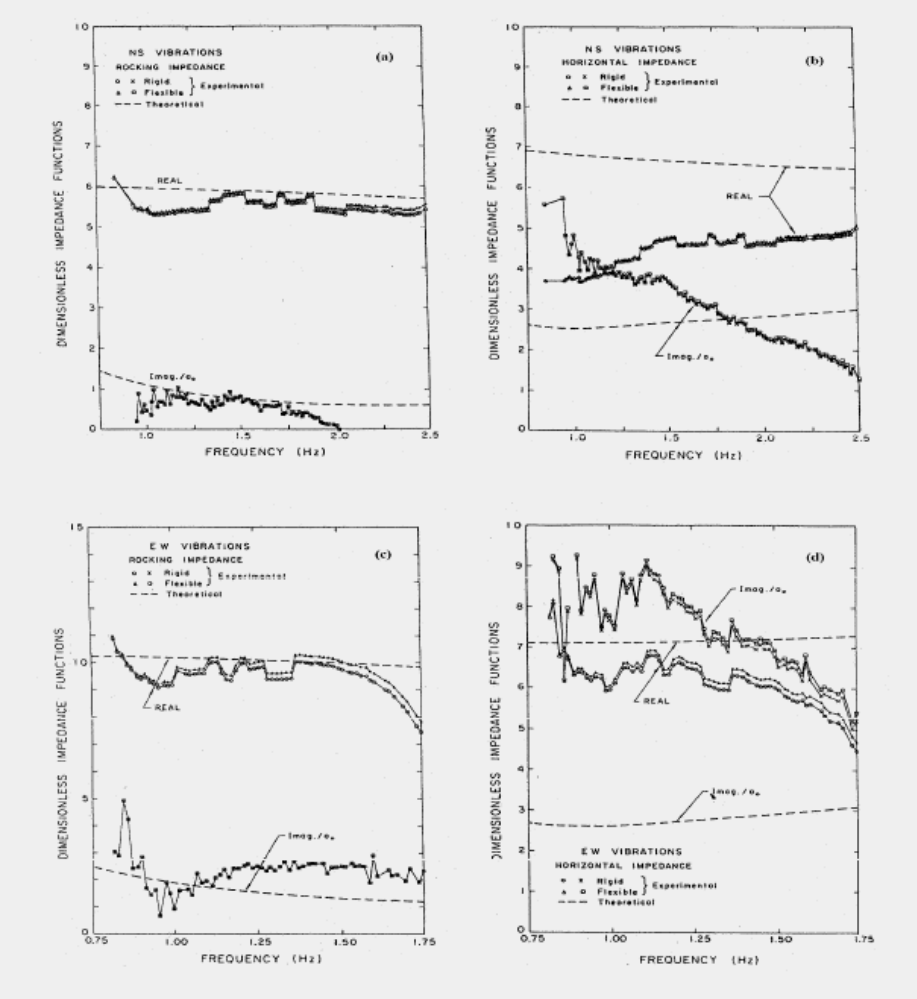

Figure 5.5: Comparison of theoretical and experimental estimates of impedance functions (after Wong et al., 1988)

de Barros and Luco (1995) evaluated impedance functions from vibration tests on the Hualien containment model. The tests were carried out in the frequency ranges of 2-20 Hz and 2-25 Hz for horizontal and vertical excitations, respectively. For the horizontal excitations, the shaker was placed at the top of the structure as well as the base of the structure. Combining the data obtained from the tests in which the shaker

was placed at the top and base of the structure allowed the estimation of translational and rotational impedance functions as well as the coupled translation and rotation impedance (referred to as $\bar{k}_{f\theta}$ and $\bar{k}_{\theta f}$). This was accomplished by setting up a system of equations in which a matrix of foundation displacements and rotations is multiplied by a vector of foundation impedance coefficients, the product being set equal to a vector of base shear forces and moments. Data from both top and base excitation is used to populate the matrices and vectors, which leads to four equations with three unknowns (the three unknowns being translational, rotational, and coupled foundation impedance; the two coupled terms $\bar{k}_{\theta f}$ and $\bar{k}_{f\theta}$ were assumed to be equal). The equations are solved in a least squares sense to estimate the impedance coefficients. Figure 5.6 compares the results obtained from the experiments to theoretical predictions. Three models were considered for the theoretical predictions (A, B and C in Figure 5.6). These models differ from one another in terms of the shear wave velocity considered at shallow depths. Model A considered the average measured shear wave velocity whereas the shear wave velocity profile for models B and C consider the effect of confining pressure due to excavation. The useful frequency range is described as 5 Hz to 14 Hz, as the data at low and high frequencies appear to be noise-dominated and were disregarded by de Barros and Luco (1995). Within this frequency range, in general the soil model "Model A" predicts the experimental data better than the other models. The tests were carried out in two directions, referred to as D1 and D2. Results show that the stiffness coefficients are higher in the D2 direction.

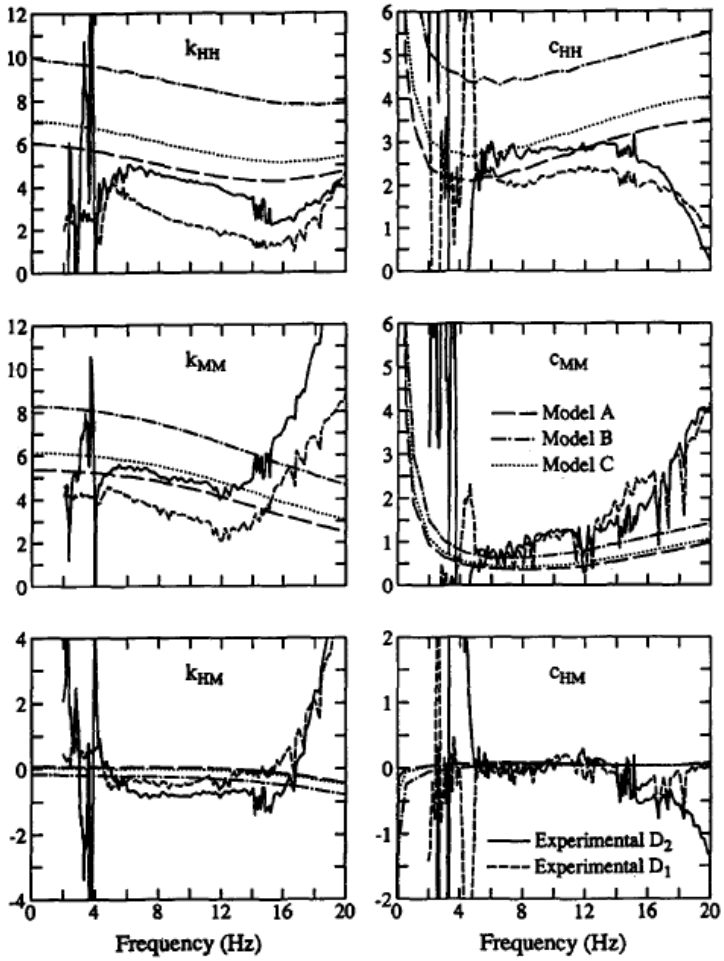

Figure 5.6 Experimental impedance functions compared to theoretical predictions for soil models A, B and C (after de Barros and Luco, 1995)

5.4 EVALUATION OF IMPEDANCE FUNCTIONS FROM FORCED VIBRATION TESTS

In this section, equations are derived for the calculation of impedance functions from measurements of acceleration in an SDOF structural system, which is depicted in

Figure 5.7. The equations of motion for the system excluding the coupled foundation damping and stiffness were given in Chapter 4 as:

$$m_s(\ddot{u}_f + h\ddot{\theta}_f + \ddot{u}_s) + m_f\ddot{u}_f + c_f\dot{u}_f + k_f u_f = F_s \text{ foundation translation} \quad (5.8)$$

$$m_s h(\ddot{u}_f + h\ddot{\theta}_f + \ddot{u}_s) + I_f\ddot{\theta}_f + c_\theta\dot{\theta}_f + k_\theta\theta_f = hF_s \text{ foundation rotation} \quad (5.9)$$

$$m_s(\ddot{u}_f + h\ddot{\theta}_f + \ddot{u}_s) + c_s\dot{u}_s + k_s u_s = F_s \quad \text{structure translation} \quad (5.10)$$

The equations include motions recorded from the structure and foundation (notation for motions is defined in Figure 5.7), the above-foundation stiffness and damping of the SDOF oscillator (k_s, c_s), masses of the SDOF oscillator and foundation (m_s, m_f), foundation moment of inertia (I_f), structure height (h), and the desired foundation stiffness and damping terms for rotational and translational vibration modes. Equations (5.8) and (5.9) contain the foundation stiffness and damping terms. Applying Fourier transforms and writing equations (5.8) and (5.9) in terms of displacements yields (overbar indicates variable in frequency domain):

$$-\omega^2 m_s\left(\bar{u}_f + h\bar{\theta}_f + \bar{u}_s\right) - \omega^2 m_f\bar{u}_f + i\omega c_f\bar{u}_f + k_f\bar{u}_f = \bar{F}_s \quad (5.11)$$

$$-\omega^2 m_s h\left(\bar{u}_f + h\bar{\theta}_f + \bar{u}_s\right) - \omega^2 I_f\bar{\theta}_f + i\omega c_\theta\bar{\theta}_f + k_\theta\bar{\theta}_f = h\bar{F}_s \quad (5.12)$$

Rearranging the equations above gives:

$$-\omega^2 m_s\left(\bar{u}_f + h\bar{\theta}_f + \bar{u}_s\right) - \omega^2 m_f\bar{u}_f + \left(\bar{k}_f\right)\bar{u}_f = \bar{F}_s \quad (5.13)$$

$$-\omega^2 m_s h\left(\bar{u}_f + h\bar{\theta}_f + \bar{u}_s\right) - \omega^2 I_f\bar{\theta}_f + \left(\bar{k}_\theta\right)\bar{\theta}_f = h\bar{F}_s \quad (5.14)$$

where, the terms $\bar{k}_f$ and $\bar{k}_\theta$ are the complex translational and rotational foundation stiffnesses, respectively, as given previously in equation (5.1) and in Figure 5.7.

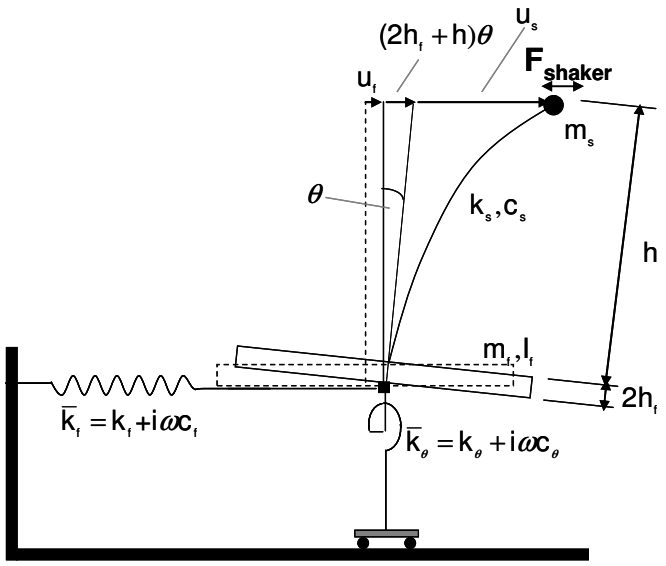

Figure 5.7 Simple SSI model for deriving impedance functions

Hence, the translational and rotational stiffness and damping can be determined by evaluating the following equations in the frequency domain:

$$\bar{k}_f = \frac{\bar{F}_s + \omega^2 m_s \left(\bar{u}_f + h\bar{\theta}_f + \bar{u}_s\right) + \omega^2 m_f \bar{u}_f}{\bar{u}_f} \tag{5.15}$$

$$\bar{k}_\theta = \frac{h\bar{F}_s + \omega^2 m_s h\left(\bar{u}_f + h\bar{\theta}_f + \bar{u}_s\right) + \omega^2 I_f \bar{\theta}_f}{\bar{\theta}_f} \tag{5.16}$$

In equation (5.15) the complex stiffness term is equal to the ratio of the base shear to the foundation displacement. The complex rotational stiffness term (5.16) is equal to the ratio of base moment to the foundation rotation. The real parts of these terms give the stiffness coefficient; the complex parts include the corresponding damping coefficient. In the next section, Equations (5.15) and (5.16) are validated using simulated data extracted from analysis of a model structure.

5.5 VALIDATION OF THE OUTLINED PROCEDURE

Before estimating impedance functions for the Garner Valley structure, the procedure outlined for calculating impedance functions is validated. This validation is similar to the one presented in Section 4.5. The response of a soil-structure system is calculated for a prescribed load history, with the soil-foundation interaction represented by theoretical impedance functions. Using the simulated responses, impedance coefficients are calculated using equations (5.15) and (5.16). The soil-structure system matches System 1 in Chapter 4 (Figure 4.5). The results are depicted in Figure 5.8 and 5.9 for the stiffness and damping coefficients respectively. It was found that theoretical impedance values can be back calculated exactly with equations (5.15) and (5.16).

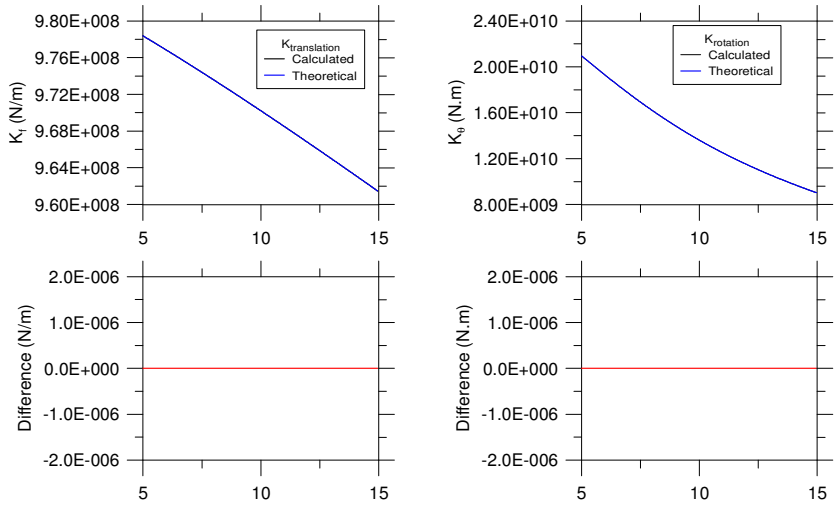

Figure 5.8 The assumed theoretical and back calculated translational and rotational stiffness

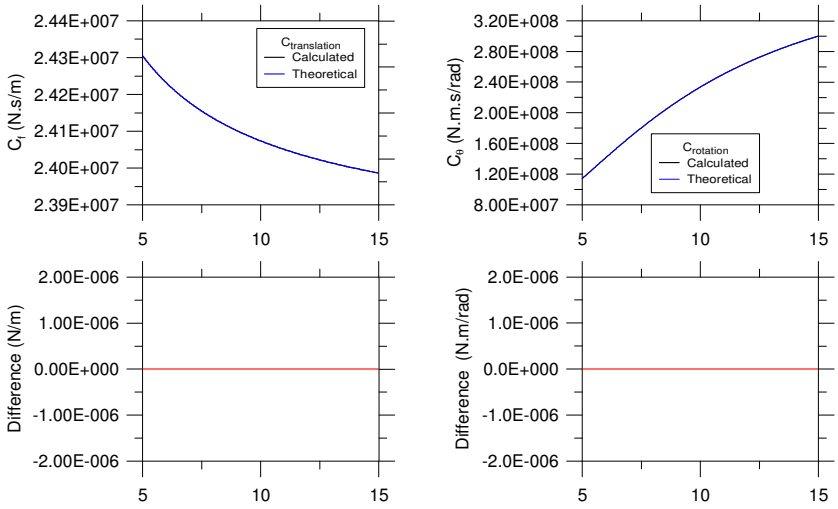

Figure 5.9 The assumed theoretical and back calculated translational and rotational damping

One of the shortcomings of using equations 5.15 and 5.16 to calculate impedance coefficients is that they do not include the coupled translational-rotational stiffness terms. To investigate the errors associated with this simplification, the verification

analysis is repeated by this time considering the coupled impedance terms in the response analysis. The motions computed from this analysis are entered into equations 5.15 and 5.16, which produces the results shown in Figures 5.10 and Figure 5.11. As expected, the back calculated values do not match the assumed values. However, the results are close (errors < 9%).

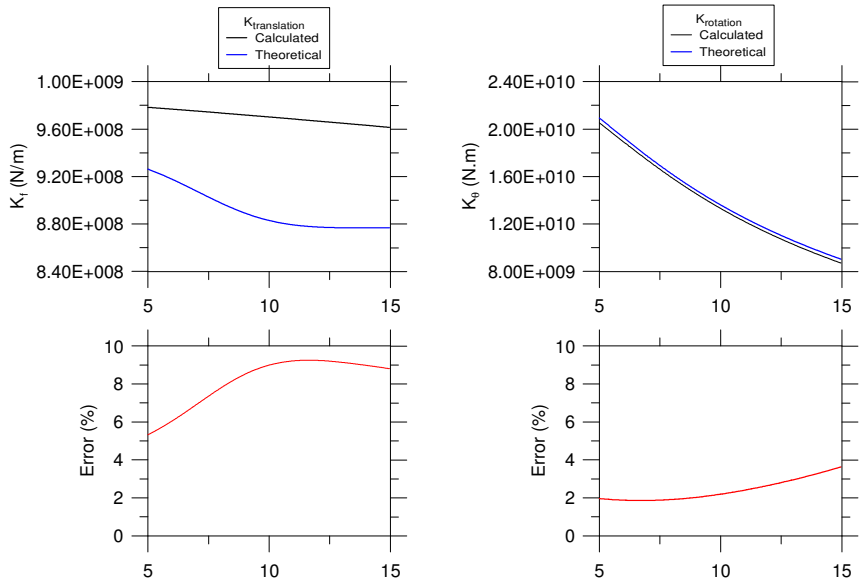

Figure 5.10 The assumed theoretical and back calculated translational and rotational stiffness

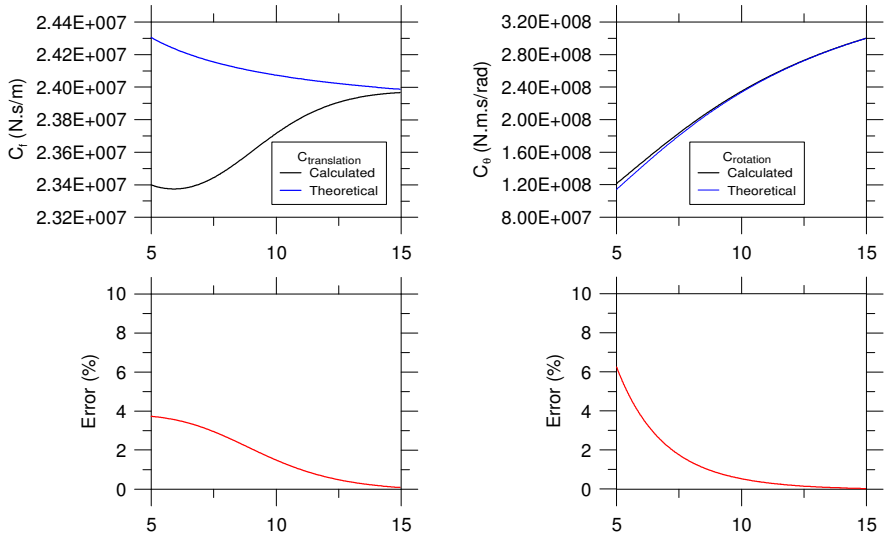

Figure 5.11 The assumed theoretical and back calculated translational and rotational damping

5.6 APPLICATION OF PROCEDURES TO GARNER VALLEY TEST STRUCTURE

5.6.1 Structure and site overview

In this section, the procedure outlined in Section 5.3 is applied to the Garner Valley test structure, which is shown in Figure 4.7. The structure can be configured with or without steel bracings in the direction of shaking, and both conditions are considered here. Forced vibration tests were carried out on the test structure using the shaker mounted at the bottom of its roof. Figure 5.12 shows a schematic of the structure and the sensors used to evaluate impedance functions. The condition depicted in Figure 5.12 is without bracings in the direction of shaking. The shaker acceleration used in calculating the shaker force is recorded with Sensor 13. The top of foundation

acceleration is recorded with Sensor 1, while the top of structure acceleration is recorded with Sensor 4. Foundation rotation is calculated by taking the difference of two vertical sensors located on opposite sides of the foundation and dividing by the horizontal distance between the sensors. The shaker force is in the North-South direction and therefore the rotation is calculated from the difference of Sensors 10 and 8 (or Sensors 11 and 7).

As shown in Figure 5.13, the site soil conditions consist of a thin layer of organics underlain by silty sand extending to a depth of 18 *m*, which then transitions to decomposed granite. Relatively intact crystalline bedrock occurs at a depth of 88 *m*. The ground water table is at the surface in rainy seasons and drops to about 3 *m* in dry seasons. Geophysical tests (suspension logging and SASW) have been carried out to measure P-wave and S-wave velocity profiles in the free-field (i.e., away from the structure). As shown in Figure 5.13, the SASW analysis indicates near-surface shear wave velocity of approximately V_s = 207 *m/s*.

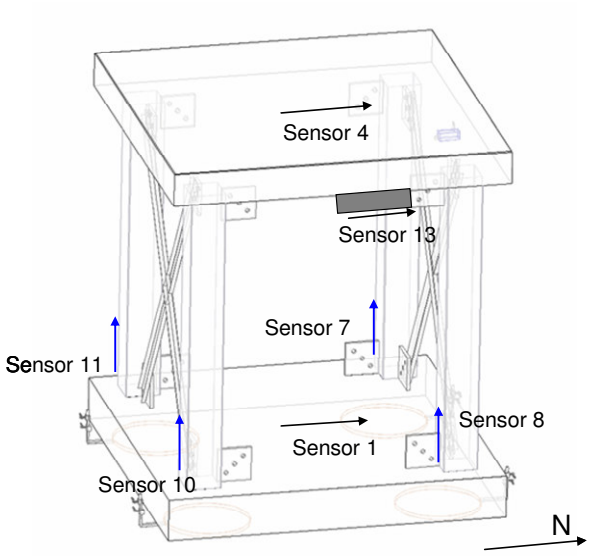

Figure 5.12 Schematic of test structure and the sensors used to evaluate impedance functions

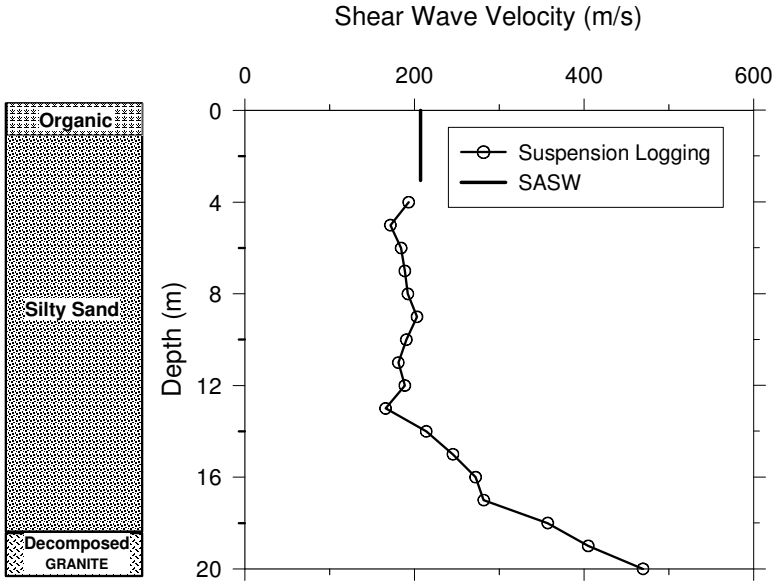

Figure 5.13 Near surface soil profile with shear wave velocities obtained from suspension logging and SASW tests

5.6.2 Theoretical impedance functions

An important variable in calculating theoretical impedance functions for a soil-structure system is the shear wave velocity (V_s) taken to represent the properties of an equivalent halfspace. As stated earlier, NEHRP (2003) guidelines recommend the use of an average V_s over effective depths of $0.75\times r_f$ for translation and $0.75\times r_\theta$ for rocking impedance coefficients. This provides effective depths of 1.72 m from the surface for both translational and rocking modes for the Garner Valley test structure. The SASW test carried out in Garner Valley predicts constant V_s of 207 m/s for 3 m from the surface. However these measurements were taken in the free-field (yet close to the structure) and do not include the additional stress due to the structure's weight. General correlations for soil shear modulus (G) indicate a dependence on mean effective stress (σ_m') as follows (Seed et al., 1986):

$$G = 1000 K_2 \sqrt{\sigma_m'} \tag{5.17}$$

where K_2 is a dimensionless parameter related to the relative density of the soil. For the Garner Valley site, G is calculated from equation (5.17) first with respect to the free-field overburden pressure only (equation 5.18), and next for the combined pressure of overburden and structural self weight (equation 5.19).

$$\rho V_s^2 = 1000 K_2 \sqrt{\sigma_o'} \tag{5.18}$$

$$\rho V_{s,new}^2 = 1000 K_2 \sqrt{\sigma_o' + \Delta\sigma_s} \tag{5.19}$$

The term $\Delta\sigma_s$ in equation (5.19) is the depth-dependent vertical stress increment associated with the structure's self weight. Classical elastic solutions allow evaluation of $\Delta\sigma_s$ under the corner of a rectangular loaded area using influence factors (e.g., Fadum, 1948), and superposition enables evaluation of $\Delta\sigma_s$ in intermediate areas beneath a slab. The new V_s at any depth is calculated by taking the ratio of equation (5.19) to equation (5.18). Note that the density term ρ and relative density term K_2 drop out in the ratio. Figure 5.14 shows the original (SASW) V_s profile and the modified V_s profile evaluated in the manner described above.

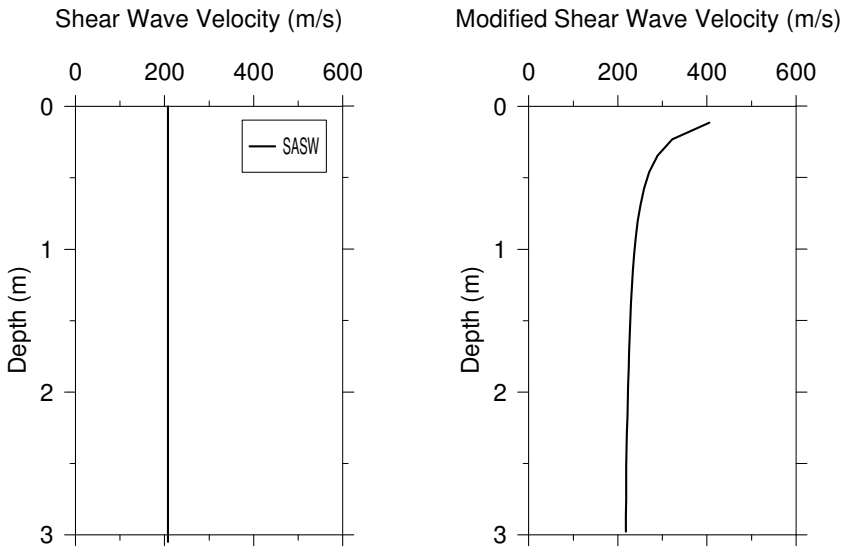

Figure 5.14 The SASW test data and shear wave velocity profile at the corner of the foundation modified to consider effects of structure self-weight

The effective halfspace shear wave velocity to be used in the theoretical equations is calculated as the ratio of effective depth to shear wave travel time through that

effective depth. Using the modified V_s profile and an effective depth of 1.72 m, an effective V_s of 236 m/s is found.

5.6.3 Analyses of impedance functions for model test structure

Impedance coefficients calculated from the unbraced structure are presented first. The forced vibration test was a fast sweep in the frequency range of 15-5 Hz over a time increment of 60 sec. Figure 5.15 shows the acceleration histories of the motions used in the calculation of impedance functions. The bottom-of-foundation motion in the figure is obtained by subtracting the contribution of rocking from the translation recorded at the top of the foundation.

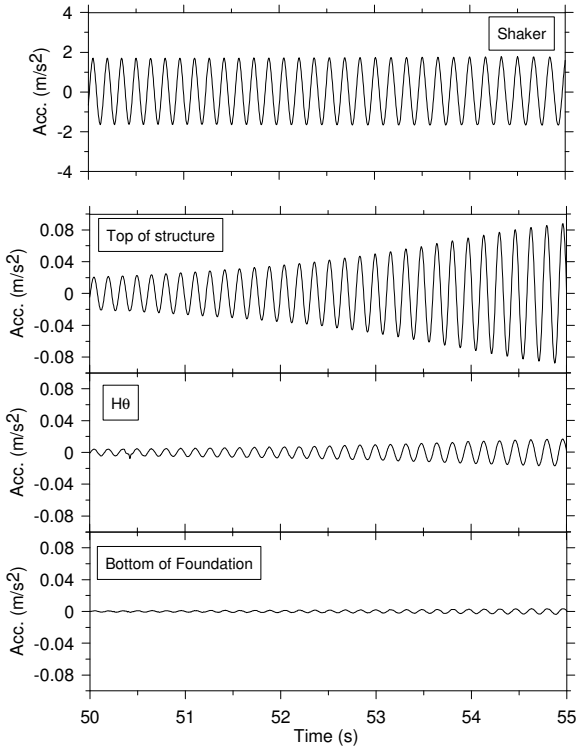

Figure 5.15 Motions used in analysis of impedance functions (data from unbraced structure)

Fourier transformation of the motions in Figure 5.15 is performed without zero padding and equations (5.15) and (5.16) are used to calculate impedance functions. Figures 5.16 and 5.17 depict the translational and rotational impedance functions, respectively. Also shown in those figures are predictions of theoretical impedance function models for a uniform halfspace with effective V_s=236 m/s. The data and model predictions are generally consistent at the lower end of the tested frequency band (near 5 Hz). This suggests that the static stiffness predicted by the theoretical models is consistent with the data, indicating that the effective V_s used in the calculations is likely reasonable. However, the data show a stronger reduction of stiffness and damping with frequency than predicted by the models.

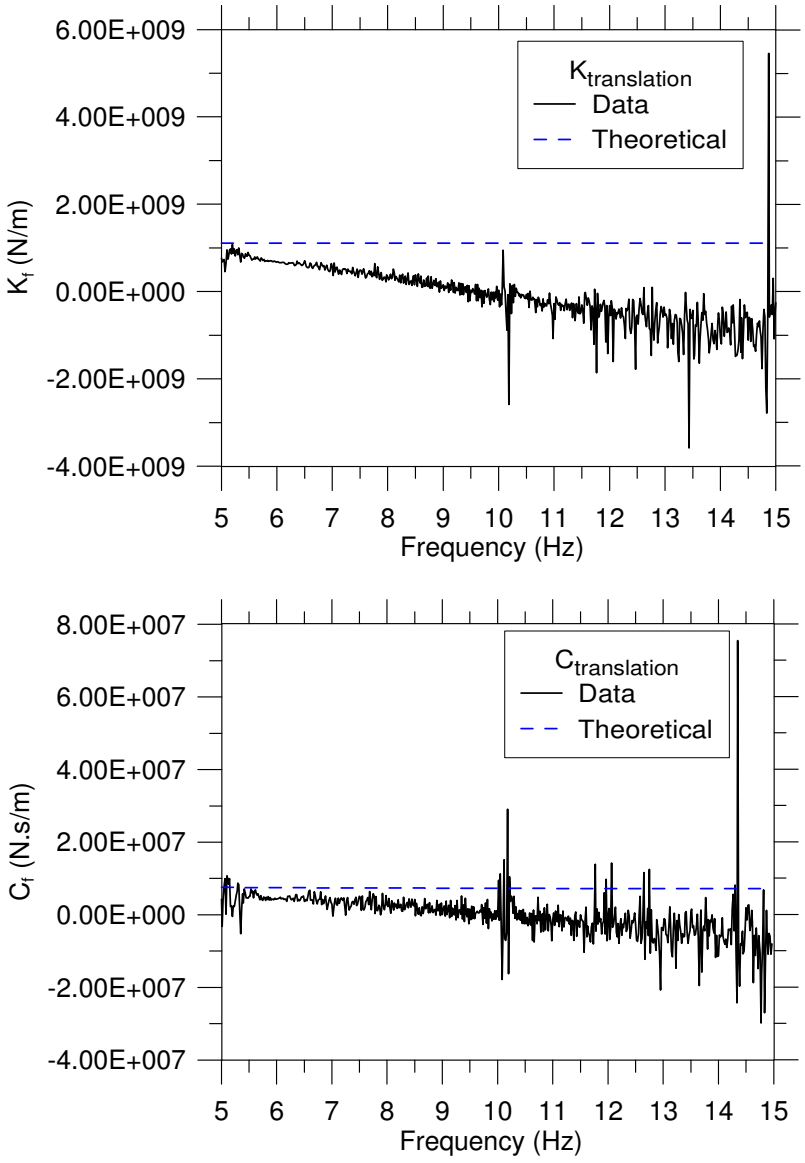

Figure 5.16 Translational impedance functions from data (unbraced structure) and theory

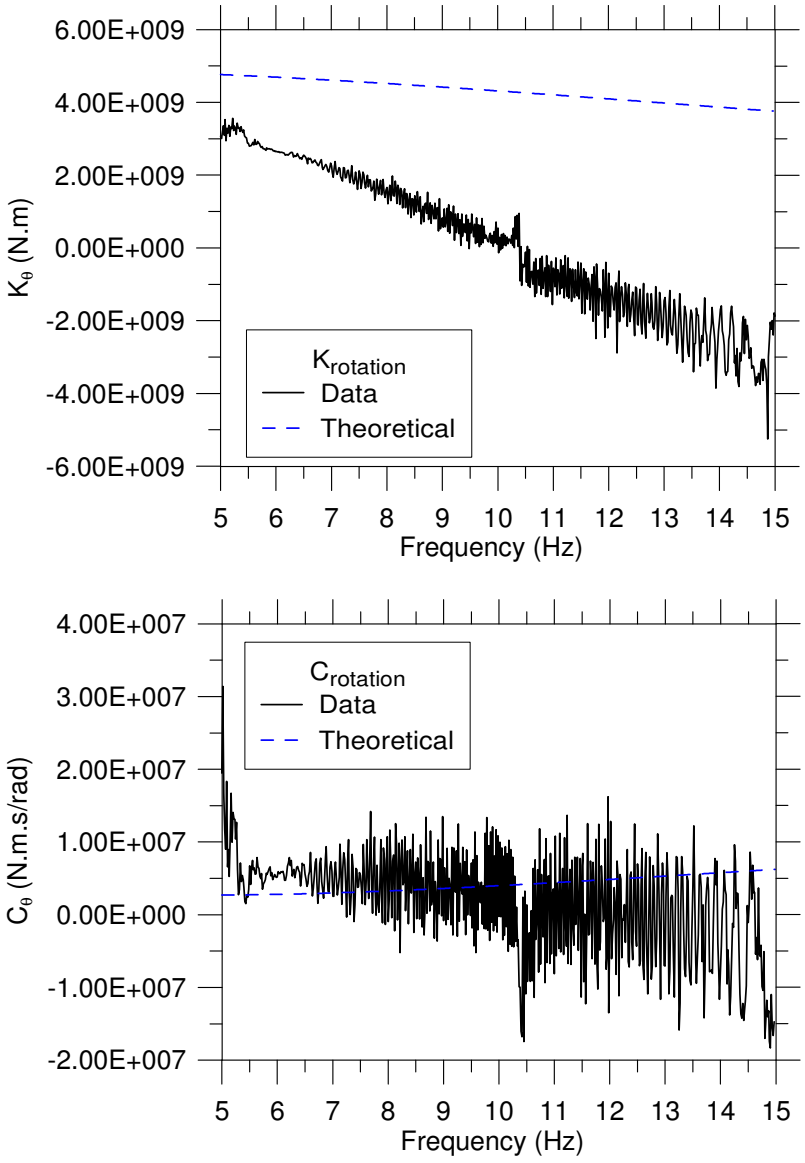

Figure 5.17 Rotational impedance functions from data (unbraced structure) and theory

Two types of tests were carried out on the braced structure. In addition to the 60 second sweep tests (fast sweep) from 15-5 Hz (the same tests that were carried out on the unbraced structure), harmonic tests at a series of individual frequencies were

conducted. As opposed to the fast sweep tests, the harmonic tests involve shaking the structure at a single frequency until a steady state response is reached. Similar to the fast sweep tests, shaker forces were applied to the structure over the frequency range of 5-15 Hz in the harmonic tests. Results of both the fast sweep and harmonic tests are shown in Figures 5.15 and 5.16 for translational and rotational impedance functions, respectively. As before, also shown are the predictions of theoretical impedance function models using an effective halfspace V_s=236 m/s.

As shown in Figures 5.18-5.19, the data from the braced structure are remarkably consistent for the fast sweep and harmonic tests. As with the unbraced structure, the impedance coefficients estimated from data are consistent with theoretical estimates at the end of the tested frequency band, but show a faster decay of stiffness and damping with frequency than implied by the halfspace model.

As described above, data from both the braced and unbraced structure show some departures from theoretical predictions. While the theoretical predictions are identical for both structure configurations, the impedance coefficients implied by the data are not identical. The braced and unbraced experiments were carried out on the same day for both structural configurations, which reduces the opportunity for variability in environmental conditions to affect the results. Figures 5.20-5.21 show the experimental impedance coefficients for both configurations. The low-frequency (5 Hz) ordinates are nearly identical, except for the case of rotational stiffness. However, the reduction of stiffness and damping with frequency is faster for the unbraced structure than for the braced structure. This is especially the case for stiffness ordinates, with damping values

for the two cases being relatively comparable. These results are discussed further in Section 5.8.

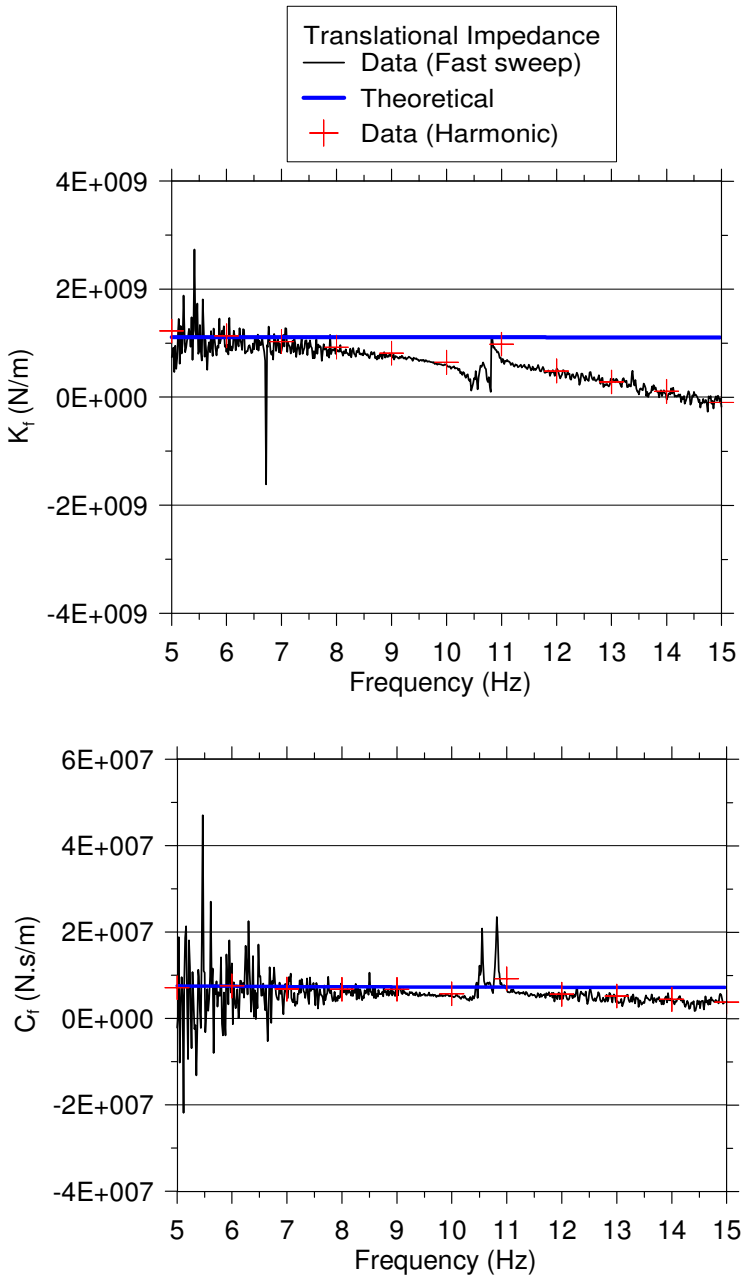

Figure 5.18 Translational impedance functions from data (60 second sweep and full harmonic test on braced structure) and theory

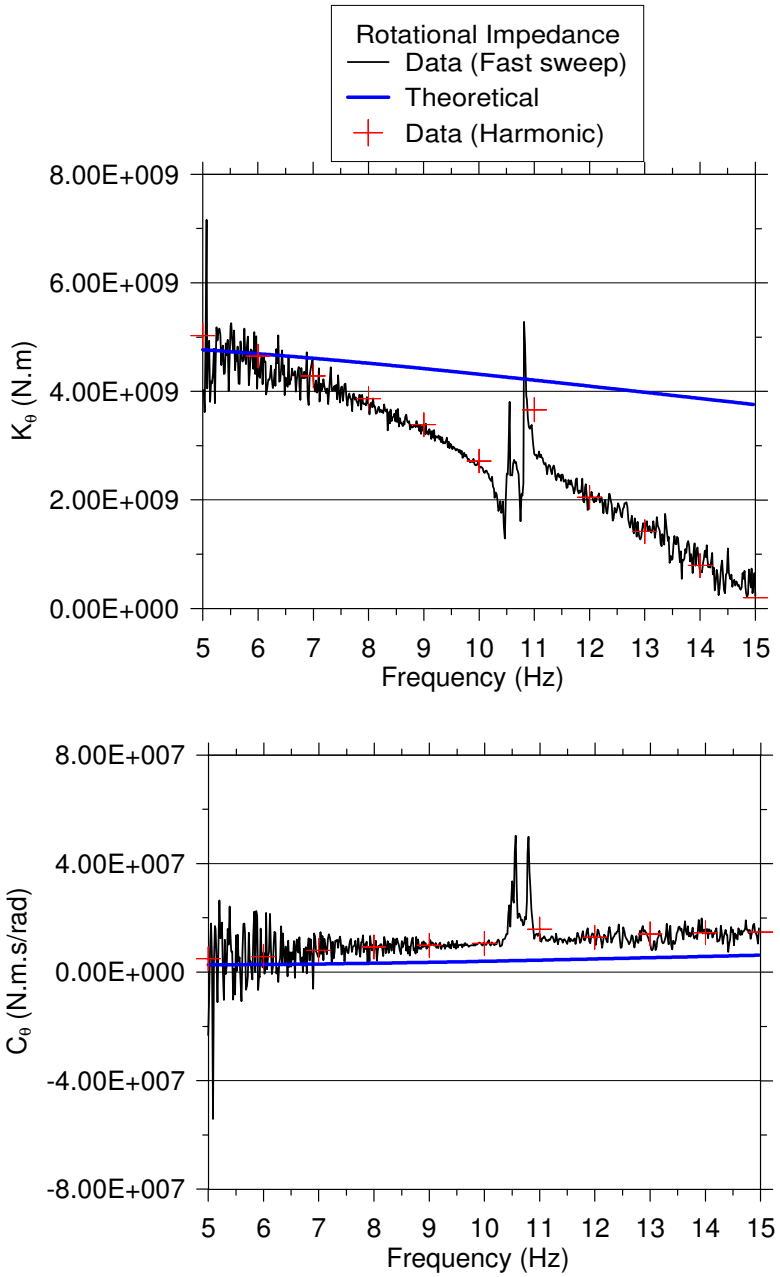

Figure 5.19 Rotational impedance functions from data (60 second sweep and full harmonic test on braced structure) and theory

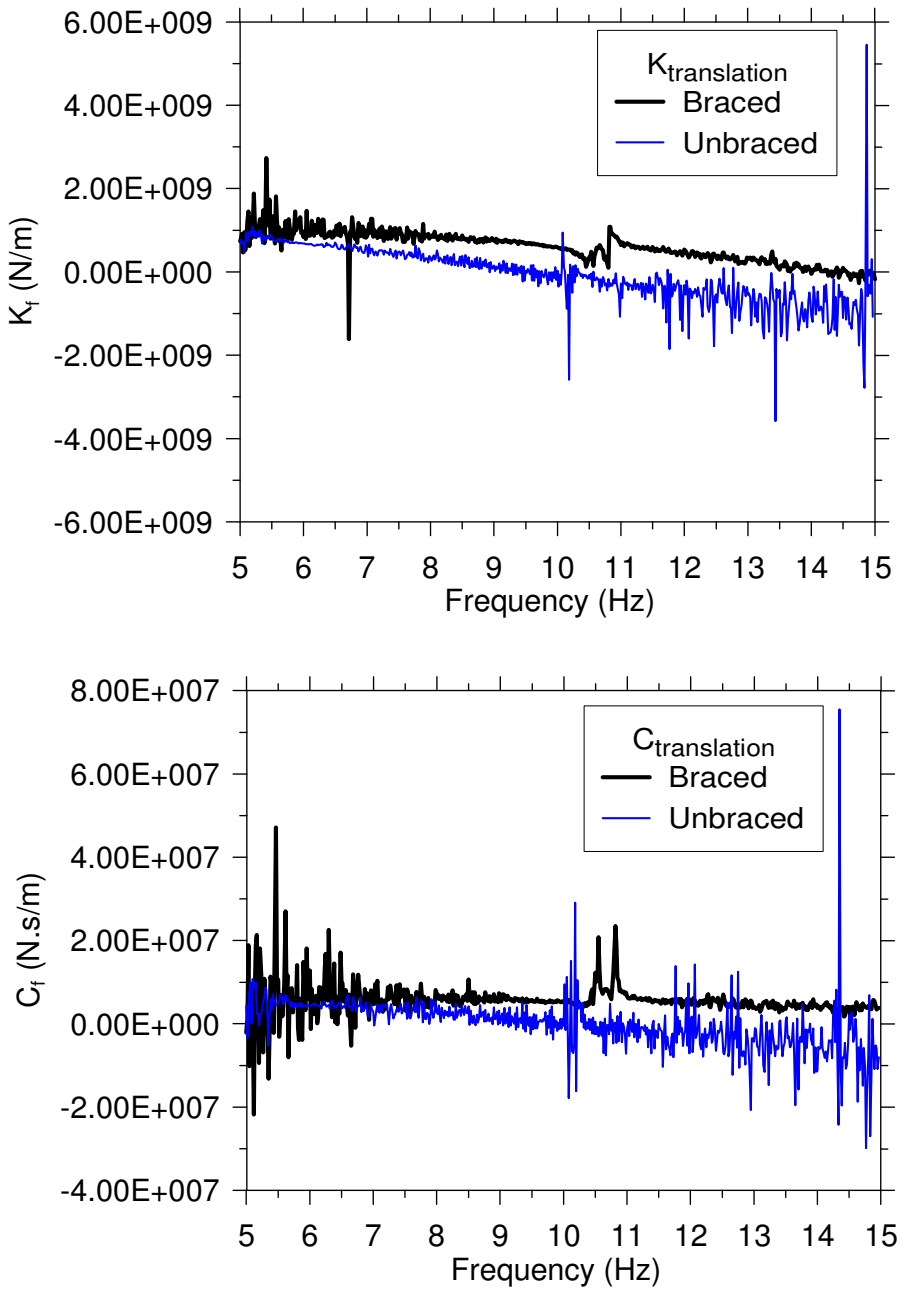

Figure 5.20 Comparison of translational impedance functions estimated from the braced and unbraced structural configurations

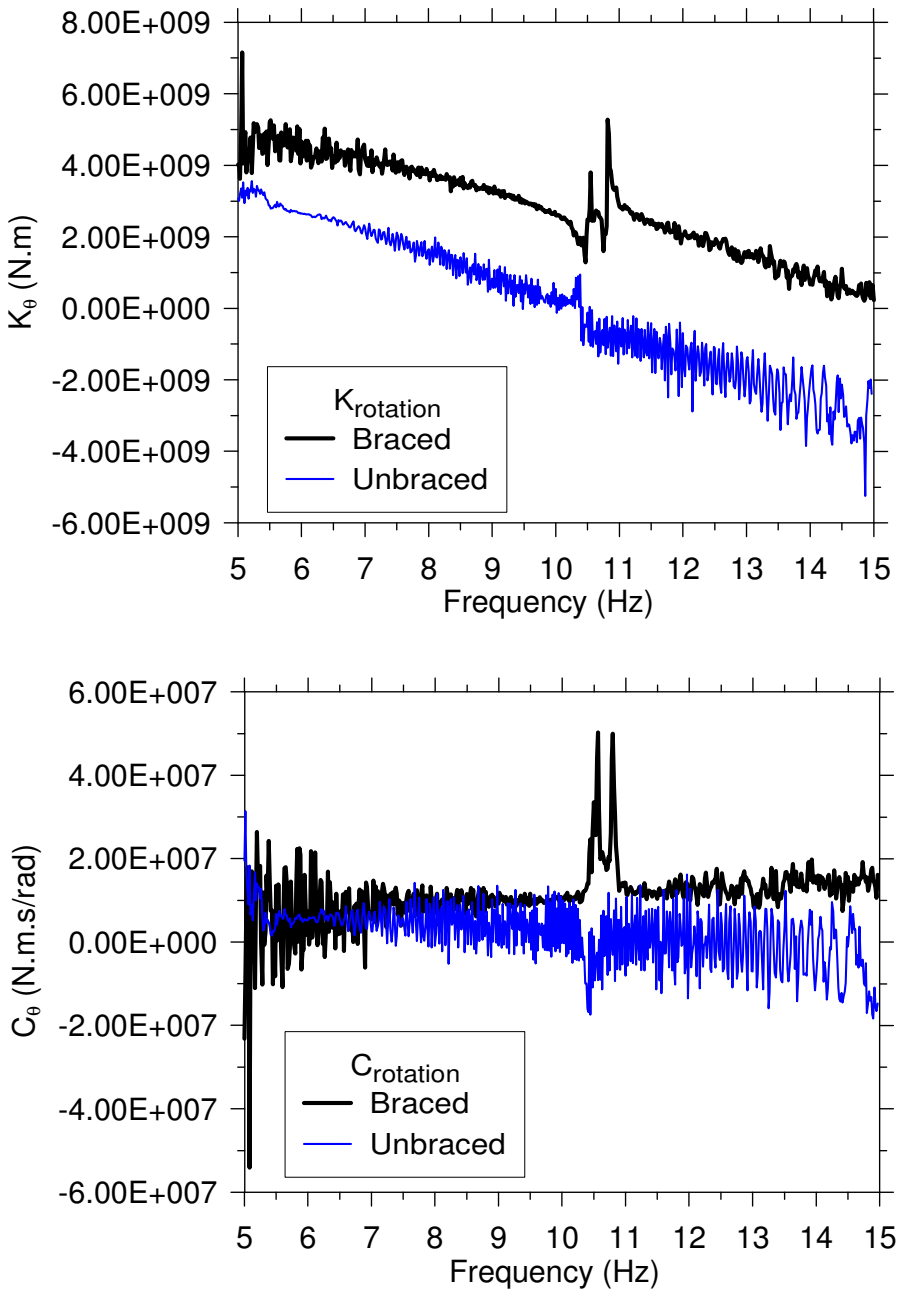

Figure 5.21 Comparison of rotational impedance functions estimated from the braced and unbraced structural configurations

5.7 EFFECT OF GROUND WATER TABLE LEVEL ON IMPEDANCE FUNCTIONS

The study presented in the preceding section is taken a step further to investigate an important environmental effect, namely the depth of the ground water table. Rainfall data and ground water table level measurements were recorded at the Garner Valley site for a 2 month period between January 2008 and March 2008. During this period the structure was unbraced. Figure 5.22 shows the rainfall data and the ground water depth. Several dates were selected in which the ground water table was high, at moderate depth, and deep (marked with "x" on Figure 5.22). Sweep tests were carried out on those dates and impedance coefficients were calculated. Translational and rotational impedance values obtained at various dates are shown in Figures 5.23-5.24.

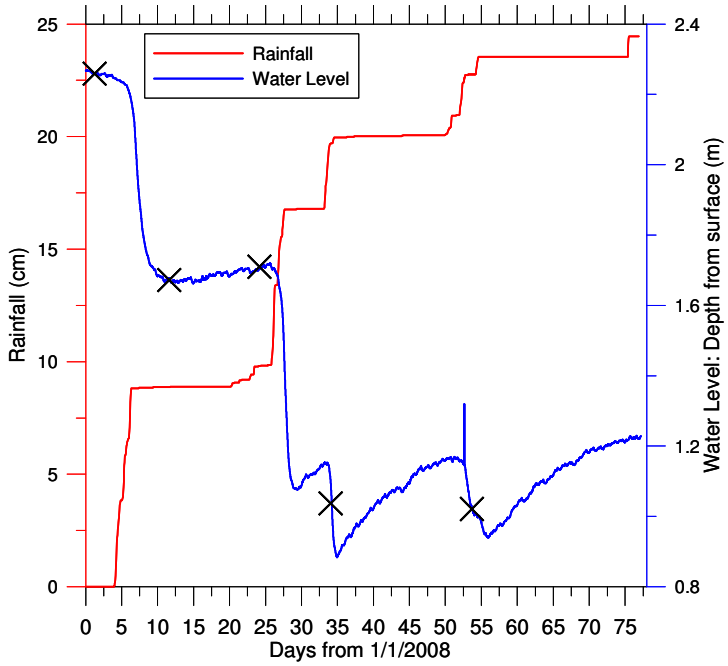

Figure 5.22 Rainfall and ground water table depth at the Garner Valley site

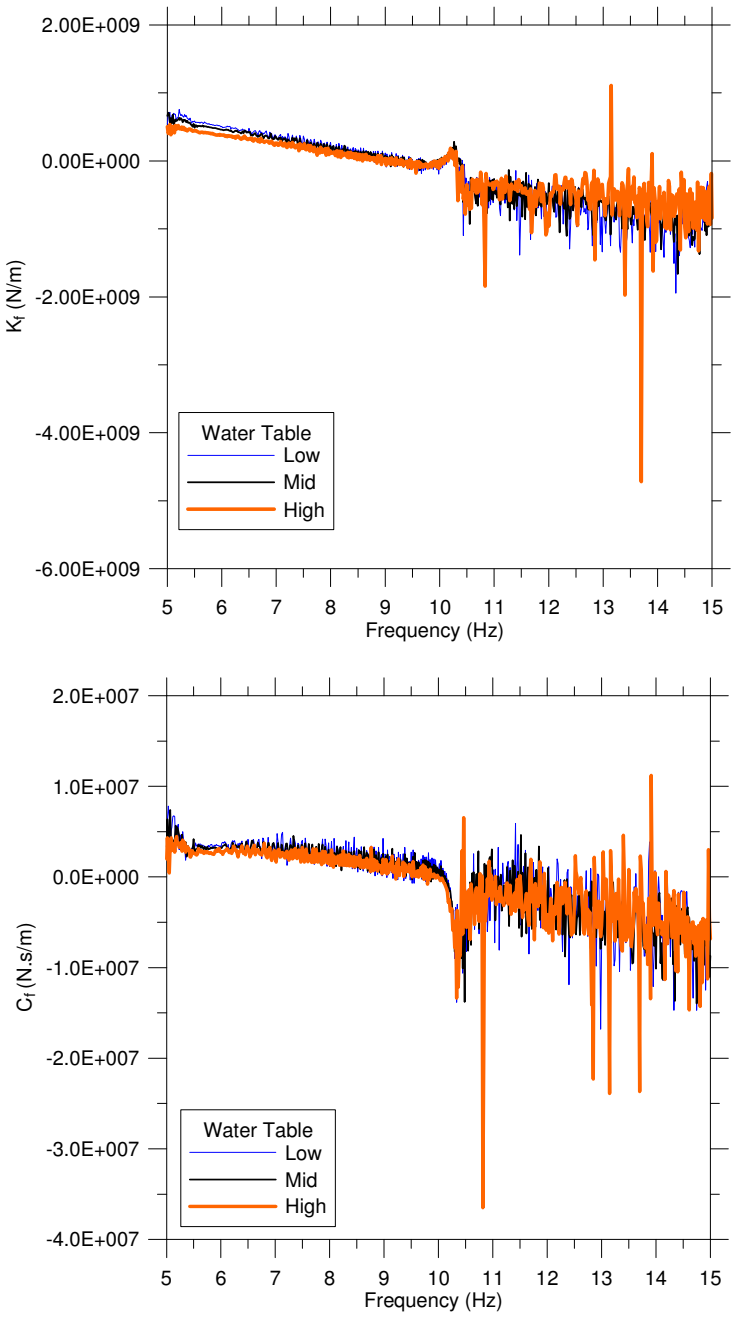

Figure 5.23 Translational impedance coefficients for different ground water depths

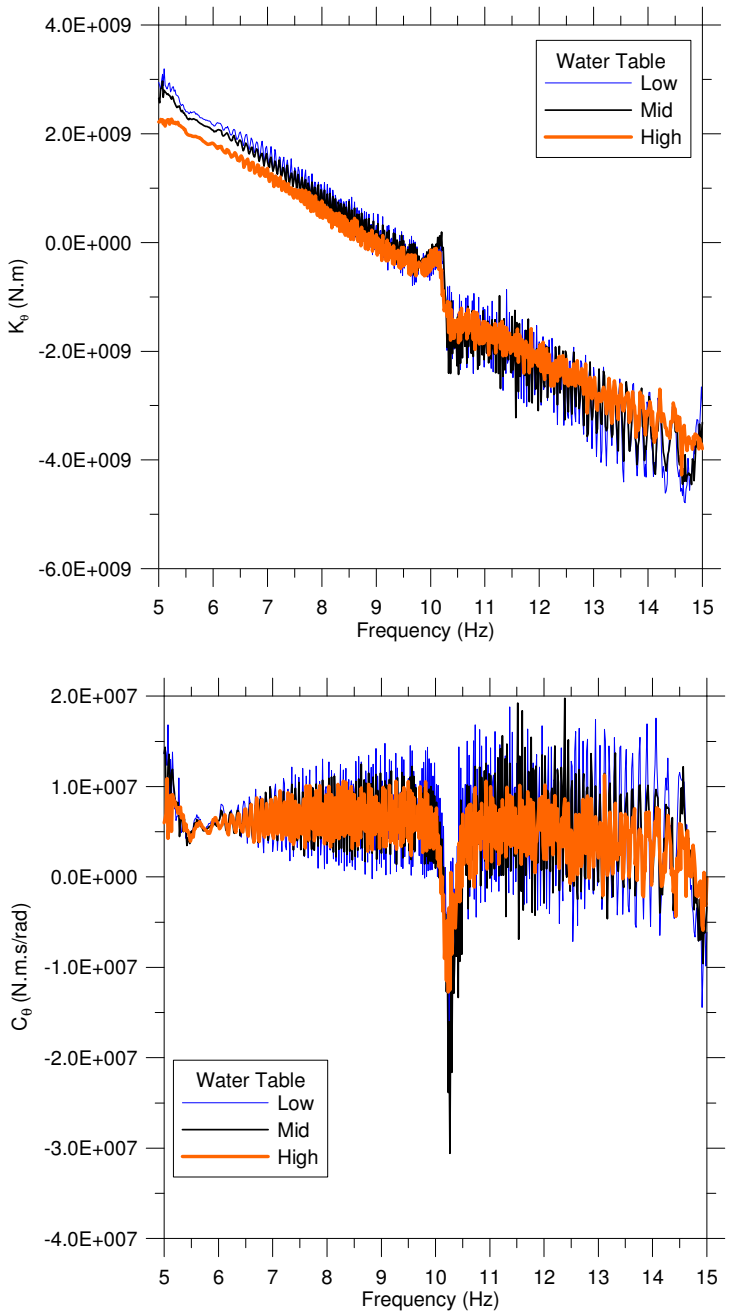

Figure 5.24 Rotational impedance values for different ground water depths

In the examination of this data, it is important to consider whether the small variations that are observed from date-to-date are random or systematically related to

water table depth. To provide insight into the variability for a given water table depth, I show in Figure 5.25 the rotational stiffness for nearly common depths. The two results are seen to nearly overlie each other. Similar results are obtained for other impedance coefficients. Hence, the date-to-date variability for a given water table depth is small. Looking then again at the results in Figures 5.23-5.24, we see a systematic decrease in the low-frequency (near 5 Hz) stiffnesses as the water table rises. This is consistent with reduced effective stress associated with reduced matric suction in the vadose zone. These variations in stiffness are not significant (or are within the data scatter) at high frequencies (higher than approximately 10 Hz). Interestingly, the damping coefficients show no clear dependence on water table depth.

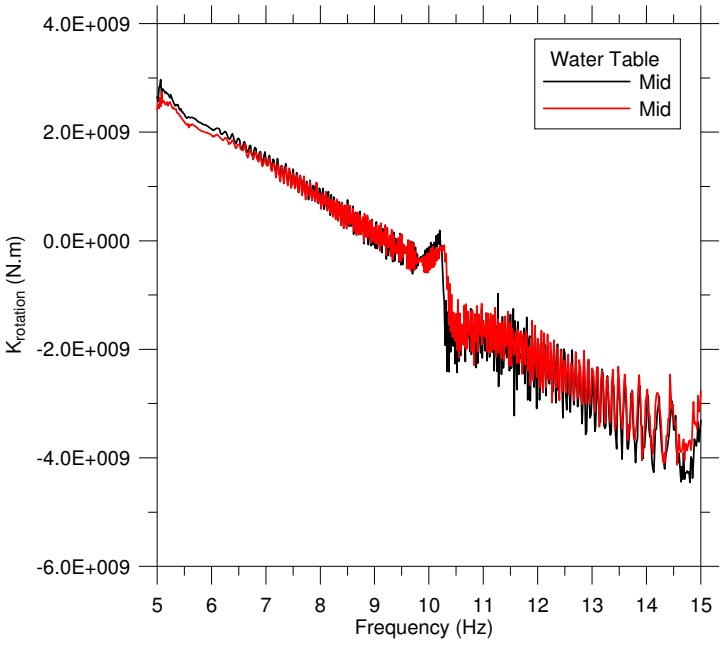

Figure 5.25 Rotational stiffness at two dates for ground water table at approximately common depths

5.8 DISCUSSION

This section focuses on the interpretation of several features of the results that are not immediately intuitive. These include:

1. Impedance coefficients evaluated from data for the braced and unbraced structure were different. The differences are especially noteworthy for the rotational and translational stiffnesses. Given that the tests for the braced and unbraced configurations were conducted on the same day, in which the environmental effects (ground water table level) are essentially the same, the results are somewhat surprising.
2. The experimental impedance coefficients show a faster reduction with frequency than is predicted by theoretical models for a halfspace.
3. Negative damping is obtained from the unbraced structure at frequencies higher than approximately 10 Hz. This is not observed for the braced structure although there are a few negative spikes. The physical meaning of negative damping is unclear.

When faced with somewhat surprising phenomena such as these, one must first check carefully the results to make sure they are reliable. There are several possible sources of bias that I examined. One is the effect of noise in the measurements. If the measurements are noise-dominated over a portion of the considered frequency range, then those results are unreliable. Another possible issue is limitations of the model of the structure used to derive equations (5.15) and (5.16). In particular, the model does

not incorporate coupling stiffness terms and there is potential sensitivity to uncertain fixed base stiffness and damping terms. After discussing these issues, I investigate more deeply the frequency dependence of the stiffness and damping, to highlight the time-domain characteristics associated with phenomena such as negative stiffness and damping as well as unusual spikes in the results. Finally, this chapter is concluded with speculation as to physical mechanisms that may be responsible for the observed trends.

5.8.1 Noise effects

The forced vibration tests were carried out for both structural configurations in the frequency range of 5-15 Hz. The braced structure has a flexible-base frequency of 10 Hz whereas the unbraced structure has a flexible base frequency of 6 Hz. In order to confirm that the results obtained are reliable, the signal and noise is compared in this section. The signals considered are the top of foundation acceleration and foundation rotation since the denominators of Equations (5.15) and (5.16) are essentially calculated from these terms. The noise for these terms is taken from data recorded immediately prior to the experiments. Figure 5.26 and Figure 5.27 show the Fourier amplitude spectra of the considered signal and the associated noise for the unbraced and braced structure configurations, respectively. For the unbraced structure, the signal power for the translations is near the noise for frequencies beyond approximately 10 Hz. For rotations, the signal remains comfortably above the noise over the full range of frequencies. In the case of the braced configuration, the signal spectrum comfortably exceeds the noise over the full 5-15 Hz frequency range. The relatively high S/N ratio

for the braced structure likely results from more significant SSI in this case, which causes larger foundation displacements. Non-physical results for the unbraced structure at high frequencies (such as apparent negative damping) are not considered to be reliable as a result of the low S/N ratio.

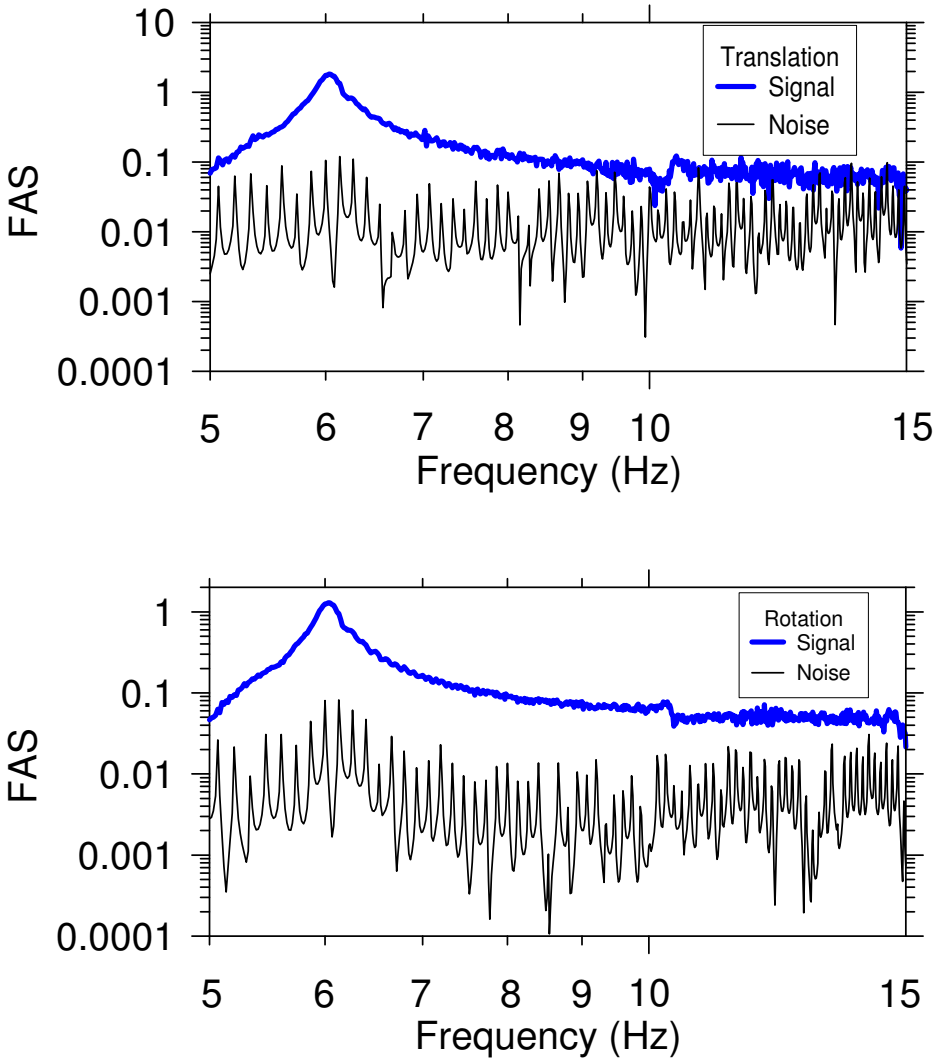

Figure 5.26 Fourier amplitude spectra of signal and noise (unbraced structure)

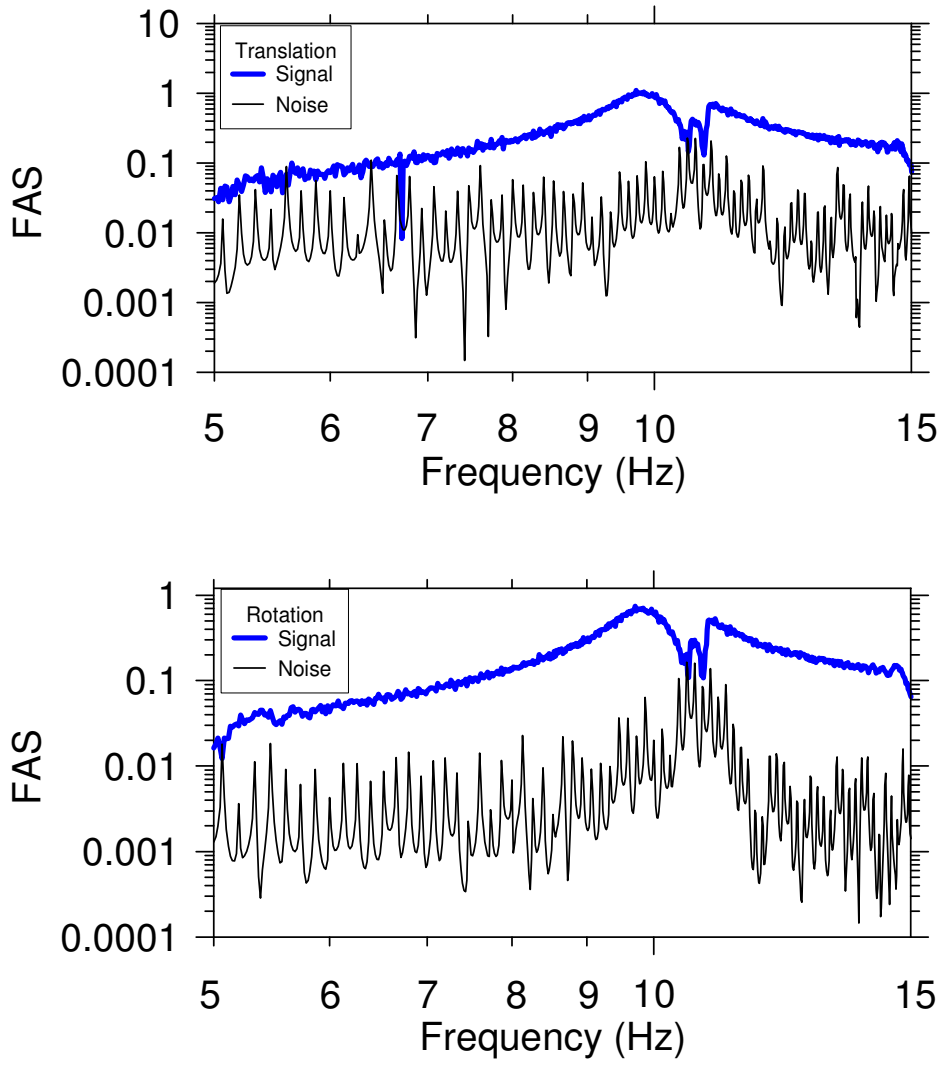

Figure 5.27 Fourier amplitude spectra of signal and noise (braced structure)

5.8.2 Limitations of underlying physical model

The physical model of the soil-foundation-structure system used to derive equations (5.15) and (5.16) is not a perfect representation of the true structure in the field. We have considered whether omissions from this model may have led to bias in

the inferred impedance coefficients. One obvious omission is the coupling impedance terms, which have a minor effect as shown previously in Section 5.5.

5.8.3 Time-domain interpretation of trends in impedance coefficients

The negative stiffness values obtained from the experimental data are due to the base shear and base moment being out of phase with the foundation displacement and foundation rotation, respectively. This can be illustrated most clearly with the harmonic test data for the braced structure. In Figure 5.15 it can be observed that the translational impedance becomes negative at 15 Hz for both the fast sweep test and the full harmonic test. Figure 5.28 shows the base shear and displacements (the numerator and denominator, respectively, of Equation 5.15) when the system is harmonically excited at 15 Hz. It can be observed that at the time of the peaks of the base shear force the displacement is negative. Hence, the force and displacement are more than 90 degrees out of phase, causing the negative stiffness.

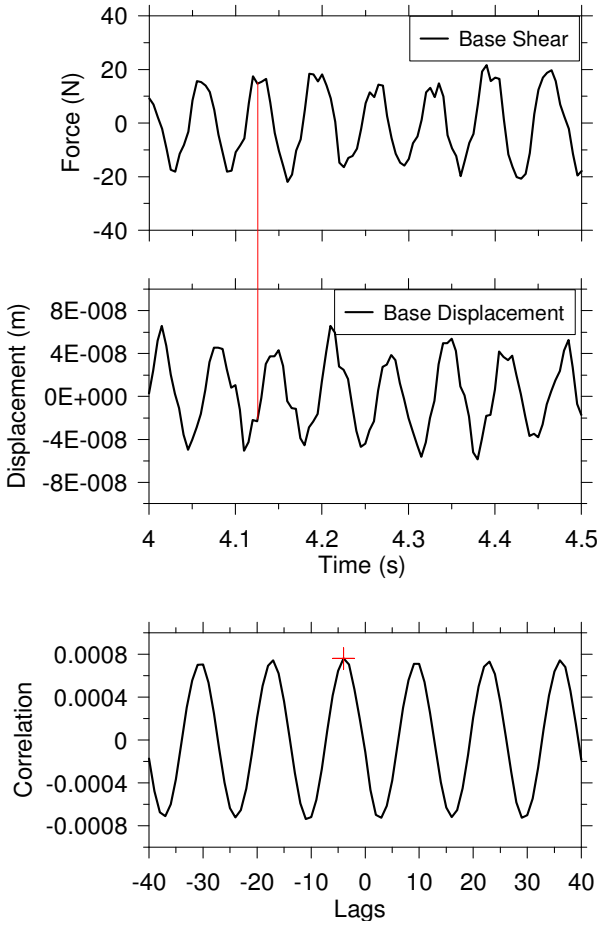

Figure 5.28 Base shear and foundation base displacement at 15 Hz and the cross correlation of the two signals (braced structure)

As described earlier the complex stiffness term is composed of the real part which is essentially the stiffness coefficient and the imaginary part which includes the damping coefficient (Equation 5.1). For both translation and rotational modes, stiffness and damping coefficients are related through the phase shift ϕ:

$$\tan \phi_j = \frac{\omega c_j}{k_j} \tag{5.20}$$

where *j=f* for translation and *j=*θ for rotation. Writing equation (5.1) for the translational mode yields $\bar{K}_f = k_f + i\omega c_f$. This equation may be written in the form:

$$\bar{K}_f = r_f e^{i\phi_j} \tag{5.21}$$

where, $r_f = \sqrt{k_f^2 + \omega^2 c_f^2}$

Term ϕ_j in equation (5.20) is the phase shift between the base shear and base displacement or base moment and base rotation. This can be shown by examining the base shear and base displacement, or the base moment and base rotation, in the frequency domain. For brevity, the verification is shown for base shear ($\bar{F}$) and base displacement ($\bar{U}$) only:

$$\begin{aligned} \bar{F} &= a + ib = r_1 e^{i\phi_1} \\ \bar{U} &= c + id = r_2 e^{i\phi_2} \end{aligned} \tag{5.22}$$

where, $r_1 = \sqrt{a^2 + b^2}$, $r_2 = \sqrt{c^2 + d^2}$ and ϕ_1 and ϕ_2 are the phase angles of the force and displacements. The complex translational impedance then becomes:

$$\bar{K}_f = \frac{r_1}{r_2} e^{i(\beta)} \tag{5.23}$$

where, $\beta = \phi_1 - \phi_2$. For equations (5.21) and (5.23) to be equal, the real parts and the imaginary parts of the equation have to be equal. Hence $r_f = r_1 / r_2$ and $\beta = \phi_f$. Hence, the phase angle observed from non-parametric system identification using equation (5.15) is the phase difference between base shear and foundation displacement.

Similarly, the phase angle derived from equation (5.16) is the phase difference between base moment and rotation.

The above concepts are illustrated with an artificial data set consisting of two arbitrary sine waves, one being the base shear and the second being the displacement. Both signals have a frequency of 5 Hz. The displacement signal is defined to lag the sine signal by 0.005 seconds. Figure 5.29, shows the sine waves as well as the cross-correlation of the motions, which yields a 0.005 second lag of displacement with respect to the force (as defined). Performing a Fourier transform of the signals yields:

$$\begin{aligned} \overline{F} &= -7.8217\times10^{-1} - i4.982\times10^{3} \\ \overline{U} &= -3.1236\times10^{2} - i1.9683\times10^{3} \end{aligned} \tag{5.22}$$

The phase angle of the force $\overline{F}$ is $\phi_1 = 1.571$ whereas it is 1.413 radians for the displacement $\overline{U}$. The difference β of these angles is 0.158. The complex impedance is defined as the ratio of the force $\overline{F}$ to the displacement $\overline{U}$:

$$\overline{K} = 2.4690 + i0.3914 \tag{5.23}$$

The phase angle ϕ for the complex impedance term is found to be 0.158 radians, matching β.

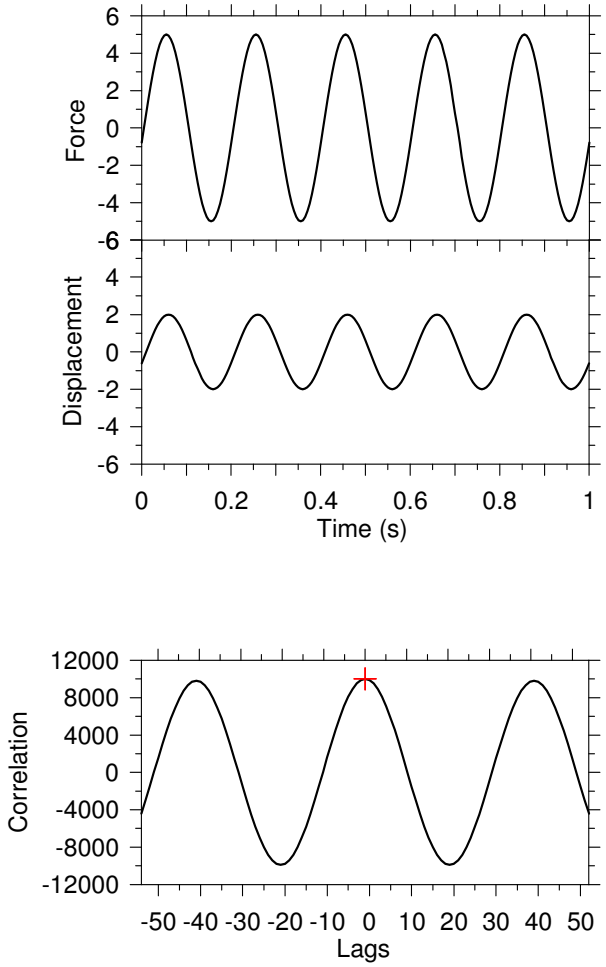

Figure 5.29 Force and displacement and the cross-correlation of the two sine waves

To examine the effect of increasing phase shift on identified impedance ordinates, the force is kept constant and the phase of the displacement is increased. In Figure 5.30, the complex plane is shown. The case analyzed above falls into the first quadrant (Case I). Three additional cases (II, III, IV) are investigated, with the associated force and displacement signals shown in Figure 5.30 (each having a 5 Hz frequency). The complex force and displacement obtained by performing a Fourier transform on the

signals is presented in Table 5.2. The table also presents the complex impedance obtained from the force and displacement.

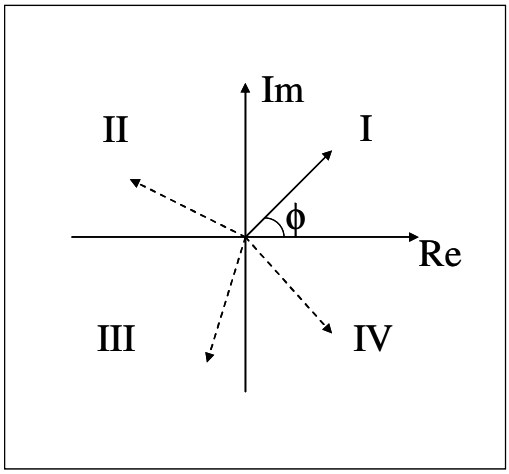

Figure 5.30 The complex plane

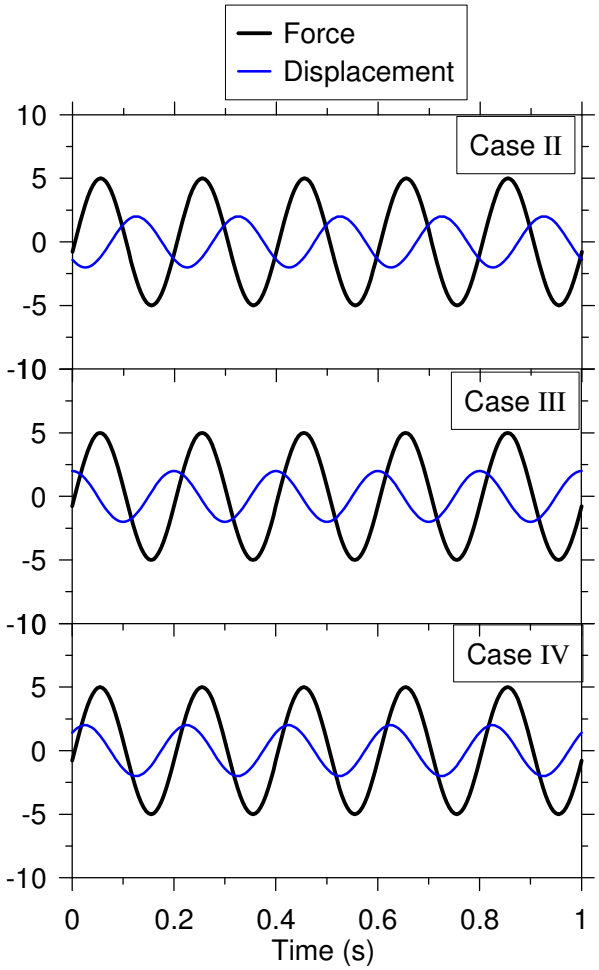

Figure 5.31 The force and displacements investigated

Table 5.2 Complex force, complex displacement, complex impedance

Case No	Complex Force	Complex Displacement	Complex Impedance
Case II	-0.782-i(4982)	-16113+i(1171.3)	-1.4675+i(2.0222)
Case III	-0.782-i(4982)	1970.3+i(311.74)	-0.3907-i(2.4668)
Case IV	-0.782-i(4982)	16113-i(1171.3)	1.4675-i(2.0222)

From Table 5.2, it can be seen that the imaginary part of the impedance terms (corresponding to damping) are negative for Cases III and IV. The two cases are in the

3rd and 4th quadrant in the complex plane as shown in Figure 5.30 ($\pi < \phi < 2\pi$). Similarly, the real part of the impedance terms (corresponding to stiffness) are negative for Cases II and III ($\pi/2 < \phi < 3\pi/2$).

The procedures applied to sine waves in the previous paragraphs are now applied to the data from Garner Valley. For the braced structure at 15 Hz the number of lags between the base shear and displacement based on the cross-correlation of the two motions was found to be 4 (Figure 5.28). That is, the base shear is leading the base displacement by 0.02 seconds (200 samples per second recordings). This corresponds to a phase angle of 1.88 radians. The phase angle calculated in the frequency domain was found to be 1.83 radians. Hence, the phase angle falls in the $\pi/2 < \phi < \pi$ quadrant. Furthermore, the estimated damping is positive. Thus, the negative stiffness and positive damping has physical meaning and can be explained by the phase shift.

For the case of the unbraced structure, a harmonic test is not available. However, earlier it was shown that the harmonic test and fast sweep test results agree well for the braced structure. Hence, the investigation carried out on the harmonic test results for the braced structure is repeated here for the unbraced structure with fast sweep tests. The stiffness and damping coefficients for the unbraced structure is plotted with the phase angle in Figure 5.32.

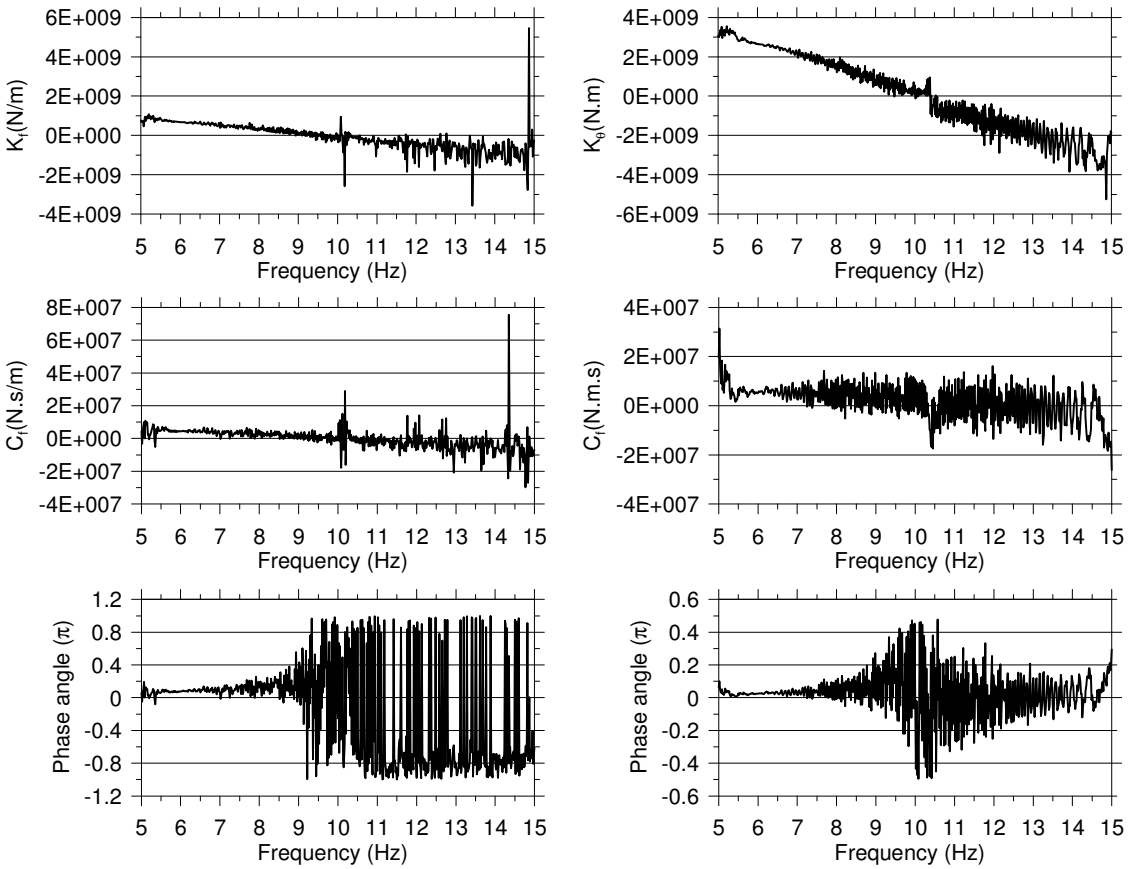

Figure 5.32 Translational stiffness and damping coefficients and the phase angle (unbraced structure)

For brevity only translational components are considered. The frequency is incremented in fast sweep tests such that the frequency range of 15-5 Hz is covered in 1 minute. Time windows containing two predominant frequencies are chosen to gain insight into the stiffness and damping values obtained from the transfer functions.

Figure 5.33 shows the base shear and displacement for a time window near 6 Hz. According to Figure 5.33, the foundation displacement lags the base shear by 1 time step (0.005 seconds). This compares well with the phase obtained from the frequency

domain analysis (0.19 radians from time domain compared to 0.23 radians from frequency domain). This places the response in the first quadrant ($0 < \phi < \pi/2$), providing positive stiffness and damping.

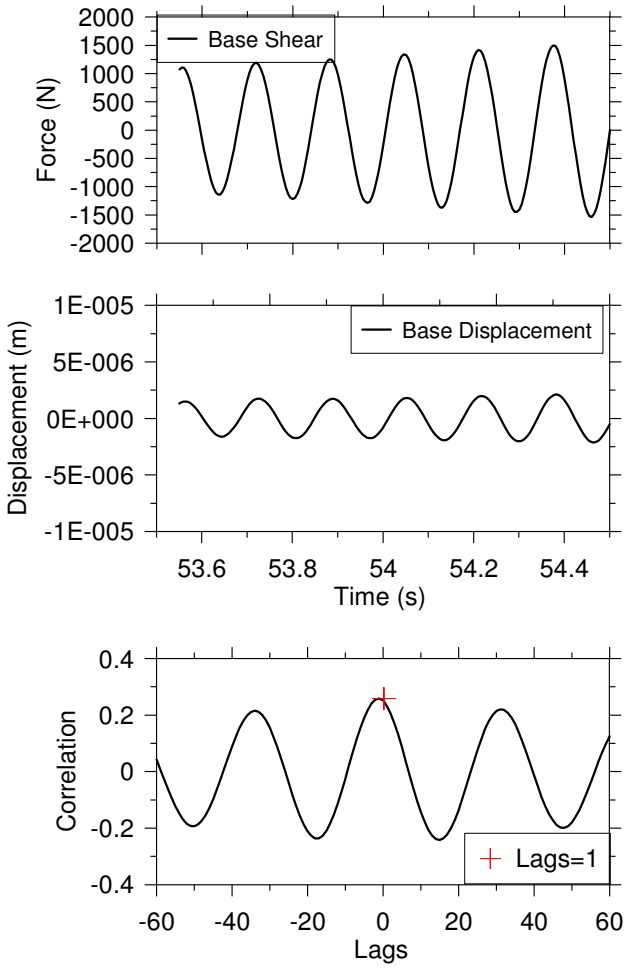

Figure 5.33 Base shear and foundation base displacement in the vicinity of 6 Hz and the cross correlation of the two signals (unbraced structure)

As stated earlier, at frequencies higher than 10 Hz the damping becomes predominantly negative, although some frequencies show positive damping as well.

Figure 5.33 shows base shear and displacement histories for a time window near 11 Hz, where negative damping was obtained. In this case, the base shear lags the displacement. The phase angle calculated in the time domain is -2.76 radians whereas the frequency domain calculations yielded a phase angle of -2.79 radians. This places the response in the third quadrant ($\pi < \phi < 3\pi/2$), providing negative stiffness and damping. However, as shown in Figure 5.32, the phase variations at these high frequencies are highly sporadic and random, suggesting a strong influence of noise on the results. This is consistent with the low S/N ratio observed for the translational data in this range (Figure 5.26). Accordingly, the phase measurements in this region are not considered reliable; hence the damping is also unreliable.

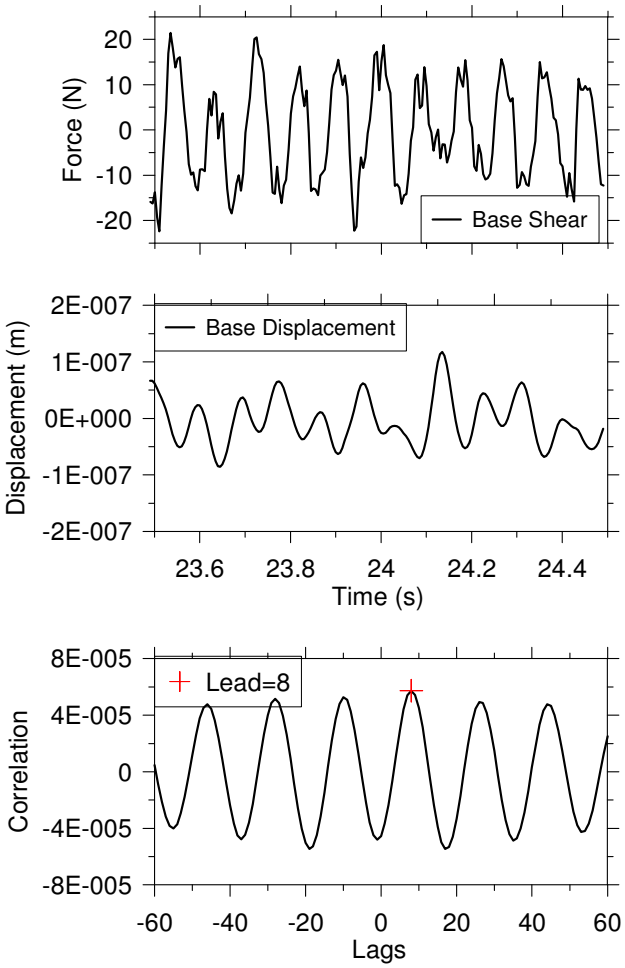

Figure 5.34 Base shear and foundation base displacement in the vicinity of 11 Hz and the cross correlation of the two signals (unbraced structure)

5.8.4 Speculation on physical mechanisms

Figure 5.2 depicts the theoretical predictions of foundation impedance for a non-uniform site. As opposed to a uniform site, the impedance functions for a non-uniform site decay relatively rapidly with frequency. The impedance coefficients estimated from forced vibration tests for the Garner Valley soil-structure system also have a

relatively fast decay with frequency. It is possible, therefore, that the misfit of the theoretical predictions results in part from the assumption of uniform soil stiffness with depth. The theoretical impedance coefficients were calculated using an effective halfspace shear wave velocity profile, which was calculated using an effective profile depth from the literature. This appears to have been satisfactory for low-frequency impedance coefficients. At higher frequencies, SSI produces shorter wavelengths of excitation in the ground, which in turn may excite intervals of the site profile having different effective velocities. To what extent that this is the case at the Garner Valley site requires further research.

6 SUMMARY AND CONCLUSIONS

6.1 SCOPE OF THE RESEARCH

The main objectives of the research were to evaluate soil-structure interaction effects by using data collected from forced vibration tests as well as earthquakes. Theoretical models that describe the primary effects of soil structure interaction exist in the literature. Those models however are not validated against field data and therefore the reliability with which they can be applied to realistic conditions in the field is unknown.

One purpose of this research was to describe modeling procedures that would be expected to realistically simulate this soil-foundation-structure interaction problem and to contrast those procedures with modeling approaches commonly used in practice (Chapter 2). Simple models are presented that take into account kinematic interaction effects which cause reductions of ground motion translation and introduce rocking for embedded rigid cylinders. Those models are implemented for several instrumented buildings with subterranean levels to evaluate their effectiveness for realistic field conditions. In Chapter 3, this work was expanded by performing detailed analysis of a

single building with subterranean levels and recordings of earthquake response. Both kinematic and inertial interaction effects were considered in developing the model for the building. The goal was to gain insight on the impact of different modeling procedures on various metrics of building response. A detailed model of the building was first created such that the response of the model matches the actual response of the building during the 1994 Northridge earthquake. The elements of the foundation are stripped away and the resulting errors are examined.

The remainder of the research focused on the development and implementation of specific parametric (Chapter 4) and nonparametric (Chapter 5) system identification procedures for soil-structure systems. First, a procedure that enables parametric system identification for a soil-structure system excited by forced vibrations was developed. Fixed-base and flexible-base frequency as well as damping of the system can be identified with the developed procedure. The procedure was applied to data collected from forced vibration tests carried out on the NEES model test structure in Garner Valley, California (http://nees.ucsb.edu). The results obtained from the field data was compared to the theoretical predictions

Nonparametric system identification procedures were developed to compute foundation stiffness and damping (impedance coefficients) from forced vibration tests. Previous work on this topic using field data is very limited. These studies are needed because engineering models for impedance coefficients, derived from analytical or numerical methods, are based on simplified conditions and may not apply under realistic field conditions. The equations required to calculate impedance functions from

forced vibration tests were first derived and then verified against a known solution. The procedure was then implemented using data collected from forced vibration tests carried out on the Garner Valley test structure. Translational and rotational impedance coefficients were obtained and compared to theoretical predictions.

6.2 RESEARCH FINDINGS

The results of the study presented in Chapter 2 are:

1. The rigid foundation models for kinematic interaction of embedded foundations produce estimates of top-of-foundation ground motions that are biased on the low side. There are a number of possible explanations for this difference, including amplification through the subterranean portion of the structure (which is affected by the mass and flexibility of those portions of the structure), effect on demand introduced to the system of foundation non-rigidity between the base and top of the foundation, possible torsional effects on the ground-level motions, and potential effects of surface waves (stronger at the ground surface than at depth).
2. The base rocking for very tall, long period buildings is reasonably well predicted by rigid cylinder models for kinematic interaction. Short-period buildings, such as at the Lotung site can have much larger base rotations than what is predicted by rigid cylinder models due to pronounced inertial interaction effects.

The investigation in Chapter 3 produced the following findings:

1. Properly accounting for foundation/soil deformations does not significantly affect vibration periods for the tall building investigated (which is expected), but does impact significantly the distribution of inter-story drifts over the height of the structure. To the best of my knowledge, the latter observation is new to this study.
2. The exclusion of kinematic effects on base rocking and translation does not change the vibration periods of the building nor interstory drifts above ground. However, kinematic interaction does significantly affect below-ground drifts. Hence, to accurately characterize the demand in subterranean levels, kinematic interaction effects should be considered. Exclusion of depth-variable ground motions did not significantly affect either below-ground or above-ground response for this building.
3. Two approximations commonly used in practice gave poor results: (i) fixing the structure at ground line with input consisting of free-field translation and (ii) fixing the structure at the base level, applying free-field motions as input at the base level, and using horizontal foundation springs along basement walls with their end condition fixed to the free-field ground motion.

The results of the non-parametric and parametric system identification investigation are summarized below:

1. Parametric system identification procedures originally developed for earthquake excitation have been extended to the case of forced vibration. To

evaluate flexible-base modal parameters, which incorporate flexibility and damping associated with foundation translation and rocking along with structural translation, recordings of shaker acceleration and roof translational acceleration are needed. Shaker mass and fundamental-mode participating mass are also needed. To evaluate fixed-base modal parameters, recordings of foundation translation and base rocking (measured using vertical accelerometers on opposite sides of the foundation) are needed in addition to those for the flexible-base case.

2. The input-output pairs for parametric system identification were verified using numerical analysis of various structures for which the fixed-base parameters are specified a priori and the flexible-base parameters can be computed using theoretical analysis. The verification involved the use of computed structural motions in parametric system identification procedures, which reproduced the a priori specified (fixed-base) and theoretically derived (flexible-base) parameters. The input/output pairs are found to be exact for single degree-of-freedom structures and to provide approximate results for multi degree-of-freedom structures.
3. The system identification procedures were applied to recordings obtained during forced vibration testing of a test structure at the Garner Valley Differential Array. The results were generally consistent with those obtained from earthquake recordings, both in terms of the values of fundamental mode vibration properties and the levels of soil-structure

interaction effects inferred from comparison of fixed- and flexible-base parameters.

4. Nonparametric system identification procedures were developed to compute foundation impedance coefficients from the results of forced vibration tests. An analytical model of a generic soil-structure system was created and the equations required to calculate impedance coefficients were derived. These equations were verified with respect to a known solution as well as existing equations in the literature. Coupling impedance terms were not included in the analysis, however were found to have little effect on computed impedance coefficients. The translational impedance coefficients are taken as the ratio of base shear to base displacement. The base shear is essentially made up of the inertia of the structure and foundation. Similarly, the rotational impedance coefficients are equal to the ratio of base moment to base rotation. Both equations were evaluated in the frequency domain. As a result, these equations give a complex impedance term made up of the corresponding stiffness and damping at the excitation frequency.
5. The equations for foundation impedance were applied to data recorded from forced vibration tests on the Garner Valley test structure. Tests were repeated for the structure with and without bracing. Theoretical predictions of the impedance functions were found to be close to the experimental results at lower frequencies. However, the experimental results decay more rapidly with increasing frequency than do theoretical predictions. Some of

the stiffness terms reduce sufficiently that they become negative at high frequencies. In one case (translational impedance for unbraced structure) damping coefficients also became negative.

6. Negative foundation stiffness was found to occur when the base shear is out of phase with the base displacement by 90 to 180 degrees (similarly results apply for base moment/rotation). Negative damping, which has no physical meaning, occurs when the phase angle is more than π, but was found to be associated with low signal-to-noise ratios and frequency band with sporadic (non-physical) variations of phase angle with frequency. This occurred at frequencies higher than 10 Hz in the unbraced structure. On the other hand, the braced structural configuration experiences more SSI and the damping coefficients obtained in the frequency range of interest were all positive.
7. Foundation stiffness was found to decrease at low frequencies when ground water table rises. The effects of ground water table for the damping coefficients were small.

6.3 RECOMMENDATIONS FOR FUTURE RESEARCH

The following are recommended for future research:

1. The effects of foundation modeling on the response of a structure were investigated on a single structure. In order to generalize some of the conclusions, more analysis on different structures using the procedures outlined in this research should be carried out.

2. The parametric system identification procedures developed were for a single input and single output system. Multiple-input and multiple- output parametric identification procedures exist. These procedures may be adapted to an MDOF structure system subjected to forced vibrations.
3. An important part of soil-structure interaction is governed by impedance functions. Whether it is through earthquake excitations or forced vibration tests, there is still a lack of impedance functions obtained from field performance data. The impedance values obtained in this study are for a test structure with a slab on grade foundation. Further field testing should be carried out on structures resting on different types of soils. It is important to cover a variety of such conditions, calculate impedance values and to compare with theoretical predictions.
4. The identified impedance coefficients were found to be highly frequency dependant for the Garner Valley site. Further research should be carried out to investigate the causes of this phenomenon. Numerical modeling of the soil-foundation system may give some insight into the causes.
5. The effects of groundwater table fluctuation on impedance values and system parameters are another area where further research should be carried out. A long term monitoring of the model test structure and the application of the procedures outlined in this research will give more insight on this topic.

REFERENCES

Apsel, R.J. and Luco, J.E (1987). "Impedance functions for foundations embedded in a layered medium: an integral equation approach," *J. Earthquake Engineering Structural Dynamics*, **15**(2), 213-231.

Chajes, M. J. Finch, W. W., Jr., and Kirby, J. T. (1996). "Dynamic analysis of a ten-story reinforced concrete building using a continuum model," *Computers & Structures*, 58 (3), 487-498.

Chopra, A.K, "Dynamics of Structures" (2007), Prentice-Hall, Upper Saddle River, NJ.

Chen, J-C., Lysmer, J., and Seed, H.B. (1981). "Analysis of local variations in free-field seismic ground motions," *Rpt. No. UCB/EERC 81-03*, Earthquake Engrg. Research Ctr., Univ. of California, Berkeley.

Computers and Structures, 2008, *ETABS version 9 User Manuals*, Berkeley, CA.
EPRI, Electrical Power Research Institute (1993). "Guidelines for determining design basis ground motions. Volume **1**: Method and guidelines for estimating earthquake ground motion in eastern North America," *Rpt. No. EPRI TR-102293*, Palo Alto, CA.

Crouse, C.B., Hushmand, B., Luco, J.E., and Wong, H.L.(1990). "Foundation impedance functions: Theory versus Experiment," *J. Geotech. Engrg*. ASCE,**116**(3), 432-449.

Crouse,C.B, McGuire,J., (2001) "Energy Dissipation in Soil-Structure Interaction",*Earthquake Spectra*; **17**, 235-259

Crouse, C.B, Liang, G.C and Martin G.R, (1984). "Experimental study of soil-structure interaction at an accelerograph station", *Bulletin of the Seismological Society of America*; **74**, 1995-2013

Day, S.M. (1978). "Seismic response of embedded foundations," *Proc. ASCE Convention,* Chicago, IL, October, Preprint No. 3450.

de Barros. C.P. and Luco, J.E (1995). "Identification of foundation impedance functions and soil properties from vibration tests of the Hualien containment model," *Soil Dynamics and Earthquake Engrg.*; **14**(4), 229-248

Elsabee, F. and Morray, J.P. (1977). "Dynamic behavior of embedded foundations," *Rpt. No. R77-33*, Dept. of Civil Engrg., MIT, Cambridge, Mass.

EPRI, Electrical Power Research Institute (1993). "Guidelines for determining design basis ground motions. Volume **1**: Method and guidelines for estimating earthquake ground motion in eastern North America," *Rpt. No. EPRI TR-102293*, Palo Alto, CA

Fadum, R.E (1948). "Influence values for estimating stresses in elastic foundations", *Proceedings 2nd International Conference SMFE, Rotterdam,* Vol.**3**

Gazetas, G. (1991). "Formulas and charts for impedances of surface and embedded foundations," *J. Geotech. Eng*, **117** (9), 1363-1381.

Idriss, I.M. and Sun, J.I. (1992). "SHAKE91: A computer program for conducting equivalent linear seismic response analyses of horizontally layered soil deposits," Center for Geotech. Modeling, Univ. of California, Davis.

Iguchi, M. and Luco, J.E. (1982). "Vibration of flexible plate on viscoelastic medium," *J. Eng. Mech.*, ASCE, **108**(6), 1103-1120.

Kausel, E., Whitman, R.V, Morray, J.P. and Elsabee, F (1978), "The Spring Method for embedded foundations", Nuclear Engineering and Design, (48). 377-392, North Holland.

Kim, S. (2001). Calibration of simple models for seismic soil structure interaction from field performance data, Ph.D. Dissertation, Univ. of Calif., Los Angeles.

Kim, S. and Stewart, J.P. (2003). "Kinematic soil-structure interaction from strong motion recordings," *J. Geotech.. & Geoenv. Engrg.*, ASCE, **129** (4), 323-335.

Kramer, S.L. and Stewart, J.P. (2004). Chapter 4: "Geotechnical Aspects of Seismic Hazards," in *Earthquake Engineering. From Engineering Seismology to Performance-Based Engineering*, Y. Bozorgnia and V.V. Bertero (editors), CRC Press, 85 pages.

Kunnath, S. K., Nghiem, Q., and El-Tawil, S. (2004). "Modeling and Response Prediction in Performance-Based Seismic Evaluation: Case Studies of Instrumented Steel Moment-Frame Buildings," *Earthquake Spectra*. 20 (3), 883-915.

LeRoy Crandall Associates, LCA (1981). "Report of Geotechnical Investigation, Proposed High Rise Development, Bounded by Harbor Freeway and 7th, 8th, and Figueroa Street, Los Angeles, California," *Job. No. ADE-81040.*

Liou, G.-S. and Huang, P.-H. (1994). "Effect of flexibility on impedance functions for circular foundations," *J. Eng. Mech.*, ASCE, 120(7), 1429-1446.

Liu, H., Yang, Z., and Gaulke, M. S. (2005). "Structural identification and finite element modeling of a 14-story office building using recorded data," *Engineering Structures*, **27** (3), 463-473.

Luco, J.E, Trifunac, M.D, and Wong, H.L. (1988). "Isolation of soil structure interaction effects by full-scale forced vibration tests*," J. Earthquake Engrg. Struct. Dynamics*, **16**(1), 1-21.

Luco, J.E., "Soil-structure interaction and identification of structural models", Proc. 2nd *ASCE Conf. on Civil Engng. and Nuclear Power*, Vol. **2**, 10/1/1-10/1/31/1980

Luco, J.E and Westman, R.A (1971)."Dynamic response of circular footings,"J. Engrg. Mech., ASCE, **97**(5), 1381-1395.

Mita, A. and Luco, J.E. (1989). "Dynamic response of a square foundation embedded in an elastic halfspace," *Soil Dyn. Earthquake Eng.*, **8**(2), 54-67.

Mylonakis, G., Gazetas, G., Nikolaou S., and Chauncey, A. (2002). "Development of Analysis and Design Procedures for Spread Footings" Technical Rpt MCEER-02-0003, City University of New York and the University of Buffalo, State University of New York, 246 pgs.

Naeim, F., Lee, H, Hagie, S., Bhatia,H. And Skliros, K. (2005), *CSMIP-3DV Technical Manual*, John A. Martin & Associates, Inc, Los Angeles, CA.

Naeim, F., Lee, H, Hagie, S., Bhatia,H., Alimoradi,A. and Miranda, E. (2006), "Three-dimensional analysis, real-time visualization, and automated post-earthquake damage assessment of buildings," *The Structural Design of Tall and Special Buildings*, 15, 1, pp. 105-138, Wiley InterScience, London.

Pandit, S.M. (1991). *Modal and Spectrum Analysis*, John Wiley, New York, NY.

PEER, 2008, Open system for earthquake engineering simulation (OpenSees) – development platform by the Pacific Earthquake Engineering Research Center (PEER). *http://opensees.berkeley.edu/*

Riggs, H.R. and Waas, G. (1985). "Influence of foundation flexibility on soil-structure interaction," *J. Earthquake Eng. Struct. Dynamics*, **13**(5), 597-615.

Roesset, J.M (1980). "A review soil-structure interaction," in Soil-Structure interaction: *The status of current analysis methods and research, J.J. Johnson, ed*., Rpt. No. NUREG/CR-1780 and UCRL-53011, U.S Nuclear Regulatory Com., Washington DC, and Lawrence Livermore Lab., Livermore, CA.

Safak, E. (1991) "Identification of linear structures using discrete –time filters" *J.Struct. Engng*. ASCE **117**, 3064- 3085

Seed, H.B. and Idriss, I. M. (1970). "Soil moduli and damping factors for dynamic response analyses," *Report EERC 70-10*, Earthquake Engineering Research Center, University of California, Berkeley.

Sohn, H (2004). "A Review of Structural Health Monitoring Literature: 1996-2001," Los *Alamos National Laboratory Report, LA-13976-MS*. Los Alamos NM 87545.

Stewart, J.P., Whang, D.H., Nigbor, R.L., Wallace, J.W., and Kim, S. (2005). "Role of field performance data in development and calibration of seismic soil-structure interaction analysis procedures," in *Soil-Structure Interaction: Calculation Methods and Engineering Practice*, Proc. of the International Geotechnical Conference Dedicated to the Tercentenary of St. Petersburg, St. Petersburg, Russia, V.M. Ulitsky (ed.); **1**, 47-58.

Stewart, J.P, and G.L. Fenves (1998), 'System identification for evaluating soil-structure interaction effects in buildings from strong motion recordings', *Earthquake Engng. and Struct. Dynamics*; **16**, 1-21.

Stewart, J.P., Kim, S., Bielak, J., Dobry R., Power, M.S, (2003)." Revisions to Soil Structure Interaction Procedures NEHRP Design Provisions." *Earthquake Spectra*; **19** No.3, 677-696.

Stewart, J.P., Seed, R.B. and Fenves, G.L. (1998). "Empirical evaluation of inertial soil-structure interaction effects," *Rpt. No. PEER-98/07*, Pacific Earthquake Engineering Research Center, University of California, Berkeley, 205 pgs.

Stewart, J.P., Fenves, G.L. and Seed, R.B. (1999). "Seismic soil-structure interaction in buildings. I: Analytical aspects," *J. Geotech. & Geoenv. Engrg.*, ASCE, **125** (1), 26-37.

Stewart, J.P., Seed, R.B., and Fenves, G.L. (1999). "Seismic soil-structure interaction in buildings. II: Empirical findings," *J. Geotech. & Geoenv. Engrg.*, ASCE, 125 (1), 38-48.

Stewart, J.P. and Stewart, A.F. (1997). "Analysis of soil-structure interaction effects on building response from earthquake strong motion recordings at 58 sites," *Rpt. No. UCB/EERC-97/01*, Earthquake Engineering Research Center, University of California, Berkeley, February, 742 pgs.

Stewart, J.P. and Tileylioglu, S. (2007). "Input ground motions for tall buildings with subterranean levels," *Structural Design of Tall and Special Buildings*, 16(5), 543-557.
Tileylioglu, S. Nigbor, R.L, and Stewart J.P. (2008), "Determination of soil-structure interaction effects for a model test structure using parametric system identification procedures," in *Geotechnical Engineering and Soil Dynamics IV,*, May 18-22, 2008, Sacramento, CA, ASCE Geotechnical Special Publication No. 181, D. Zeng, M.T. Manzari, and D.R. Hiltunen (eds.), 10 pages (electronic file).

Stewart, J.P. and Tileylioglu, S. (2007). "Input ground motions for tall buildings with subterranean levels," *Structural Design of Tall and Special Buildings*, **16**(5), 543-557.

Todorovska, M. I., Hayir, A., and Trifunac, M.D. (2001). "Antiplane response of a dike on flexible embedded foundation to incident SH-waves," *Soil Dyn Earthquake Eng*. 21(7), 593-601.

Veletsos A.S and Meek, J.W 'Dynamic behavior of building-foundation systems,' E*arthquake Engng. and Struct. Dynamics* 1974; **2**, 121-138

Veletsos A.S and Verbic B. (1973). "Vibration of viscoelastic foundations" *Earthquake Engng and Struct. Dynamics*; **2,** 87-102

Veletsos,A.S. and Wei, Y.T. (1971). "Lateral and rocking vibrations of footings." *J.Soil Mech. And Found. Div., ASCE*, **97(**9), 1227-1248.

Welch, P.D.(1967), "The use of Fast Fourier Transform for the estimation of power spectra: a method based on the time averaging over short, modified periodograms," *Transactions on Audio and Electroacoustics*, IEEE, AU-15(2), 70-73.

www.nees.ucsb.edu

Yang, Z., Lu, J., and Elgamal, A., (2004). "A Web-based Platform for Live Internet Computation of Seismic Ground Response," *Advances in Engineering Software*, Elsevier, Vol. 35, pp. 249-259